Shaping Living Matter

Direct Ink Writing of Cellulose Producing Bacteria

Kevin Krüger

Delft University of Technology

TU Delft

Shaping Living Matter

Direct Ink Writing of Cellulose Producing Bacteria

For obtaining the degree of Master of Science in Aerospace Engineering at Delft University of Technology

Kevin Krüger

25 June 2022

TU Delft

Delft University of Technology
Faculty of Aerospace Engineering
Department of Aerospace Structures and Materials

GRADUATION COMMITTEE

Chair holder:

Dr. K. Masania

Committee members:

Dr. M.E, Aubin-Tam

Prof. CA. Dransfeld

Acknowledgement

With this thesis coming to an end, I want to express my deepest gratitude to everyone who has helped me over its course. First and foremost, I would like to thank my supervisor Dr. Kunal Masania, who's trust and guidance over the past year, has given me the opportunity to work on a truly extraordinary topic and who's motivational words have allowed me to push through even the most frustrating of days, which when working with bacteria, mostly occurred when said bacteria decided to perish for reasons of unknown (fungi) origin.

I furthermore want to thank Dr. Marie-Eve Aubin-Tam, who provided me with invaluable insights into the biological aspects of my thesis and all members of the Shaping Matter Lab who made every part of this thesis so much more enjoyable.

In addition, I would like to extend special gratitude towards Satya Ammu, who for some reason, which in my opinion must be related to his old-age, listened to my endless monologue's about the intricacies of bacteria growth for the past 9-months and always found the right words to allow me to see a path forward.

Lastly, I want to thank my family and friends, I simply could not have done this without your support, you mean the world to me.

Kevin Krüger
Delft, June 2022

Abstract

One of the biggest challenges of the 21st century will be the need to reduce the impact of climate change, requiring a drastic rethinking of how products are designed, build, operated and recycled. This similarly applies to the current design approaches used for structural components in the aerospace industry, which place large emphasis on mass reduction, thus decreasing fuel consumption in the process, but neglect to consider the environmental impact of components over their entire life-cycle. One prominent example of this is the frequent use of carbon fiber, which from an operational standpoint can reduce CO2 emissions due to the lightweight parts it allows for, but crucially requires high energy input during its production while being neither biodegradability nor easily recyclable.

As a result, there has been a concentrated effort to find novel, more sustainable materials and production techniques, with one of the most promising alternatives being Bacterial Cellulose (BC). BC combines the high specific mechanical properties of cellulose, with the use of microbes as micron-sized factories, which are leveraged to digest glucose in an oxygen-rich environment to metabolise a highly pure and crystalline intertwined network form of cellulose. In spite of its advantageous properties, the lack of shaping freedom in current BC manufacturing techniques has hindered its implementation. To remedy this, research has focused on embedding cellulose-producing bacteria into hydrogel inks from which 3-dimensional living structures can subsequently be printed using direct ink writing. However current iterations of this process lack the ability to manufacture geometries with complexities in excess of single layer patterns. The goal of the MSc thesis at hand was to investigate if the addition of inorganic silicone dioxide platelets to the hydrogel ink, which act as a scaffold for the bacterial cellulose to grow around, can be leveraged to increase both the printability of the ink and structural integrity of the resulting BC material.

Given the novelty of this approach, the thesis work commenced with a parametric study to determine the effect of ink formulation and processing parameters on the bacterial cellulose metabolism, the results of which were used to optimise the ink formulation while quantifying for the first time the BC yield as a function of input nutrient solution, a parameter that is crucial to understand the nutrient utilisation efficiency of the developed ink.

The increased printability and shaping freedom of the so-created ink and process was then investigated by printing a range of multi-layer geometries, demonstrating improved part complexities which were no longer limited to single layers.

Next to demonstrating the improved printability, the microstructure of the so produced BC composite was examined using SEM imaging, revealing a core-shell morphology, whereas the BC formed an enclosing shell around the platelet-rich printed scaffold. Furthermore, by tracking the BC overgrowth around one layer thick printed scaffolds, a diffusion model for the nutrient flow during the BC growth was established. This revealed that not all nutrients from within the printed scaffold could be utilised by the active bacteria in the shell layer, as a result limiting the maximum BC shell thickness to $19.7\mu m$. Lastly the effect of the in-situ BC overgrowth on the reduced Youngs modulus was investigated using nano-indentation which found an increase by a factor of 6x compared to scaffolds without BC growth and an increase by 1.7x compared to pure BC. These results show that the BC growth and subsequent shrinkage during drying compacts the core and gives rise to loading response, whereas the material acts more integral, resulting in a more effective loading of the stiff silicone dioxide platelets contained in its core.

The increased printability and mechanical integrity observed leads to the conclusion that the addition of inorganic fillers, in the form of silicon dioxide platelets, to act as a scaffold for bacterial cellulose overgrowth, can be leveraged to improve the geometric complexity and structural integrity of the printed and overgrown structures.

Contents

List of Figures

Nomenclature

Abbreviations

Abbreviation	Definition
BC	Bacterial Cellulose
AM	Additive Manufacturing
DIW	Direct Ink Writing
HA	Hyaluronic Acid
k-CA	k-Carrageenan
FS	Fumed Silica
CNF	Cellulose Nanofibre

Symbols

Symbol	Definition	Unit
ρ	Density	[kg/m^3]
η	Viscosity	[Pa $\cdot s$]
D	Diffusion Coefficient	[m$^2/s$]
T	Temperature	[K]
k	Boltzmann Constant	[J/K]
r	Radius	[mm]
h	Height	[mm]
w	Width	[mm]
l	Length	[mm]
l	Length	[mm]
t	Thickness	[mm]
v	Volume	[mm^3]
m	Mass	[kg]

1

Introduction

The approach of the aerospace industry to the synthesis of many of its most high performance materials is no longer sustainable in today's era dominated by issues of climate change and environmental pollution. A primary example of this, is carbon fiber, which due to its high specific mechanical properties, is used throughout the aerospace industry to design and manufacture lightweight parts, consequentially giving rise to more efficient structures which exhibit a reduced environmental impact during their operation. Despite of this, carbon fiber, in its current form, is no longer considered a sustainable material, as a result of the impact it has on the environment over its entire life-cycle. The origin for this is two-fold. On the one hand, its production requires the use of temperatures in excess of 1000°C, which severely increases its carbon dioxide footprint[22], while furthermore not being easily recyclable.

In contrast to this, natural materials are synthesised by organisms at ambient conditions and are shaped through millions of years of evolution to be extremely efficient in their use of energy during growth. Intriguingly, while there tends to be the perception that man-made materials are far superior to those made by nature, many natural materials such as bone, nacre, and wood offer a exceptional mix of toughness, strength, and stiffness[24], while displaying additional functionalities such as nutrient transport and self-healing capabilities. Most noteworthy of the above for large scale structural applications, is wood, whichs impressive performance can best be highlighted when considering the size *Sequoia sempervirens* trees, shown in Figure 1.1, a species which grows to heights in excess of 100 meters, towering over many of humanities most iconic landmarks and exhibiting a lifetime in excess 2000 years.

Figure 1.1: *Sequoia sempervirens* towering over the surrounding forest. [25]

On a microscopic level, woods impressive structural performance can be traced back to the intertwined chains of cellulose fibrils which interlace with lignin and hemicellulose providing it structural integrity. This is schematically shown in Figure 1.2, which highlights the basic building blocks of plants from a micro to a macroscopic scale. While in its molecular form, cellulose shows similar strength and stiffness to carbon fiber, these properties are reduced in wood due to the occurrence of impurities making is extraction from natural sources cumbersome.

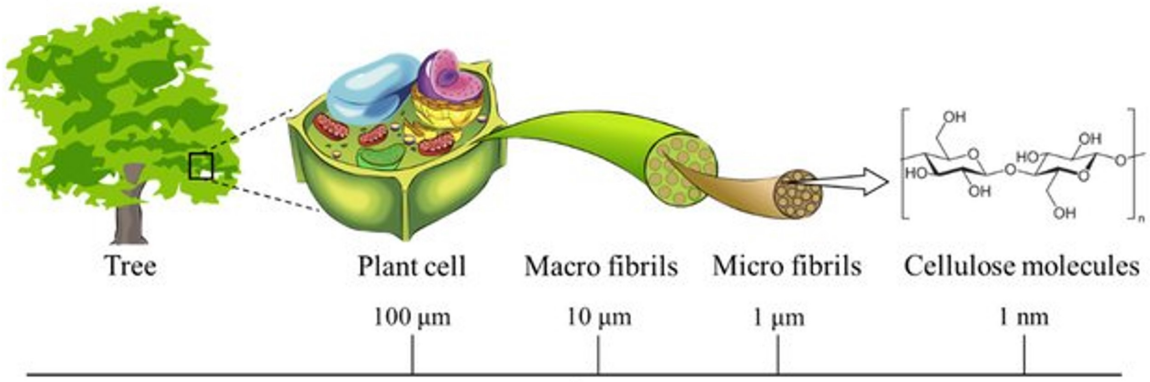

Figure 1.2: Breakdown of a plants microstructure [16], showing cellulose, the molecule which forms the basis its mechanical performance.

Crucially next to its occurrence in wood, a highly pure and crystalline form of cellulose is further produced by some bacteria strains, from here on referred to as bacterial cellulose, under ambient conditions when provided with a source of glucose and access to oxygen. As a result of its low energy intensive production and high purity, the utilisation of cellulose metabolised from bacteria strains has long been a topic of interest, given that structural components made from bacterial cellulose promise to offer both similar performance to currently used materials in the aerospace industry while being fully bio-degradable and having a low impact on the enviroment during production. Despite this, bacterial cellulose has yet to be widely applied as a consequence of the limited geometrical freedom which can be achieved by the need to retain its network like structure of intertwined cellulose fibrils for high mechanical properties and its preferential growth as a thin film. An example of the pellicle formed by static bacterial cellulose growth is shown in Figure 1.3(a), together with its respective microstructure in Figure 1.3(b).

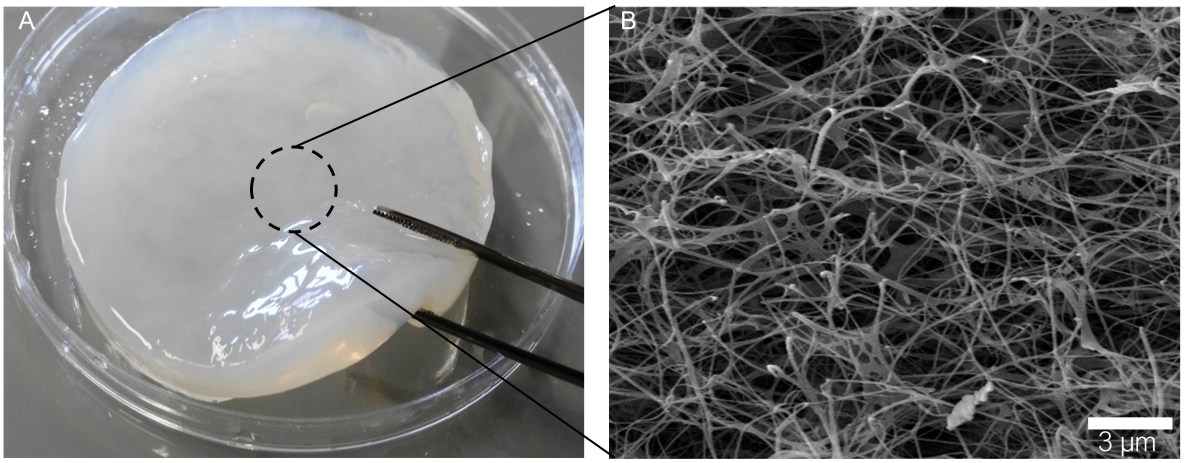

Figure 1.3: Bacterial cellulose grown using static fermentation (A)[26], and its microstructure of intertwined cellulose (B). [3]

1.1. Shaping Bacterial Cellulose using Additive Manufacturing

One approach to remedy the lack of shaping freedom, has been to embed the cellulose producing bacteria into a hydrogel ink from which 3-dimensional living structures are subsequently printed using direct ink writing, a form of Additive Manufacturing(AM), where geometries are build-up one layer at a time through the deposition of a paste like ink. These are subsequently incubated in order to allow the embedded bacteria to convert nutrients included in the hydrogel into a cellulose network to stabilise the structure. While using this approach some success has been achieved, the ability to construct multi-layer structures of significant thickness and structural integrity has yet to be demonstrated. The origin

for this has been found to steam from the two main and opposing functions required of the hydrogel ink. On the one hand the hydrogel ink has to have a high enough shape retention to allow for the construction of multi-layer parts which gives rise to hydrogel inks with high viscosities, while the need for easy and widespread diffusion of nutrients to allow for ample cellulose formation by the embedded bacteria requires low viscosity inks. In addition the high liquid content of these hydrogels in comparison to the low cellulose output observed means that the resulting structures lack a high degree of structural integrity.

As a result the approach taken in the thesis work is to improve on the current shape restrictions and low mechanical properties by the addition of inorganic platelets to the hydrogel which act as a scaffold for the bacterial cellulose to grow around, giving rise to both a higher printability and structural integrity of the resulting bacterial cellulose material.

1.2. Outline

This dissertation first provides a literature review in chapter 2, subsequent to which the research objective, question, scope, and hypothesis are outlined in chapter 3. This is then followed by a presentation of the core research results, which are split inbetween the characterisation of the bacteria strain in chapter 4, the investigation of the improvements in geometric freedom provided by the addition of the inorganic platelets in chapter 6, and an analysis of the so-produced material in terms of its microstrucutre in chapter 7, and mechanical properties in chapter 8. Lastly the significance and conclusions drawn from the here presented work are highlighted in chapter 9, with an outlook for future research furthermore given in chapter 10.

2

Literature Review

In order to provide the necessary framework for the thesis, this chapter first introduces the metabolism and characteristics of bacterial cellulose in section 2.1, followed by an explanation of its production using static fermentation, in section 2.2. Next, direct ink writing and its applications to create living structures from cellulose producing bacteria are detailed in section 2.3, after which the literature review is finished by highlighting previously investigated reinforcement regimes for BC networks in section 2.4, and a summary of the main outcomes in section 2.5.

2.1. Introduction to Bacterial Cellulose

Bacterial cellulose is formed by a multitude of bacteria strains, including but not limited to the here studied strains *G.xylinus* and *G.hansenii*. From a chemical perspective it does not deviate from the cellulose found in natural materials such as wood, with its molecular structure being made up of individual glucose monomers rings linked together by β 1-4 glycosidic bonds[9]. More simply put this β 1-4 glycosidic bond refers to the covalent bonding between the carbon atom of one glucose ring with the carbon atom of the adjacent glucose ring via an oxygen atom. In addition to this strong covalent bonding, two further hydrogen bonds exist between the hydroxyl groups of adjacent glucose rings.[1] The translation of this to the buildup of individual cellulose molecules is visually depicted in Figure 2.1.

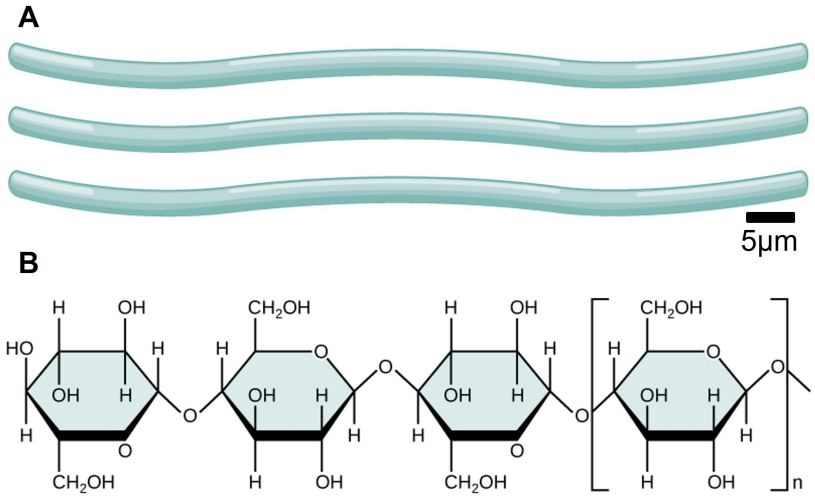

Figure 2.1: Individual cellulose fibres (A) with its respective molecular structure (B) [14].

On a high level the bacterial cellulose fibres are constructed through the breakdown of a carbon source in the form of saccharides by enzymes inside the bacterium. The so-created cellulose polymer is then expelled from the bacterium. These individual cellulose molecules subsequently self-assemble into crystalline micro-fibrils, with a mean diameter of 2nm-4nm promoted by the abundance of hydroxyl

groups present in their molecular structure. On the next higher level these nanofibres group into ribbon like structures showing both crystalline regions of highly aligned individual fibrils and disorganised amorphous regions, see Figure 2.12 **A**. On the highest level said ribbons then interlock and intertwine with each other forming a porous 3D network, Figure 2.12 **B**, held together by a combination of hydrogen bonding, van der Waals forces and mechanical interlocking between individual fibres.[**BondsCellulose**]

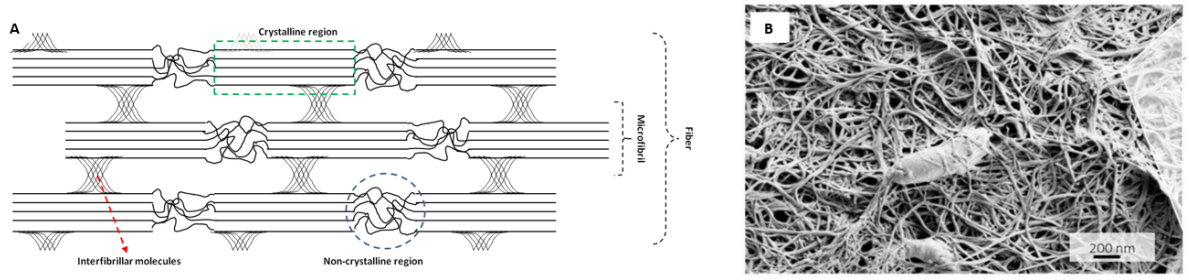

Figure 2.2: Schematic of individual cellulose fibre (A)[6] and SEM of it microstructure (B) [10].

While this represents a highly simplified view of the multi-step breakdown of saccharides such as glucose and sucrose into a form which allows for the construction of the linked glucose monomer rings a more detailed analysis of the individual enzymes involved is outside the scope of this literature review. Thus for the remainder of this review, individual bacteria will be represented as distinct entities which require a certain set of inputs in the form of a carbon, nitrogen and oxygen source together with appropriate boundary conditions such as pH and temperature to produce the desired cellulose fibres. For each aspect of the growth medium the exact compound for optimal cellulose production may vary but the following itemisation provides a summary of the most widely used options.

- Carbon Source: Glucose, Fructose, Maltose, Sucrose
- Nitrogen Source: Yeast Extract, Peptone
- pH: 3-7 possible but optimally closer to 4-6. Alter by addition of buffers. Note that bacteria may decrease pH naturally throughout the process, thus keeping it in the optimal range is vital.
- Temperature Range: 25°C-30°C

The precise formulation for the growth medium which will be implemented is based on the doctoral work of Yu [29] due to the same strain of *G.Hansenii* bacteria being used.

Next to the production of cellulose, its mechanical properties and the variables which may influence them are furthermore of utmost importance. Here on key factor is the large water retention exhibited by bacterial cellulose, exceeding 100 times its own weight [10] and the dependence of mechanical properties on the hydration level. Indicative of this, is the research done by Giuseppe Scionti [19], in which he found that the Young's modulus of a bacterial cellulose pellicle increased by 3 orders of magnitude when dried, reaching a stiffness of 10GPa and an ultimate tensile strength of 200MPa. Note that higher values have furthermore been recorded with the Young's Modulus and tensile strength of dried samples reaching up to 18GPa and 260MPa respectively. [10] [28]

2.2. Bacterial Cellulose Growth in Static Fermentation

By far the most utilised production technique in order to grow bacterial cellulose is that of static fermentation. Here the cellulose producing bacteria are added to a growth solution and fermented statically, that is without movement of the growth solution. Depending on the specific of the process this growth solution will contain a range of nutrients and pH modifiers with the most commonly used formulation being that of Hestrin & Scramm, also referred to as HS medium which consists of the following components.

1. 20 g/L Glucose
2. 2 g/L Peptone
3. 5 g/L yeast extract

4. 2.7 g/L Na2HPO4
5. 1.2 g/L citric acid monohydrate

Once added to the liquid growth culture, the bacteria move to the surface of the growth medium in order to obtain both an ample supply of oxygen, which diffuses into the growth medium from the surrounding air, and nutrients to synthesise bacterial cellulose. Note that a graphical depiction of this is provided by Figure 2.3(a). This preferential growth close to the surface and the lack of oxygen availability deeper within the growth medium, results in the bacteria forming a pellicle like film at the air-liquid interface with its shape and dimensions mirroring that of the container its grown in. Due to this characteristic growth, most applications of bacterial cellulose produced using static fermentation are limited to circumstances which require thin films. As a result one of the few commercialised applications is the treatment of burn wounds due to the positive influence of the hydrated BC pellicle on the recovery time, see Figure 2.3(b).

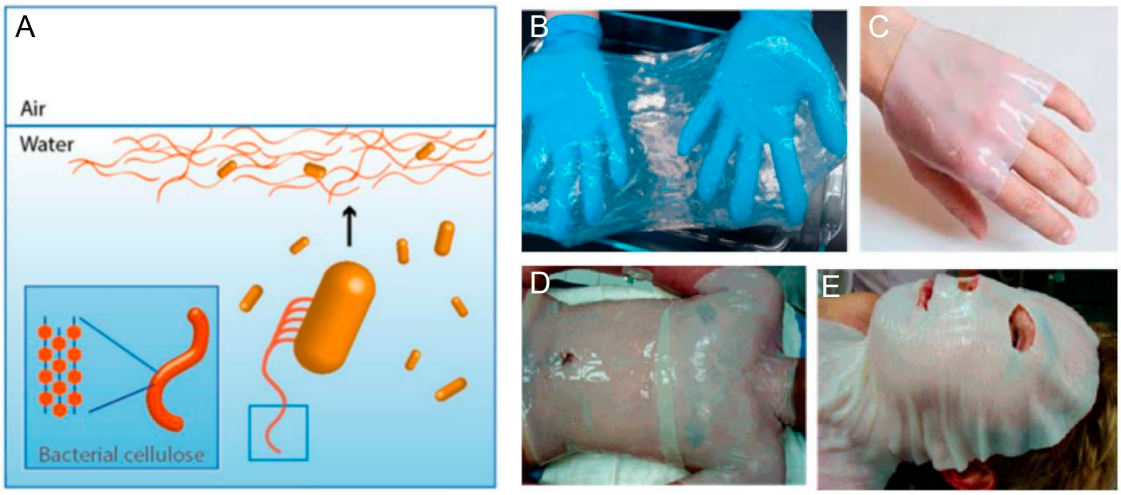

Figure 2.3: Growth of bacterial cellulose (A)[17] and its primary application for medical purposes (B-E) [11].

2.3. Direct Ink Writing of Living Inks

While the outstanding properties of bacterial cellulose together with its bio compatibility and low carbon dioxide footprint as introduced in the previous section makes it ideal from a material perspective, the lack of shaping freedom offered by current manufacturing techniques, exemplified by the static fermentation of BC films in section 2.2 has hindered its real life implementation. As a result there has been a significant effort in order to increase the shaping freedom by combining the in-situ bacterial cellulose growth with AM. To this end most research has focused on the combination of a feedstock formulation in which the living bacteria and required nutrients are combined with other additives into a paste like ink from which parts are build using direct ink writing. Given its frequent use,which extends to the thesis work at hand, this section first introduces the working principle behind DIW in subsection 2.3.1, followed by three examples of its application to living inks with cellulose producing bacteria in order to highlight both the successes and limitations of the current state of the art.

2.3.1. Direct Ink Writing

Direct ink writing is a version of AM were the part is build up layer by layer through the controlled extrusion of a paste (”ink”) from a syringe at locations which in summation form the wanted geometry, schematically shown in Figure 2.4. As such this process does not require melting of the feedstock, as required by thermoplastic based FDM processes, but rather leverages inks with shear thinning behaviour which show a reduction in their viscosity during the deposition phase and rapidly recover their shape retention properties after exciting the nozzle.

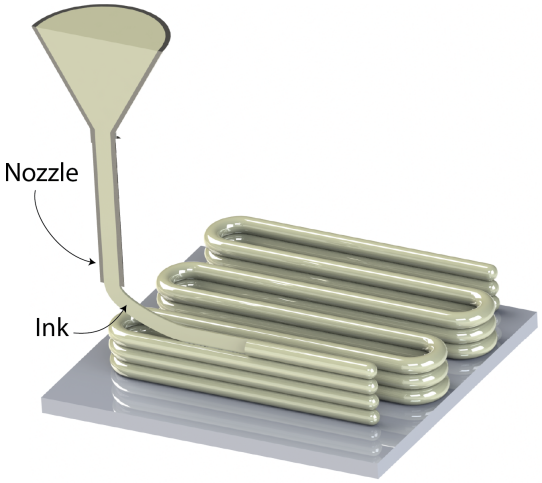

Figure 2.4: Working Principle of direct ink writing [27].

Note that while the lack of high processing temperatures makes DIW ideally suited for the printing of living materials, the reliance on the ink rheology both during and after extrusion means that the ink has to fulfil two main and conflicting functions. On the one hand, it has to flow easily during the deposition process and as such is required to exhibit shear thinning behaviour in order to reduce its viscosity and mechanical properties, while on the other hand it has to have sufficiently high at rest mechanical properties and recover those properties fast enough to allow it to retain its shape after extrusion. The result of this is two fold. First while inks which do not posses high enough at rest mechanical properties are easily extrude-able, they do not lend themselves to traditional DIW as both gravity and their own surface tension tend to distort the extruded geometry, as shown in Figure 2.5(b).

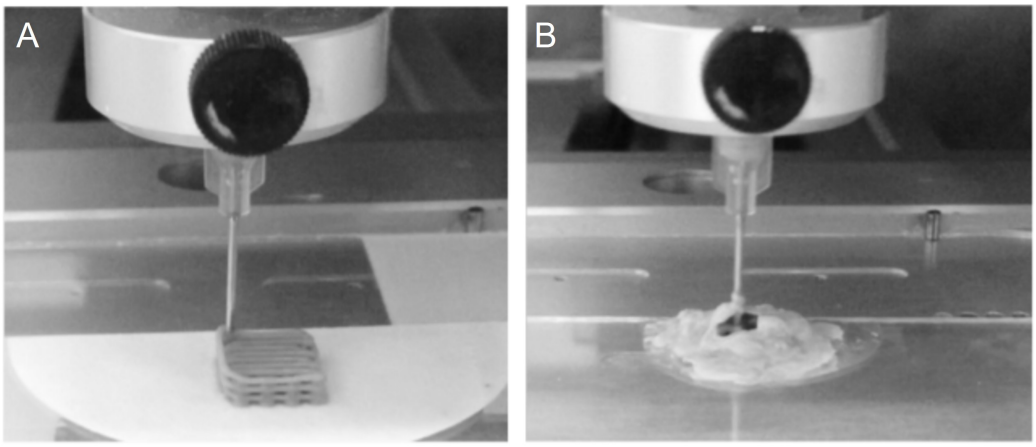

Figure 2.5: Effect of sufficient ink yield stress (A) and insufficient ink yield stress (B) on the shape retention of the extruded geometry [15].

This limits the inks which can be used for DIW to those with an at rest stiffness and yield-point in excess of 1kPa and 10Pa[15]. Secondly more complex features such as porous enclosures or overhangs which require the ink to resist collapsing under its own weight are limited due to the relatively low at rest mechanical properties of the ink as a consequence of the need to extrude them in the first place. The need to construct complex geometries is however closely linked to the efficient use of material, similarly seen in natural structures, where the materials anistropy, is leveraged by tailoring the structure for the intended function through placement of material only where it is required.

Note that while this drawback places an upper limit on the geometric complexity which can be achieved using DIW, it is nonetheless the most used AM process for printing with living materials, illustrated with the following three examples of its application to creating living structure from cellulose producing bac-

teria.

Controlling Printability through Rheological Modifiers
The research by Schaffner et al.[18] combines in-situ bacterial cellulose growth and direct ink writing using an ink, referred to as Flink, combining equal parts of bio-compatible hyaluronic acid (HA), k-carrageenan (k-CA) and fumed silica (FS) with the cellulose producing bacteria strain *A. xylinum*. Using this ink formulation, Schaffner et al[18] successfully demonstrates the ability to create thin patterns, as shown in Figure 2.6, which are overgrown with cellulose, verifying the survivability of the embedded bacteria both during and after extrusion.

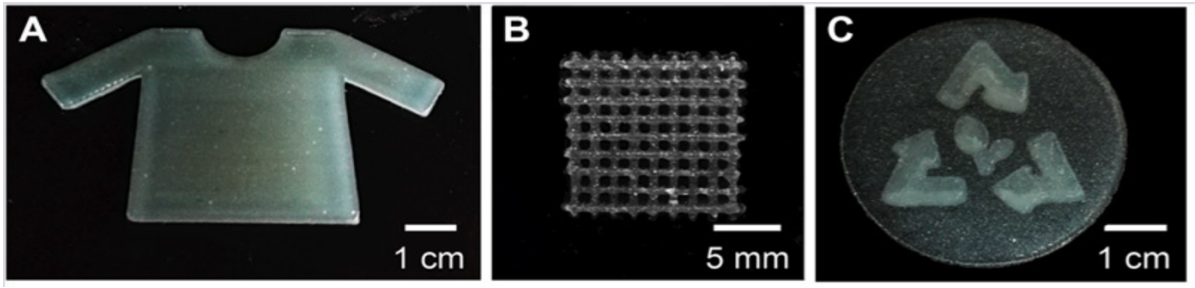

Figure 2.6: Printed geometries using direct ink writing to extrude the Flink ink formulation[18].

Crucially their work reveals the trade-off at the heart of direct ink writing with living organisms, namely the requirement to optimise the ink rheology both for printability and bacteria survivability. On the one hand, Schaffner et al.[18] demonstrate the positive relationship between print fidelity and %wt fumed silica, whichs increasing effect on viscosity, shear thinning and yield stress is found to result in better shape retention of the ink after extrusion, while on the other hand finding that the production of cellulose by the embedded bacteria is hindered by an increase in viscosity. Note that this effect is qualitatively shown in Figure 2.7, whereas the degree of cellulose formation is highlighted through the use of a UV staining agent, showing the reduced cellulose formation for for the higher ink viscosity.

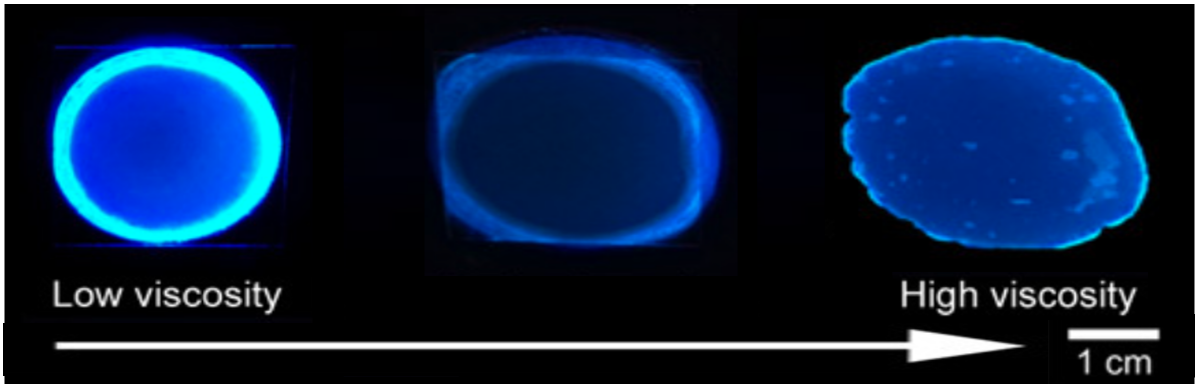

Figure 2.7: Qualitative assessment through UV staining showing that higher viscosity inks hinder cellulose metabolism[18].

Note that as a result of this balancing act, the geometries shown as part of this work are limited to relatively thin parts, indicating that the ink does not poses the shape retention capability to construct multi-layer structures.

Stabilising through In-Situ Gellation
In contrast to the approach taken by Schaffner et al.[18], whereas a careful balancing act was required to adjust the ink rheology for printability and bacteria survivability by adjusting the %wt of rheological fillers added, the work of Balasubramanian et al.[4] takes a different route, whereas a significantly less viscous bacteria loaded ink is printed and stabilised through the incorporation of sodium alginate. To this end, the process requires the ink to be extruded onto a calcium chloride loaded agar substrate which triggers gellation of the sodium alginate, subsequently stabilising the shape of the extruded ink.

Despite the difference in approach, the resulting geometries which can be produced using this method are similar in complexity to those of Schaffner et al.[18], as such being limited to thin film patterns, as seen in Figure 2.8.

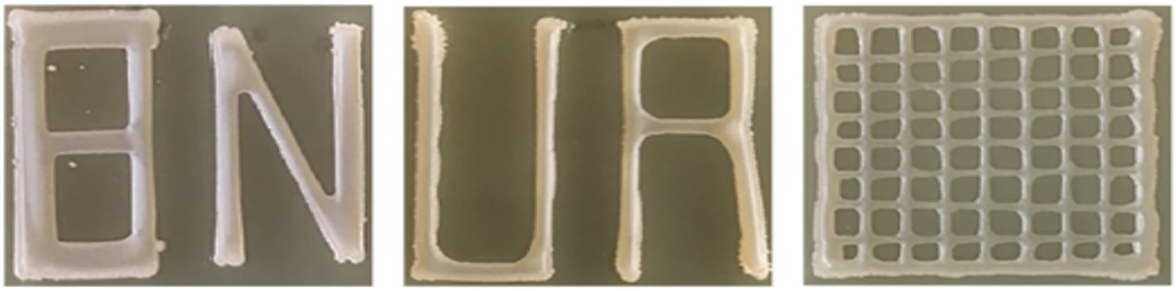

Figure 2.8: Geometries printed using direct ink writing and the ink formulation developed by Balasubramanian et al.[4].

In addition to demonstrating printability, the work of Balasubramanian et al.[4] investigates the penetration depth of oxygen into the cellulose biofilm, finding that oxygen availability is limited to the first $200\mu m$, as such giving rise to two zones within the tested biofilm, namely the aerobic zone close to the surface whereas bacterial respiration is possible and the anaerobic layer at depths in excess of $200\mu m$ whereas no aerobic bacteria can survive due to the lack of oxygen availability.

2.3.2. Print Stabilisation through a Support Matrix

In contrast to the previous two works, the work of Shin et al.[20] leveraged a bacteria loaded hydrogel ink, stabilised not by its inherent rheological properties or the gellation of one of its components after extrusion but by using a support matrix made from PTFE micro-particles. With this setup the researchers successfully demonstrated the feasibility of not only printing complex shapes from living bacteria, see Figure 2.9 but also highlighted the ability of the PTFE matrix to sustain the bacteria's metabolic activity for multiple days due to its permeability to oxygen.

Figure 2.9: Demonstration of the geometric complexity achievable when using a PTFE support bath [20]. Scale bar is 1 cm.

Next to the creation of complex shapes, one key observation noted by the researchers was the non-homogeneous distribution of cellulose throughout any given extruded filament, which is attributed to the decrease in oxygen supply away from the gel-ink interface. As a result the cross-section of a filament shows distinct BC layers on the outside with the core region consisting of a Cellulose NanoFiber(CNF) modifier,hydrogel, and BC composite. To emphasize the extend of this, Shen et al.[20] added fluorescent green dye to the bacteria previous to printing, allowing their migration to the surface to be visually observed during the incubation time. The distinction between surface layer bacteria activity and the lack thereof as a function of the distance to the surface can be clearly observed in Figure 2.11 (C). Furthermore shown are two graphical depictions, which emphasize the oxygen depletion towards the core (A) and the tube like structure formed as a consequence (B).

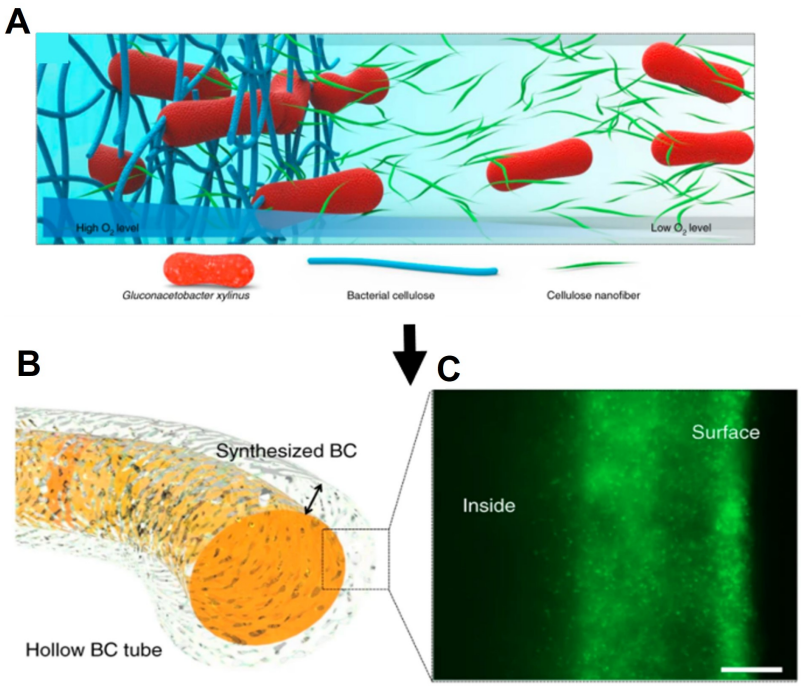

Figure 2.10: In-homogeneous bacteria distribution (A), tubular BC network produced (B), and bacteria (green) distribution within one filament (C) [20]. Scale bar is $50\mu m$ in (C).

The effect of oxygen depletion towards the core can furthermore be observed from the SEM images taken after freeze-casting the incubated prints, again showing a distinct layered composition for the surface regions where high BC production occurred(c) as compared to the composite morphology found away from the surface consisting of both BC and CNF(d).

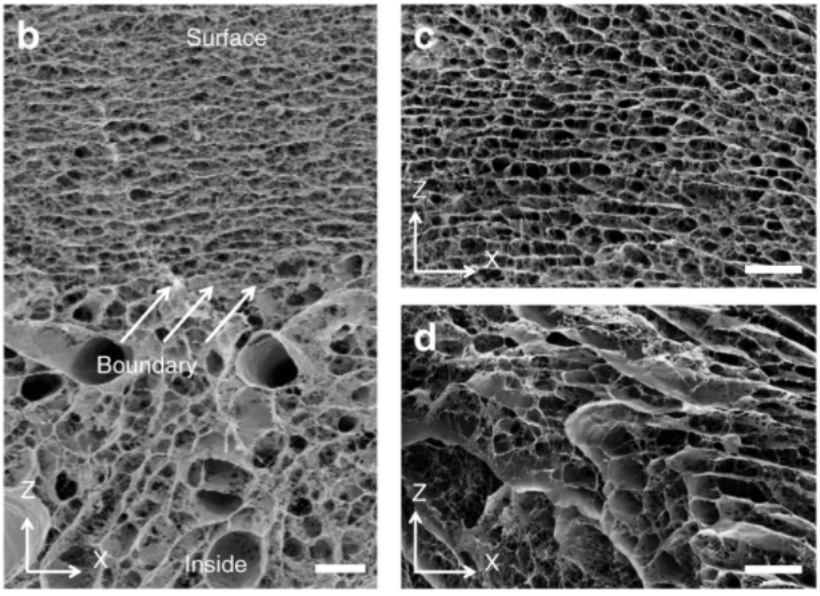

Figure 2.11: SEM of the differential microstructure created as a consequence of bacteria migration to the surface [20]. Scale bars for (b-c) are $20\mu m$.

Variations of the ink yield stress, the incubation time and percentage of mannitol added, which served as the carbon source for the bacteria, showed that these parameters could be used to effectively al-

ter the thickness of the cellulose's layer. Namely an increased yield stress allowed less bacteria to migrate from the oxygen depleted core region to the surface of the filament, causing a reduction in the thickness, while an increase in the mannitol percentage added to the print caused the thickness to increase. Similarly a longer incubation time allowed for the creation of a thicker cellulose film giving rise to a thickness of 1.5 mm after 6 days. It is important to note that while for both mannitol percentage and incubation time a positive effect on the cellulose thickness was observed, the extent was limited given that above a threshold of 2.5% with respect to the mannitol concentration and incubation times surpassing 6 days no further increases in the cellulose yield were detected. Crucially the depletion of oxygen as a function of print thickness and the subsequent lack of a bacterially formed cellulose network throughout the extruded structure was found to result in too low mechanical properties with the printed structure sacking under the influence of gravity after removal from the support matrix. This was in turn alleviated by immersion of the printed structure into a Calcium Chloride solution in order to allow for ionic cross-linking to occur between CNF's which was shown to nearly double the storage modulus of the material and allowed for it to hold its shape after removal from the gel bath.

While for the purpose of bio-medical applications the so achieved properties were deemed sufficient, direct extrapolation of this work for aerospace structural applications would not be possible, easily determined by comparing the storage modulus of the ionically crosslinked CNF/BC composite at 2kPa to that of a typical aerospace-grade polymer such as epoxy, which shows a value more than six-orders of magnitude higher at 3.5GPa.[23] As however outlined previously in section 2.1, these low mechanical properties are not caused by the inherent weakness of bacterial cellulose as a material but rather by their strong dependence on the level of hydration. Given that characterisation tests were carried out on hydrated samples, it can thus be inferred that a repeat of the mechanical testing with dried samples would yield in an increase in the mechanical performance, and as such would increase the competitiveness of the process for structural applications.

2.3.3. Summary of State of the Art

From the above state of the art research implementations of DIW and in-situ bacterial cellulose the following observations are made,

1. Ink formulations consist of three main components. Namely the bacteria stock, the nutrient source, and the rheological modifiers.
2. Higher print fidelity is achieved when increasing the amount of rheological modifiers in order to obtain inks with higher viscosity, yield strength and faster recovery
3. There is an inverse relationship between in-situ bacterial cellulose production and the viscosity of the ink used
4. Bacterial cellulose formation occurs exclusively close to the air-liquid interface, with the formed cellulose preventing oxygen penetration deeper than $200\mu m$

The conclusions which are drawn from these observations are thus two-fold. On the one hand the sole focus on bacterial cellulose overgrowth inadvertently gives rise to ink formulations with low shape retention capability's, which cannot be used to construct multi-layer parts. On the other hand, and despite optimising for bacterial cellulose growth, none of the above shown examples create structure of substantial integrity as a direct result of the bacterial cellulose only forming at the air-liquid interface, giving rise to a core-shell architecture as demonstrated by Shin et al.[20], whereas a thin film of cellulose covers a mostly liquid core.

Given these conclusions, any improvement on the process requires additional means of stabilising the core-shell microstructure created while furthermore shifting from solely focusing on the bacterial cellulose growth to a combination of bacterial cellulose growth and other stabilising mechanisms in order to allow for an ink formulation which lends itself to the printing of multi-layer structures.

2.4. Enhancing Bacterial Cellulose

While no previous work has been carried out to specifically enhance the in-situ grown bacterial cellulose network after extrusion of a living ink by using inorganic fillers, as proposed in the thesis work at hand, see chapter 3, there have been some studies on the general effect of incorporating inorganic fillers into

a bacterial cellulose network.

One such example is provided by the doctoral work of Yu[29], which placed extensive focus on increasing the mechanical performance of bacterial cellulose networks through different reinforcement techniques. Most notably, and relevant for the here presented work, is his study of bacterially induced mineralization of calcium carbonate crystals within a BC network after mechanical disintegration of it. Production of this material thus first requires the incubation of cellulose producing *G.hansenii* bacteria within a nutritional broth to produce a mm-thick cellulose pellicle followed by mechanical breakage of the cellulose network and infusion with a solution containing the calcium carbonate precipitating bacteria strain *S.pasteurii*.

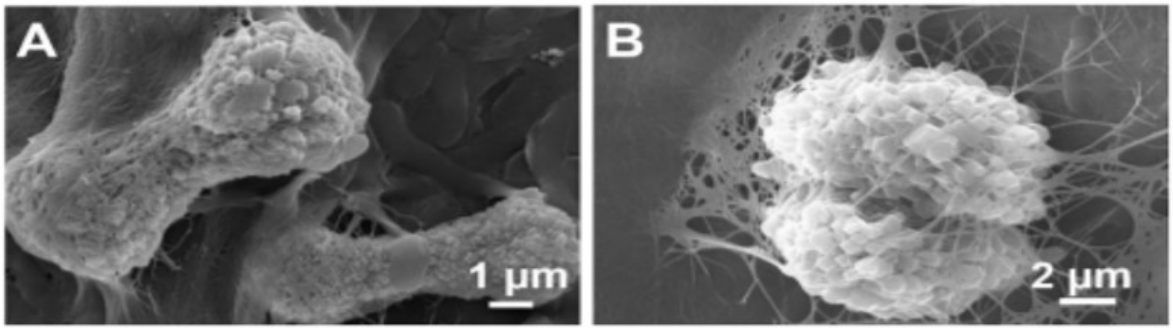

Figure 2.12: Entanglement of calcium carbonate crystals in the bacterial cellulose network[29].

Lastly self-assembly of the cellulose network with embedded calcium carbonate crystals was observed as a consequence of the air-drying step applied in order to decrease the water content in the cellulose. Mechanical testing of the so-produced material subsequently revealed that in general the insertion of calcium carbonate crystals into the cellulose network increased both elongation at break and toughness. Additional study of samples with varying calcium carbonate crystal sizes furthermore demonstrated an inverse dependency of the toughness increase on the average crystal diameter with samples of smaller embedded crystal diameters (12.5μm) showing a larger toughness increase than those with larger diameters of 110μm. The reason for this was attributed to the stress concentrations imposed on the cellulose network as a result of the insertion of larger particles into it.

Extrapolating the results of Yu[29], would thus suggest that the BC network posses the ability to entrap a brittle reinforcement phase and subsequently yields in a composite material with increased mechanical properties as compared to pure bacterial cellulose.

2.5. Outcome of the Literature Review

Based on this literature review, the conclusion is drawn that while current techniques of combining DIW with cellulose producing bacteria offer the ability to create patterns from living inks which allow for the in-situ formation of bacterial cellulose, as such increasing the shaping freedom compared to the more traditionally used static fermentation, the processes need to be improved upon to more fully utilise the outstanding properties of bacterial cellulose. To this end, three main gaps in the research field can be identified. First and foremost there is a lack of quantification on how crucial processing parameter such as ink viscosity and input nutrient volume effect the bacterial cellulose growth, which consequentially makes it impractical to assess the efficiency with which the formulated inks allow for bacterial cellulose formation. Next to this, there is a clear need to improve upon the current ink formulations to allow for multi-layer 3D printed parts. Lastly previous publications have put little focus on utilising the mechanical properties of the formed bacterial cellulose for structural applications, but rather have been concerned with the application of bacterial cellulose in its hydrated state for medical purposes, resulting in the sole focus on its hydrated properties. Resulting from this is thus the necessity to investigate how DIW with cellulose producing bacteria translates to the manufacture of structural components.

3

Research Definition

The thesis work will focus on the creation of a living ink, which combines in-situ bacterial cellulose growth with inorganic platelets to allow for the additive manufacture of 3D geometries of increased structural integrity. The research objective resulting from this, is further outlined in section 3.1, followed by the research questions derived from it in section 3.2, the scope which frames the research in section 3.3 and the main thesis hypothesis in section 3.4.

3.1. Research Objective

The objective of this research is to create and characterise a living ink suitable for direct ink writing which combines nutrients, cellulose producing bacteria and inorganic platelets in order to create 3D printed living structures on whichs surface the bacteria can survive, replicate and form a stabilising layer of bacterial cellulose.

Achieving this overarching goal first necessitates a study of how crucial ink formulation and growth conditions affect the bacterial cellulose yield which is necessary not only to optimise the ink formulation for the bacterial cellulose yield but also in order assess the efficiency with which nutrients are utilised by the bacteria during cellulose formation on top of the printed scaffold and to judge the effect of oxygen availability.

Next to establishing the ink formulation, it is imperative to demonstrate its printability and characterise the materials microstructure while furthermore assessing the underlying growth mechanism by establishing a nutrient diffusion model, followed by an assessment of how the bacterial cellulose film affects the mechanical properties of the produced BC based composite.

3.2. Research Questions

Based on the outlined research objective, the main research question which ought to be answered by the thesis work is:

"What improvements in geometric complexity and mechanical properties can be achieved by the in-situ bacterial cellulose growth on-top of a printed silicon dioxide platelet scaffold and what model can be developed to describe its growth dynamics?"

Note that the formulated main research question can subsequently be broken down into four distinct aspects, each characterised by their own sub-question.

1. How is the formation of bacterial cellulose by *G.hansenni* affected by the ink formulation and growth conditions?
2. What are improvements and limitations of the developed ink formulation?
3. What is the morphology of the microstructure and what model can be developed to describe its growth?

4. How does the overgrowth by bacterial cellulose reflect in the mechanical properties and how do these compare to bacterial cellulose produced using static fermentation?

3.3. Scope

In order to full fill the research objective and answer the associated research questions, the thesis work at hand does not only require aspects of material science and additive manufacturing but also has a biological facet, which requires some limitation in order to stay within the scope of an Aerospace Engineering MSc thesis. As a result the thesis work will be carried out in close collaboration with the Bionanoscience group at the Faculty of Applied Sciences of TU Delft, which will provide the cellulose producing bacteria strain (*G.hansenni*), as-well as the baseline ink formulation and printing procedure based on the work of Balasubramanian et al.[4], upon which the thesis presented here will iterate. Additionally the added inorganic platelets will be limited to silicon dioxide platelets (commercial named Soft Spheres), which are availlable through a collaboration with MERCK, while the added %wt will be limited to 4%wt in order to limit the number of variables to consider and ensure the thesis does not exceed the time-frame allocated.

3.4. Hypothesis

The main hypothesis of this research is that the addition of silicon dioxide platelets and fumed silica to a living ink can be utilised to act as a scaffold for in-situ bacterial cellulose growth which allows for the additive manufacture of 3-dimensional shapes giving rise to an increase in the achievable shaping freedom and micro-mechanical properties.

4

Investigating Bacterial Cellulose Formation

The primarily goal of this thesis is to investigate if the synergy of in-situ bacterial cellulose growth on top of a silicon dioxide scaffold can be used to stabilise a additively manufactured structure and impart it with improved mechanical properties while simultaneously increasing the geometric complexity attainable. In order to achieve this, the focus of this chapter is to establish how the ink formulation effects the bacterial cellulose yield while also determining the conversion factor to estimate its growth based on the input nutritional medium. Furthermore the effect of oxygen availability on the bacterial cellulose yield is investigated to define the oxygen conversion factor.

Given the above high level objectives it is thus crucial to first synthesise the appropriate parameters of interest which are established based on the requirements for the ink formulation in subsection 4.1.1, those of the estimation model in section 4.2 and those required to to analyse the effect of oxygen availability during growth in subsection 4.1.3. This is followed by a description of the methodology applied to all parameters tested in subsection 4.2.1, followed by a presentation of the results in section 4.3. The implications of these results for the ink formulation and model proposed are then discussed in subsection 4.4.2 & subsection 4.4.3 respectively, while the results of the oxygen availability experiment printing are discussed in subsection 4.4.4.

4.1. Variable Selection

4.1.1. Ink Formulation

As stated in the scope limitation, see section 3.3, the used ink formulation builds upon the work of Balasubramanian et al.[4], in which the use of a HS-based ink, supplemented with sodium alginate and printed onto agar showed promising results in terms of bacterial survivability and cellulose growth but crucially lacked the shape retention necessary to construct multi-layer structures. To improve on this, the iterated ink formulation presented here includes the addition of both fumed silica, which as outlined in subsection 2.3.1, increases the printability of the ink, while the addition of silicon dioxide platelets is proposed to yield in higher mechanical properties as compared to pure bacterial cellulose. Note that the latter is discussed in more detail in chapter 8. The resulting ink formulation is summarised below.

1. HS-medium (Basis)
2. Sodium Alginate
3. Fumed Silica
4. Silicon Dioxide Platelets
5. *G.hansenni* Glycerol Stock

To complete the above formulation it was subsequently necessary to define the concentrations of each of the components added to HS-medium which forms the basis of the ink formulation. In order to simplify this process, it was decided to use the same concentration of sodium alginate as in the work of

Balasubramanian et al.[4], while as explained in chapter 3, the %wt of the silicone dioxide is fixed to 4%wt. By simplifying the selection of the concentrations for sodium alginate and silicon dioxide, it was subsequently possible to optimise for the remaining parameters, which are the initial bacteria population size and fumed silica.

The rationale for investigating the effect of the initial population size, which is synonymously with the volume of *G.hansenii* glycerol stock added, on the bacterial cellulose yield was not only the observed lack of literature availlable on its effect and the need to select a value to use throughout the thesis but also the hypothesis that if the maximum bacteria capacity of a given growth medium was independent of the initial population size, increasing the initial density could lead to a redistribution of resource allocation away from replication and towards cellulose formation. As such the initial inoculation density defined the first parameter whichs effect on the bacterial cellulose yield was studied. The approach to determining its effect is schematically shown in Figure 4.1.

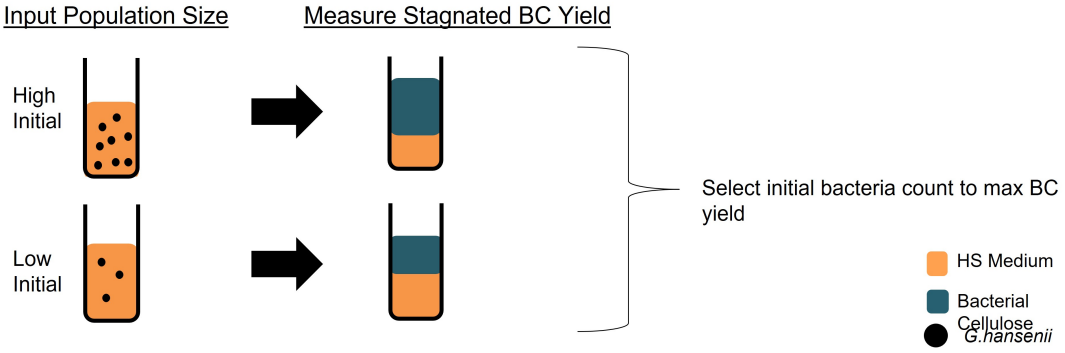

Figure 4.1: Schematic of the experimental setup for the inoculation density parametric study.

Next to the initial inoculation density, the effect of the fumed silica content on the bacterial cellulose yield was selected as a variable to study. The rational for this was its frequent usage in previous publications to increase the printability of living inks without a quantification of its effect on the bacterial cellulose yield being attempted. As a result fumed silica %wt was selected was a second variable to be studied by varying the amount added to a static growth medium and tracking the resulting bacterial cellulose yield. The general setup of the unit testing for this parameter is depicted in Figure 4.2.

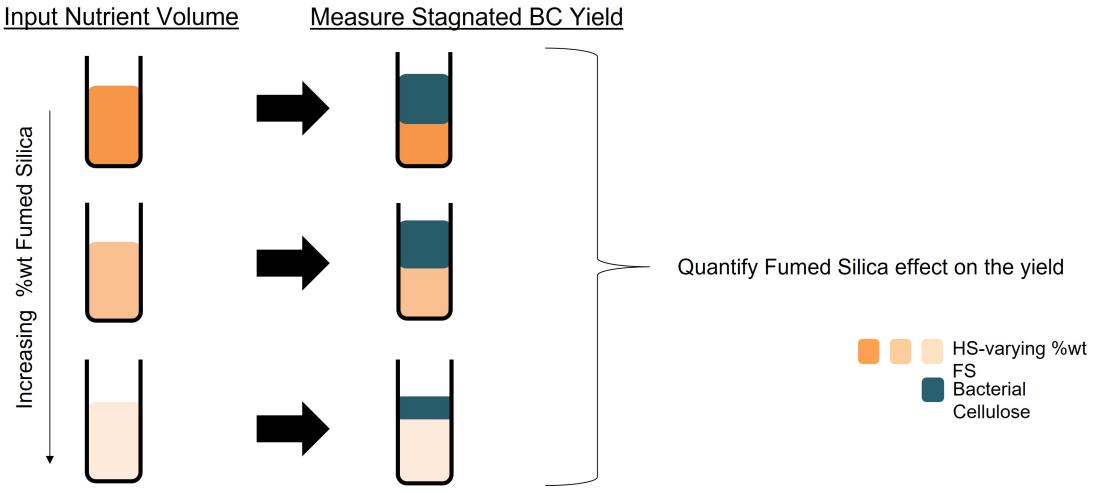

Figure 4.2: Schematic of the experimental setup for the fumed silica content parametric study.

4.1.2. Estimating Bacterial Cellulose Growth

Due to the novelty of the used ink formulation and the lack of previous work which provides quantification of the conversion factor from input nutrient (HS-medium) to bacterial cellulose within a living ink, it is imperative to quantify the conversion of nutrients to bacterial cellulose under ideal growth conditions, in order to extrapolate it towards understanding how efficiently the *G.hansenii* bacteria utilise the nutrients within the printed structure, Consequentially the second unit test experiment investigates how the volume of HS-medium supplied influences the bacterial cellulose yield, this is schematically shown in Figure 4.3.

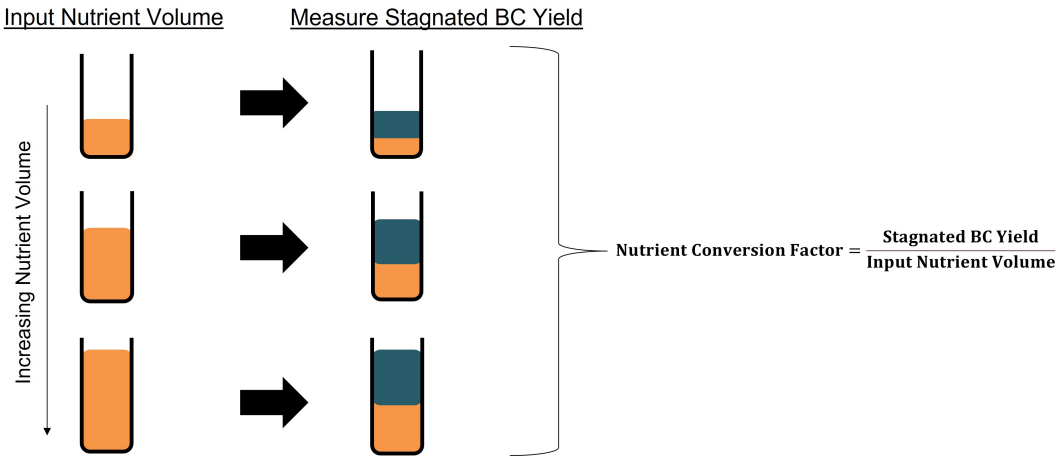

Figure 4.3: Schematic of the experimental setup for the nutrient supply parametric study.

4.1.3. Metabolism under Limited Oxygen Availability

Lastly, the effect of oxygen supply on the bacterial cellulose yield is investigated. The rationale for this is two fold, on the one hand the quantification closes a gap in literature, while on the other hand providing a basis to discuss the viability of extending the developed process and living ink to in-gel printing in chapter 10. As a consequence oxygen availability was selected as the third parameter to study in a manner that would allow for the limitation of the oxygen to a known amount such that the conversion factor could be calculated from the obtained bacterial cellulose yield, this is schematically depicted in Figure 4.4.

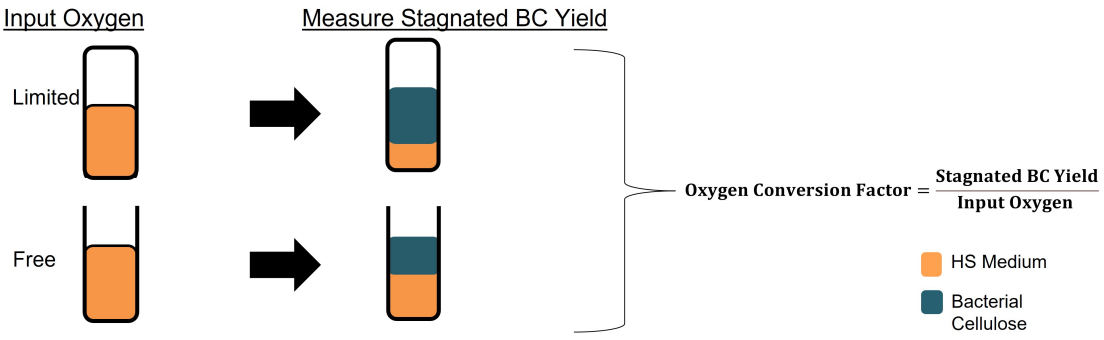

Figure 4.4: Schematic of the experimental setup for the oxygen limitation parametric study.

4.2. Methodology

This section outlines the overarching methodology and experimental setup applied to all of the four parameters selected. Note that the methodology is split inbetween aspects relating to the practical execution of the experiments and the post-processing steps applied to the obtained data.

4.2.1. Experimental Procedure

On a high level the procedure for each unit test is identical consisting of the same six steps, namely the sample preparation, the growth of cellulose in the sample under identical conditions except the controlled variation in the independent variable, the harvest of the cellulose pellicle and the subsequent determination of its hydrated (“wet”) mass, followed by its dehydration in an oven and the final dehydrated (“dry”)mass determination. These six steps are shown schematically in Figure 4.5. Here “Sample A” and “Sample B” are identical except for the controlled change of the independent variable, graphically depicted by their distinct colours. Note that for each time step additional “Type A” and “Type B” samples needed to be created. This is due to the fact that once harvested, dried and measured, the cellulose pellicle cannot simply be placed back into the growth medium to be propagated until the next timestep as all of the bacteria within it have been killed during the harvesting step.

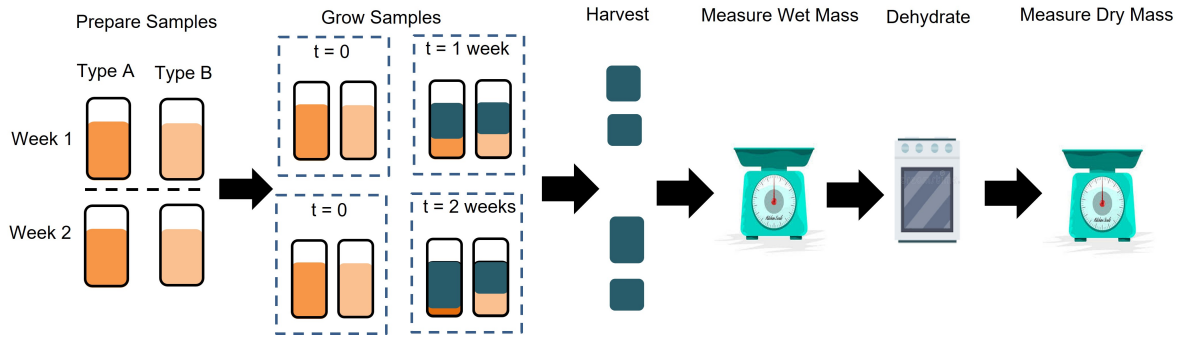

Figure 4.5: Schematic overview of the high level steps common to all parametric studies.

The following sections subsequently provide a more detailed breakdown for each of the high level steps depicted in Figure 4.5, starting with the sample preparation, followed by the sample growth & harvest, and finishing with the wet & dry mass determination.

Sample Preparation

All samples were prepared using the same standard HS medium formulation as a basis. In order to prepare the HS, first all dry ingredient were measured and subsequently mixed with distilled water using a magnetic stirrer. Stirring was continued until all dry ingridients had mixed with the distilled water and no lumps were visible after which the mixture was autoclaved in order to sterilise it. The so created HS-medium, as shown in Figure 4.6 (A), was then supplemented with the concentration of *G.hansenii* stock as required for each individual variable test and split into individual growth flask using an automatic electric pippet to dispense the amount appropriate for the given experiment, see Figure 4.6 (B). Lastly all samples, except the those which were required to be oxygen limited, were covered with parafilm into which 10 holes were punctured in order to allow for a sufficient aeration.

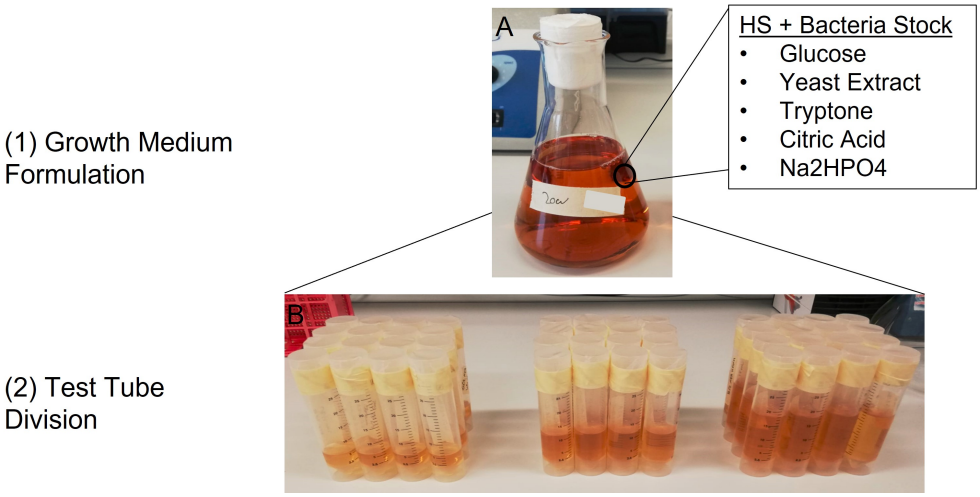

Figure 4.6: Division of autoclaved HS medium (A) into sample tubes for the parametric study (B).

Sample Growth & Harvest

Once created all samples were transported to the growth room located at TNW where they were left until harvested at a constant temperature of $30°C$ and controlled humidity. The samples were harvested by retrieving them from the growth room and removing the pellicle from the growth medium, after which it was washed in ethanol and submerged in distilled water to rinse it of any residue nutrient medium. The samples were left suspended in the distilled water for 2 days before replacing the water, followed by submersion for an additional two days in the freshly replenished distilled water. After this samples were considered sufficiently residue free for the measurement step. This process is summarised in Figure 4.8.

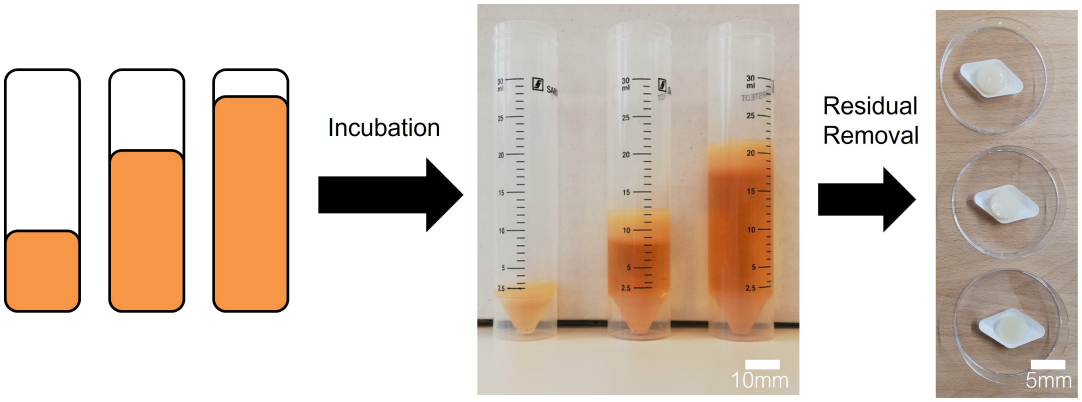

Figure 4.7: Three main steps of the sample growth and harvest, namely division of HS across the test tubes, incubation, and pellicle removal.

Wet & Dry Mass Determination

All mass measurements were carried out using a high precision scale. In order to ensure consistency in all measurements, the wet pellicle was removed from its water bath and directly transferred onto a plastic tray of known mass. The combination of tray and wet pellicle was then measured from which the wet mass of the bacterial cellulose is obtained by subtraction of the paper try mass. The plastic tray and bacterial cellulose pellicle were subsequently placed onto a open petri-dish which was stored in an oven at 50°C for 96hrs to ensure that all water had been removed from the bacterial cellulose pellicle . Hereafter the combined mass of paper tray and pellicle was once more measured from which the dry mass of the bacterial cellulose was obtained by subtraction of the paper tray mass.

Figure 4.8: Bacterial cellulose pellicle shown before(A), while(B) and after(C) drying.

4.2.2. Post-Processing & Growth Model

The so collected data was then post-processed according to the protocol below. Note that special attention is placed on the description of the trendline selection and the explanation of how growth stagnation is defined and applied in the thesis work at hand as this is crucial in determining the conversion factors.

Data Post-Processing

The raw data on the wet and dry mass yield as a function of growth conditions and time was post-processed in order to identify statistically significant trends. This was done by first calculating the average and standard deviation for the measured wet and dry bacterial cellulose mass for each variable level at each sampling point. Calculation of these was made possible by increasing the number of samples per variable level and sampling time from n=1 during an initial test run to n=4 in order to account for the variability observed in the bacterial cellulose yield which is attributed to minor discrepancies introduced in the sample preparation and growth steps. Note that while a higher number of samples per sampling interval per variable level was considered in order to increase the statistical significance of the results obtained, it was ultimately deemed too time-intensive given the objective of the thesis was focused more heavily on characterising the bacteria behaviour when applied to the direct ink writing processes rather then under static fermentation.

Trendline Selection & Growth Stagnation

Having established the average bacterial cellulose yield and standard deviation for each sampling point it was subsequently imperative to select an appropriate growth model which could be used to describe the observed bacterial cellulose yield. To this end a logistical growth model was used as it describes biological growth within a resource limited environment, which is the condition present within the growth flasks due to the purposeful limitation of nutrient supply and/or oxygen. As a result of accounting for this resource depletion, the logistical growth model shows a transition from exponential to linear and stagnated growth as vital resources within the environment are being exhausted. This behaviour can be observed in Figure 4.9, which shows the characteristic shape of a logistical growth curve, whereas the parameter A_2 quantifies the predicted maximum carrying capacity of the environment, while A_1 sets the starting population size, x_0 the growth time at which the growth rate is linear and p defines the exponential growth rate factor.

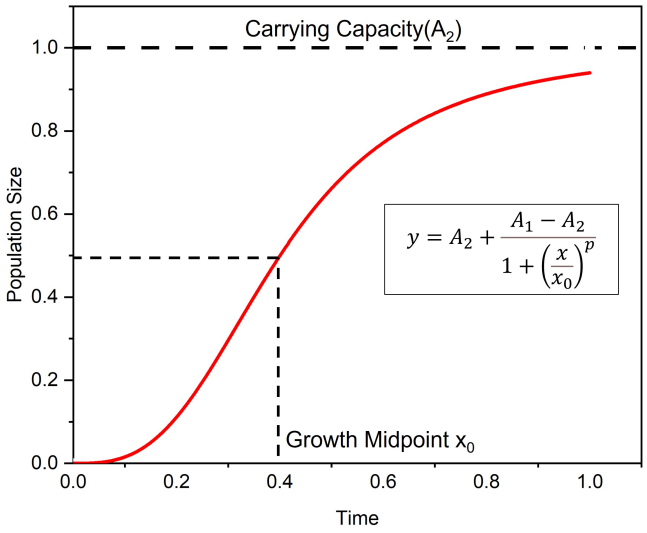

Figure 4.9: Biological growth modelled using a logistical function to predict exponential growth in a resource limited environment.

For all of three of the unit tests conducted, the predicted carrying capacity of the environment (A_2) is the crucial parameter as it defines the maximum bacterial cellulose output based on the input resources, which for the oxygen availability is the amount of oxygen enclosed within the growth flask while for the nutrient and inoculation density experiments it is the HS medium supplied. It is however important to note that the logistical growth model can only be applied and the carrying capacity accurately predicted if either the A_1, x_0, and p are known based on a deeper understanding of the biological growth mechanics or if the observed data shows growth stagnation. Given the focus of this thesis is not biological and in an effort to focus the work on the practicality of creating additively manufactured structures from a living ink, it was decided to neglect an investigation of the parameters describing the growth model, but rather establish growth stagnation and maximum carrying capacity from the observed data. Note that for the purposes of this thesis growth stagnation is said to have occurred if the maximum measured material yield at the final sampling point does not exceed that of the either one of the previous ones. As stated, this distinction is crucial as for growth conditions under which the BC yield does not show clear stagnation no accurate conclusion on the maximum carrying capacity(A2) value can be extrapolated. As a result the A2 values determined from the logistical growth model will only be used for further calculations if stagnation as defined here has occurred.

4.3. Results

The results of the inoculation density experiment executed based on the procedures discussed in subsection 4.2.1 are plotted in Figure 4.10, which displays the dry mass of the harvested bacterial cellulose (y-axis) as a function of growth time (x-axis) for samples inoculated with a higher density of bacteria stock $(300\mu l/100mL)$ and samples inoculated with a lower density of bacteria stock $(30\mu l/100mL)$.

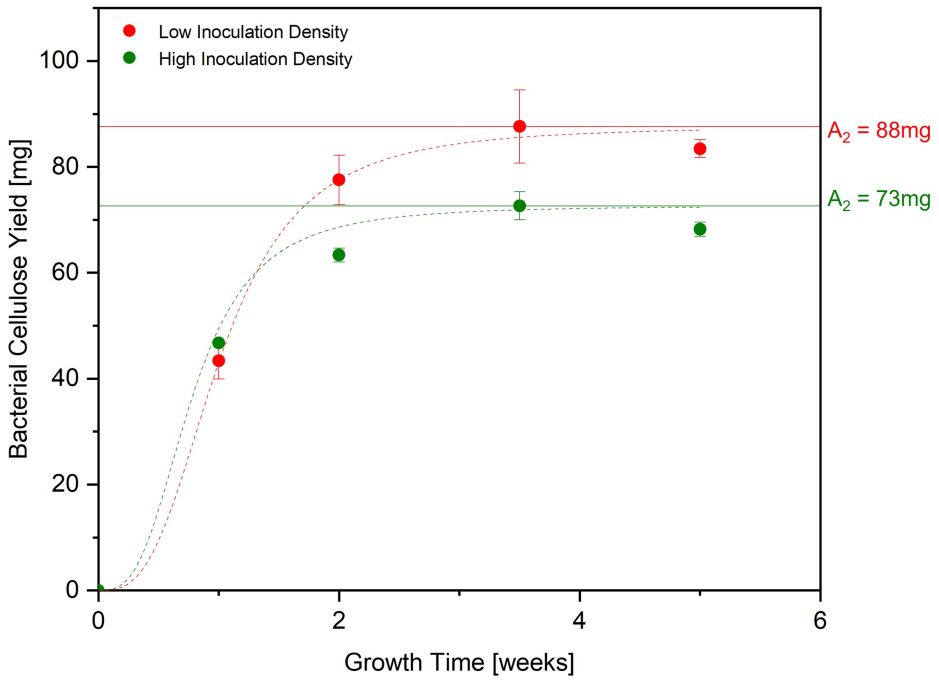

Figure 4.10: Results of the inoculation density experiment with sample size n=4.

The results of the fumed silica experiment, executed based on the procedures discussed in subsection 4.2.1, are plotted in Figure 4.11, which displays the dry mass of the harvested bacterial cellulose (y-axis) as a function of growth time (x-axis) for samples supplied with growth media containing 0%wt, 1.5%wt, 3%wt, 4.5%wt fumed silica.

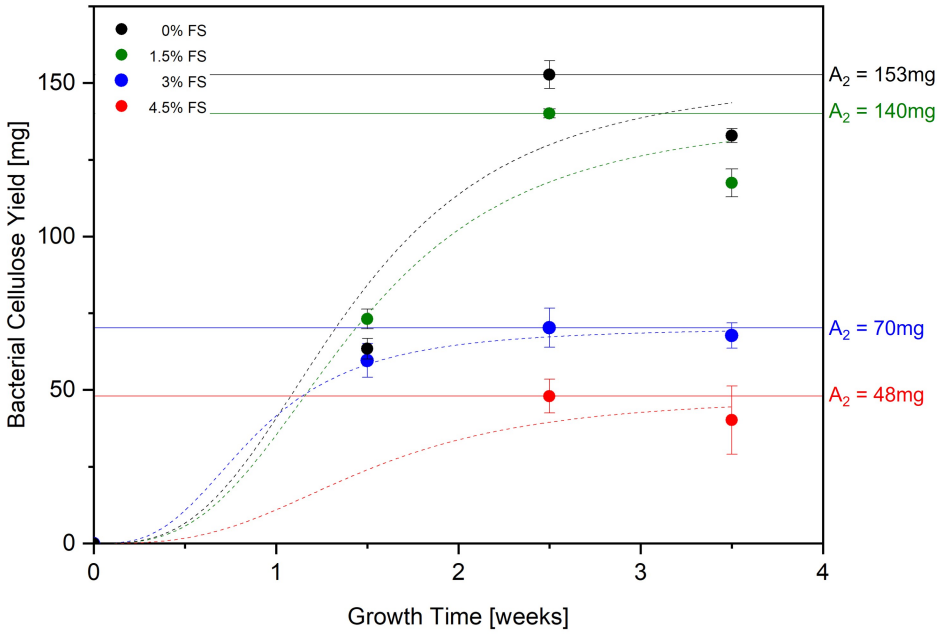

Figure 4.11: Results of the fumed silica experiment with sample size n=4.

Note that the bacterial cellulose yield for samples supplemented with the the highest amount of fumed silica (4.5%wt) could not be obtained for growth times of 1 and 2 weeks as no distinct pellicle was formed which made it infeasible to distinguish bacterial cellulose from growth medium.

The results of the nutrient supply experiment executed based on the procedure discussed in subsection 4.2.1 are plotted in Figure 4.12, which displays the dry mass of the harvested bacterial cellulose (y-axis) as a function of growth time (x-axis) for 6mL,12mL,18mL-of input nutrient medium. Note that the logistical growth function is only fitted to the data if growth stagnation occurs as defined in subsection 4.2.2.

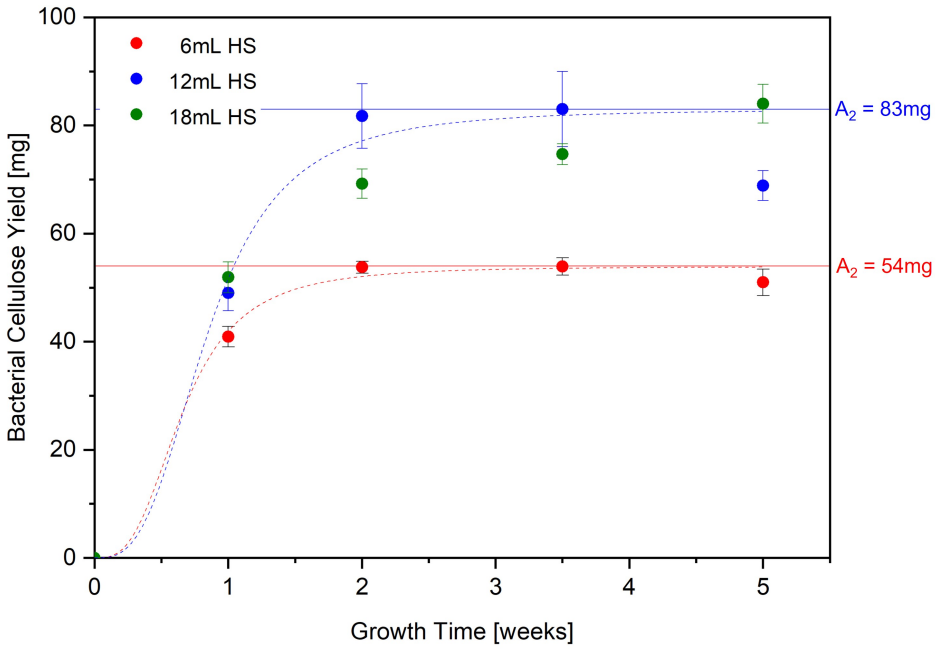

Figure 4.12: Results of the liquid nutrient volume experiment with sample size n=4.

The results of the oxygen limitation experiment executed based on the procedures discussed in subsection 4.2.1 are plotted in Figure 4.13, which displays the dry mass of the harvested bacterial cellulose (y-axis) as a function of growth time (x-axis) for oxygen unlimited and limited samples. Note that the logistical growth function is only fitted to the data if growth stagnation occurs as defined in subsection 4.2.2.

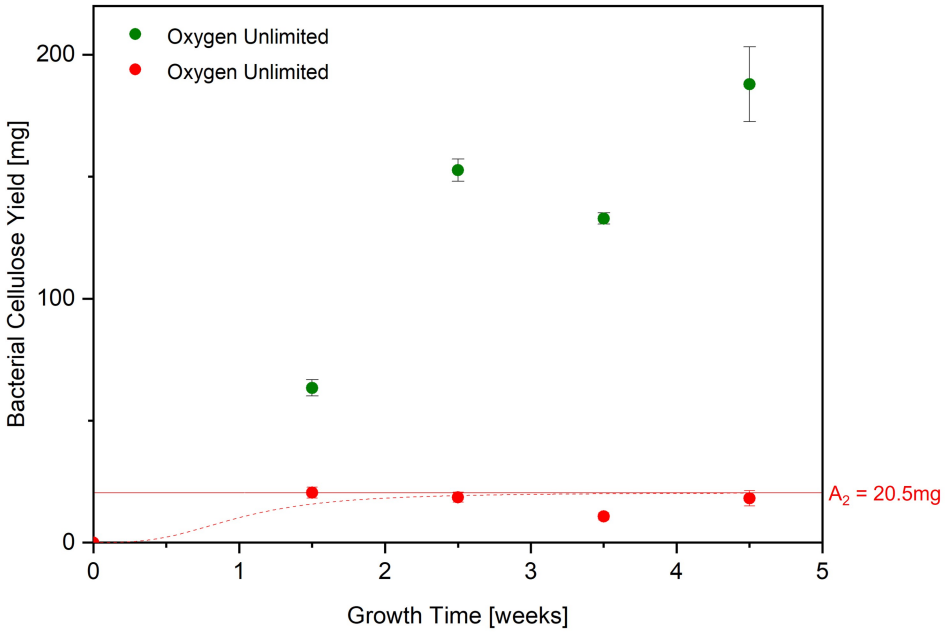

Figure 4.13: Results of the oxygen availability experiment with sample size n=4.

4.4. Discussion

The results are subsequently discussed based on their applicability to the ink formulation, growth prediction and oxygen conversion in subsection 4.4.2,subsection 4.4.3, and subsection 4.4.4 respectively.

4.4.1. Determining the *G.hansenii* Glycerol Stock Concentration

The parameter of interest for the ink formulation is the inoculation density as the hypothesis is made that the bacterial cellulose yield can be maximised by using a higher concentration of bacteria stock, which is synonymous with a higher initial bacteria population size.

Previous to drawing a conclusion on this hypothesis, it is however first important to establish that the results as plotted in Figure 4.10 show growth stagnation. This can be confirmed based on the definition established in subsection 4.2.2 as for both the bacterial cellulose yield for samples of high and low initial inoculation do not increase further after 5 growth weeks as compared to 3.5 growth weeks. As a result the conclusion is drawn that the resources availlable to the samples have been depleted to a point which allows for no further growth to occur such that the A_2 values, as noted in Figure 4.10, and obtained from the logistical curve fitted to the datapoints can be used. Having established this, it is subsequently possible to compare the effect of initial inoculation density on the bacterial cellulose yield which exposes, that while the difference in bacterial cellulose yield is relatively small, given the factor 10x variation in the input inoculation density, it is nonetheless contrary to the hypothesised effect such that a lower inoculation density yields in a 1.15x higher bacterial cellulose yield, 87.6mg and 72.6mg respectively. In other words having a smaller initial bacteria population size gives rises to a higher conversion efficiency of HS-medium to bacterial cellulose.

Note that while defining the origin for the observed reduction of bacterial cellulose yield as the inital population density increases, lies outside the scope of this thesis, the hypothesis is made that this may be due to the magnitude of the initial population size causing a shift in the distribution of resources used for replication and cellulose metabolism such that the obtained bacterial cellulose has a different distribution of bacteria to cellulose causing a difference in the measured dry mass. Despite of this, the above results can used to define the concentration of the *G.hansenii* glycerol stock, as the origin is of little concern for the ink formulation which is solely driven by the maximisation of bacterial cellulose yield such that the lower value of $30uL/100ml$ is used.

1. HS-medium (Basis)
2. Sodium Alginate [5% (w/v)]
3. Fumed Silica
4. Silicon Dioxide Platelets [4%wt]
5. *G.hansenii* Glycerol Stock [$30uL/100ml$]

4.4.2. Completing the Ink Formulation

The results of the fumed silica experiment can now be analysed in order to establish the %wt fumed silica. These show that while all four growth cultures exhibit growth stagnation according to the criteria defined in subsection 4.2.2, a significant difference in the magnitude at which said stagnation occurs can be observed. For samples incubated in a growth solution with 1.5%wt fumed silica added, the growth stagnation occurred at a average bacterial cellulose yield of 130mg, while for samples which had 3%wt fumed silica added a reduction by a factor of 1.9 to 68.5mg is observed. A further reduction can be observed when the fumed silica is increased by a factor of 2 to 4.5%wt whereas the bacterial cellulose yield dropped to 48mg, which represents a further decrease by a factor of 1.4x. These results clearly indicate that an increase in the %wt fumed silica, which increases the viscosity of the growth media, leads to a decrease in the conversion of the nutrients contained in the growth media to bacterial cellulose. Note that this trend has previously been observed [18][4], however this research is the first to attempt a quantification of this inverse relationship, with previous publications on this topic resorting to qualitative means such as cellulose staining[18], to visually observe the variation in cellulose growth. Said quantified fumed silica reduction rate can be obtained when plotting the average stagnated bacterial cellulose yield for each of the varying amounts of %wt fumed silica growth media and normalising it with the optimal, that is the static growth culture with 0% fumed silica added. This is shown in Figure 4.14 were a linear trendline is fitted to describe the observed correlation. The slope of this trendline

in turn is equivalent to the fumed silica reduction rate such that its magnitude is found to be -0.13, that is a 13%reduction in bacterial cellulose yield per 1%wt increase in the fumed silica content within the growth medium.

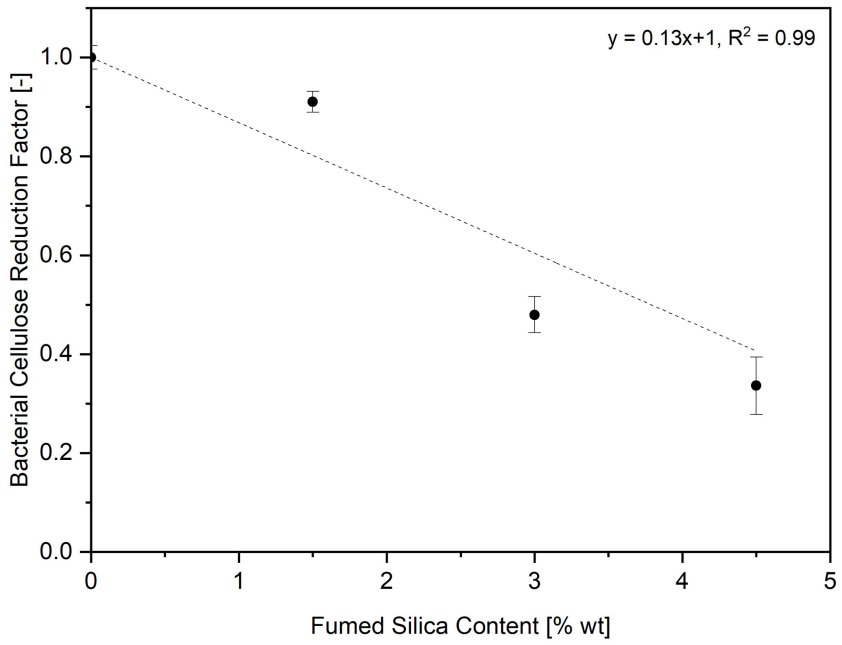

Figure 4.14: Bacterial cellulose formation as a function of fumed silica content.

As a consequence of the found significant reduction of the bacterial cellulose yield as a function of fumed silica added it was thus decided that the %wt of fumed silica added should be minimised in order to keep the ink rheology as close as possible to that of unaltered HS-growth medium. In accordance with this conclusion, the %wt of fumed silica was found by determining the minimal amount which yielded in an ink that could be used to create multi-layer structures without distortion or platelet sagging after extrusion by employing a trial and error process. The resulting ink formulation based on the inoculation density and fumed silica experiment which was used for the remainder of the thesis work is shown below.

1. HS-medium (Basis)
2. Sodium Alginate [5% (w/v)]
3. Fumed Silica [4%wt]
4. Silicon Dioxide Platelets [4%wt]
5. *G.hansenii* Glycerol Stock [$30\mu l/100mL$]

4.4.3. Nutrient Conversion Factor for Yield Prediction

The results presented in Figure 4.12, show that during the initial part of the growth, between the preparation and first sampling point after 1 week, the bacteria in each sample forms a similar amount of bacterial cellulose indicating that its growth is independent of the supplied growth medium and that all HS-media still provides sufficient resources to the bacteria. The same observation can however no longer be made after the second growth week whereas the growth rate of the samples supplied with 6mL of HS solution significantly reduces as compared to its growth rate within the first week and that of the 12mL and 18ml samples within the second growth week with the lack of further growth over the course of the remaining 3 weeks being symptomatic of resource depletion within the provided 6mL HS medium. A similar trend but delayed by 1.5 weeks can be observed for samples supplied with 12mL of growth medium, which show no further bacterial cellulose formation after 3.5 weeks, stagnating at a value of 84mg of bacterial cellulose compared to 54mg for the samples supplied with 6mL growth medium. Lastly the samples supplied with 18mL nutrients cannot be said to have depleted the nutrients within the growth medium as a further bacterial cellulose yield is found between a growth time of

4-5weeks however at a significantly reduced linear growth rate.

Given that the samples supplied with 18mL of HS medium do show further bacterial cellulose growth up until the last sampling point of 5-weeks, the conclusion is not supported that the resources within the HS-medium have been depleted by the bacteria in order to replicate and form bacterial cellulose, based on the definition established in subsection 4.2.2. Consequentially it is not possible to determine the liquid HS medium input to dry bacterial cellulose output, also referred to as the nutrient conversion factor, as it is unclear if the further bacterial cellulose growth, which is synonymous with a further conversion of nutrients to bacterial cellulose, would occur if the samples supplied with 18mL of HS medium would be observed over a longer growth period than 5-weeks. As a result, Figure 4.15 plots only the conversion ratio of the 6mL & 12mL samples which is obtained by dividing the measured bacterial cellulose yield by the input HS volume, while negating the results of the samples provided with 18mL of HS.

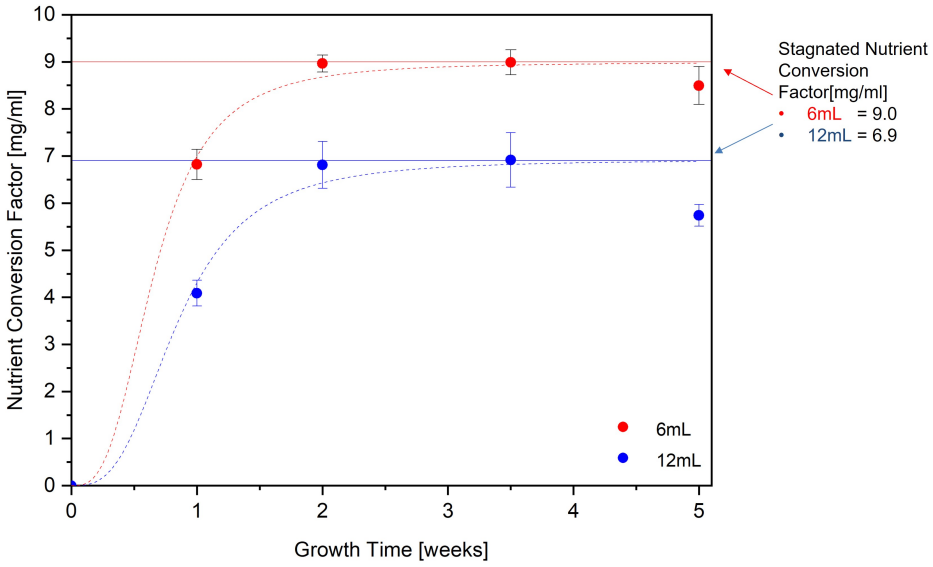

Figure 4.15: Nutrient conversion factor as a function of growth time for static cultures supplemented with 6mL & 12mL.

The above plot shows that while the growth in both the 6mL and 12mL solution samples has stagnated, the 6mL sample shows a 1.3x higher nutrient to bacterial cellulose conversion factor than that of the 12mL solution samples, 9.0mg of BC per mL HS and 6.9mg of BC per mL of HS respectively. The reason for the growth stagnation of the 12mL solution growth cultures at conversion ratio less than that shown possible by the 6mL samples is hypothesised to lie within the pellicle thickness. The rationale behind this, is that in order to replicate and metabolise cellulose the bacteria require both diffusion of nutrients from the HS solution and oxygen primarily from the surrounding air. Given this growth occurs at the interface between the cellulose and the ambient air[10], and that cellulose itself acts as a diffusion barrier[21], it is hypothesised that as the pellicle grows in thickness it increasingly inhibits the flow of nutrients to the active bacteria in the aerobic region and as such may define an upper threshold on the bacterial cellulose yield specific to the diameter of the growth flask. The distribution of aerobic and anaerobic zones within the growth of a cellulose pellicle is shown in Figure 4.16.

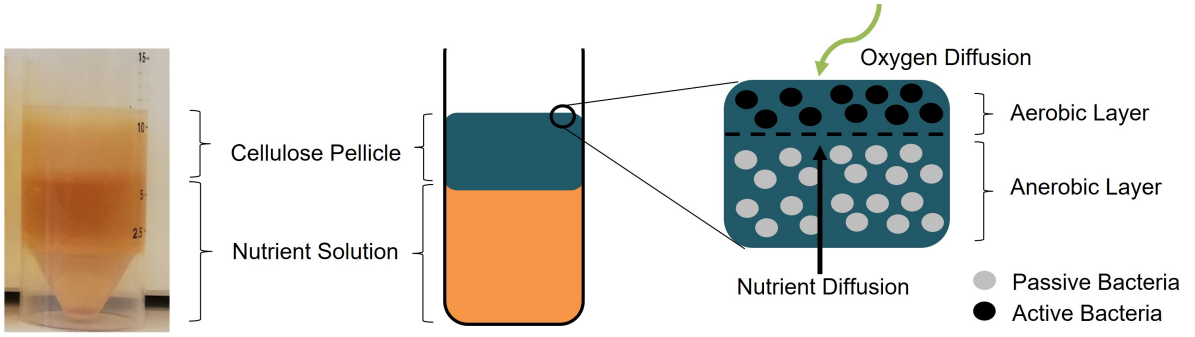

Figure 4.16: Visualisation of bacterial cellulose formation in a static growth culture, emphasising the limitation of the bacterial activity to the aerobic region.

While this is intriguing from a biological perspective, it does not have any practical implications for the thesis work at hand as the cellulose films which can be created from the nutrients within the printed scaffold does so under substantially contrasting growth conditions, such that the hypothesised pellicle thickness effect is deemed inconsequential. Furthermore the clear stagnation of the 6mL nutrient solution sample at a pellicle thickness smaller than the hypothesised critical pellicle thickness of the 12ml samples, over multiple weeks, means that the nutrient conversion factor calculated from its stagnated bacterial cellulose yield, will be used to predict the bacterial cellulose growth from a given volume of input HS-medium. This process is schematically shown in Figure 4.17.

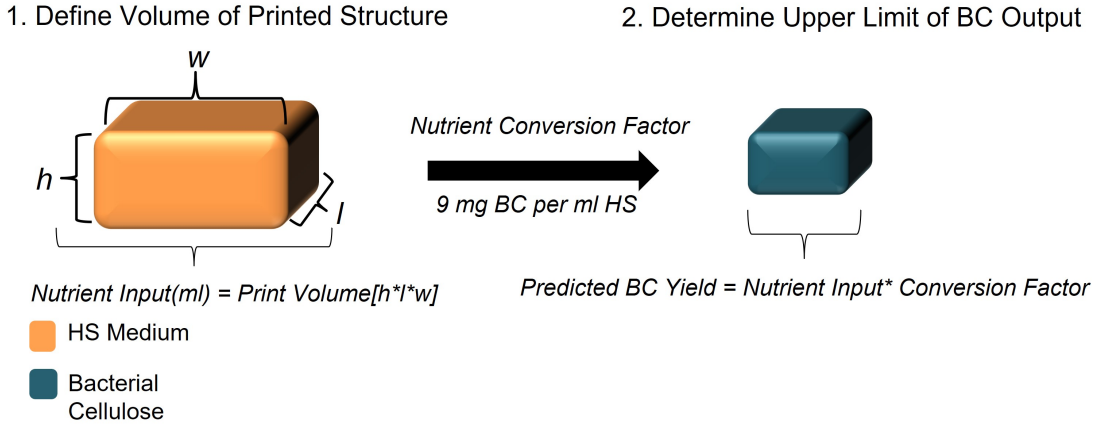

Figure 4.17: Application of the nutrient conversion factor to predict bacterial cellulose yield as a function of input nutrients.

This model is subsequently applied in chapter 7 to to judge the efficiency of the bacterial cellulose film formation on-top of the printed scaffolds.

4.4.4. Oxygen Conversion Factor

The results obtained from the oxygen availability experiment as plotted in Figure 4.13, show that limiting the oxygen supply to the samples has a severe effect on the bacterial cellulose formation by *G.hansenni* within the growth medium, showing a reduction by a factor of 3 after the first 1.5 weeks of growth and by a factor of 23 after 5.5 weeks of growth. This exponential increase in the reduction factor between the first 1.5 and the final 5.5 growth weeks is due to the lack of further bacterial cellulose formation within the oxygen limited samples which, after reaching a value of 5.08mg, show no further increase, while the oxygen unlimited samples undergo exponential and linear growth phases, reaching a average yield of 187.9 mg after 5.5 weeks. The lack of any further bacterial cellulose formation in the oxygen limited samples indicates that the bacteria within these samples have used up the availlable oxygen to an extent which does not allow for further reproduction or cellulose metabolism. As a result the samples are considered to have reached the maximum carrying capacity of their environment, as defined in subsection 4.2.2, due to a resource limitation in the form of a too low oxygen concentration.

Note that this result in turn verifies the initial assumption of sufficient sealing as outlined in subsection 4.4.4, as an improper sealing would have resulted in further bacterial cellulose growth of the oxygen limited samples such that the yield would have approached that of the oxygen unlimited samples rather than stagnating at a lower value, as observed. Given the outlined verification of the sample seals, the observed stagnation value of 5.08 mg can be used to estimate the conversion efficiency of oxygen input to bacterial cellulose output.

To calculate this, it is first required to establish the initial oxygen content within the sealed samples which can be calculated from the known volumes of air (25mL) and nutrient medium (15mL) within each test tube in combination with the oxygen concentration saturation values of air at room temperature & sea level pressure as-well as water like liquids, which are approximately 285mg/L[8] and 8mg/L[8] respectively. The so calculate oxygen input value of 7.12 mg is then divided by the found bacterial cellulose carrying capacity of the oxygen limited samples to determine the oxygen conversion factor of 0.71 mg of bacterial cellulose yield per mg of oxygen made available during growth. This calculation is schematically shown in Figure 4.18.

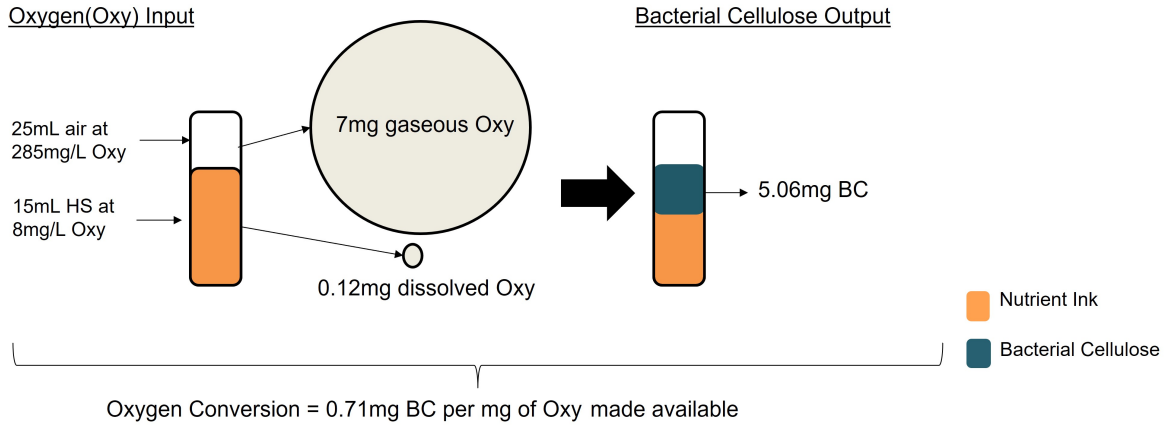

Figure 4.18: Calculation of the oxygen conversion factor from the encapsulated oxygen within each test tube and the stagnated bacterial cellulose yield.

The so-obtained oxygen conversion factor of $0.71 mg BC / mg O$ subsequently highlights the importance of maintaining a constant flow of fresh oxygen to the bacteria during fermentation due to the small BC yield obtained when solely relying on oxygen previously contained in the growth medium and overhead air. It further highlights that relying on the amount of dissolved oxygen within a liquid is not feasible due to the combination of low oxygen saturation of liquids and the low conversion factor. Lastly this quantification of the oxygen conversion factor may be applied for future iterations of the process as outlined in chapter 10.

5

Printing Methodology

The methodology developed in order to manufacture printed structures using the living ink as formulated in chapter 4 and repeated below, is described here. Note that this methodology is applied throughout chapter 7,chapter 8 and chapter 6, to manufacture all samples for analysis. On a high level the procedure can be split into the making of the agar and ink which is outlined in section 5.1 & section 5.2 respectively, followed by the printing of the living ink, which is described in section 5.3 and the BC growth on the surface of the printed structure followed by its drying, which is outlined in section 5.4.

5.1. Agar Preparation

The first step in the manufacturing methodology was the preparation of the agar plates onto which the living ink was later printed. These were prepared ahead of time as they could be easily stored and retrieved. The procedure followed first required the preparation of HS-growth medium which forms the liquid component of the agar. For each batch,the amount of HS required differed as it depended on the number of agar plates desired, with each petri-dish sized agar plate requiring approximately 20mL of solution. As a result of the varying total volume, all dry ingridients are given in terms of their respective concentrations rather than absolute values. Once the appropriate HS-growth medium was mixed and sterilised, agar and calcium chloride powder were weighted, at a concentration of 1%(w/v) and 0.05M respectively, and added to the HS-growth medium. The resulting HS-agar-CaCl2 solution was subsequently mixed using a magnetic stirrer at 400rpm for 3 minutes in order to obtain a homogeneous viscous liquid. This solution was then brought to a boil in order to sterilise it before letting it cool down to 50°C such that it could be poured into petri-dishes in which it was left cool down to room temperature and solidify. The so prepared agar dishes were subsequently stored at 5°C until the were required for printing.

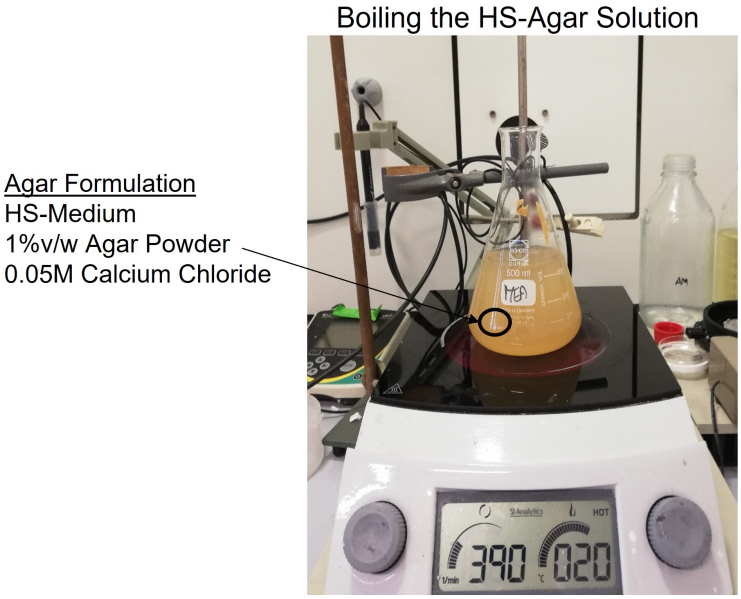

Figure 5.1: Composition of the agar solution and its sterilisation by boiling

5.2. Ink Synthesis

As shown in the ink formulation the basis of the ink is made up of a mixture of HS-medium and sodium alginate at a concentration of 5% (w/v). Consequentially the first step in making the ink was to prepare HS-growth medium, into which sodium alginate powder was mixed using a magnetic stirrer at 500rpm for 15 minutes. The so fabricated HS-Sod.Alg solution was subsequently autoclaved to sterilise it before it was used further in the ink making procedure. Note that while the HS-Sod.Alg solution was prepared 1L at a time, each syringe only required 12mL of ink such that only one batch needed to be created for all samples analysed as part of this thesis. The volume of ink created at a time was in turn dependent on how many syringes where required for the number of parts to be printed such that the procedure below is given in terms of concentrations rather than specific volumes/weights as these varied.

Once the HS-Sod.Alg solution was prepared, the next step was to weight the dry ingridients at a concentration of 4%wt fumed silica and 4%wt silicon dioxide. The dry ingridients were subsequently combined with the HS-Sod.Alg solution in sterilised plastic cup and homogenised using a planetary speed mixer at 3500rpm for 5 minutes which resulted in a smooth silky paste.

This paste was then inoculated with *G.hansenii* glycerol stock at a concentration of $30\mu l/100mL$ using a micropipet after which it was mixed by hand using a sterilised metallic spatula. Note that the choice was made to mix the ink by hand instead of using the speed mixer to prevent excessive shear forces acting on the bacteria. The so-inoculated ink was then filled into the appropriate number of 12mL syringes which could then be used for printing.

5.3. Printing Process

As stated in chapter 2, DIW was selected as a printing process given its compatibility with living inks due to the low pressure and temperatures required in combination with its simplicity. For the purpose of this thesis, a low cost DIW setup was build by replacing the stock FDM printhead of an Ultimaker 2+ with a custom build DIW printhead which was sized in order to allow for easy mounting and dismounting of various syringe sizes. The working principle of this printhead is purposefully kept simple, such that the rotation of the 12V stepper motor is transformed into linear movement by a threaded rod which applies pressure to the syringe through the plunger pusher. The pressure imbalance so created causes the ink to flow out of the nozzle at a rate proportional to the input stepper motor rotation. Thus the stepper motor rotation, which can be controlled via g-code, determines the rate of material deposition while the

x,y,z motors of the stock printer, which are similarly controlled via g-code determine the movement of the printhead. Combining the g-code with the printer setup thus allows for the deposition of living inks in any pre-determined shape only limited by the print volume and ink rheology.

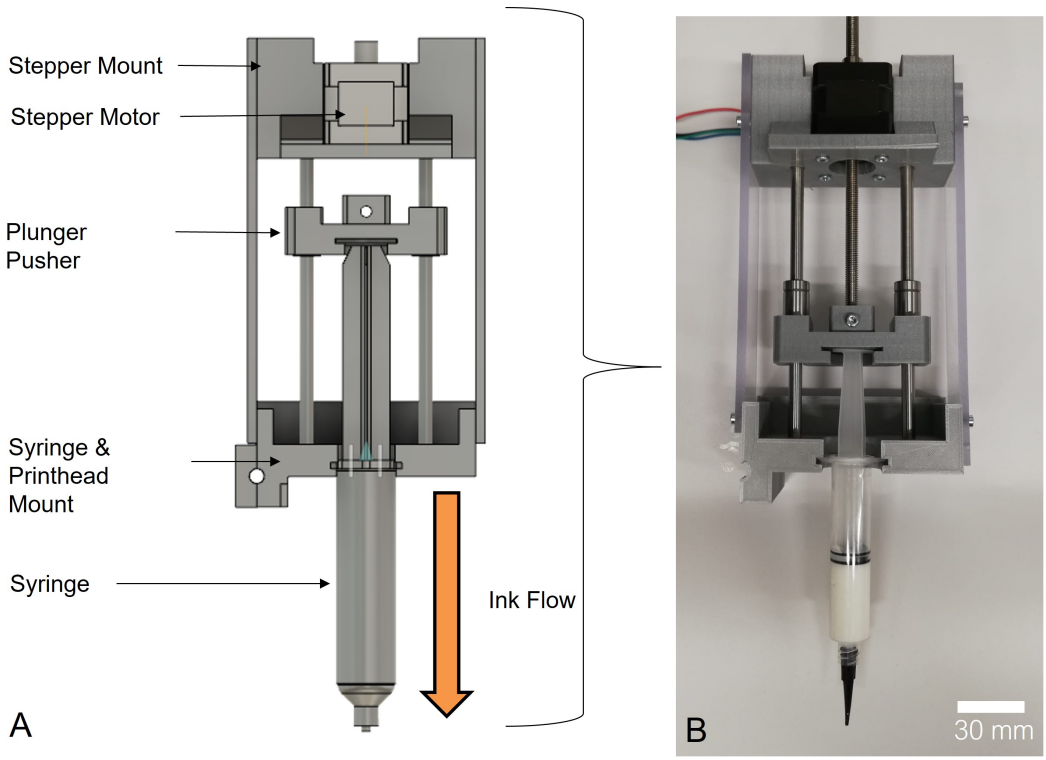

Figure 5.2: Self-build DIW setup as designed (A), and implemented (B)

The procedure applied for all prints thus first required the formulation of the appropriate g-code commands which described the desired geometries. For this grasshopper, a plugin for the rhino software was used, as its graphical user interface allows for simple parametric modelling. G-codes were generated based on three steps. First the geometry was defined as a point cloud matrix, with the the print path being defined by the order of the points. Once the geometry was defined, the extrusion volume required between every two points was calculated assuming a filament diameter equal to that of the nozzle size and the know distance between two subsequent points. The g-code was subsequently put together by combining the X,Y,Z coordinates of each point with the respective extrusion volume required to deposit filament when moving inbetween them.

Once the g-codes were generated, it was subsequently necessary to calibrate the z-offset of the 0.84 nozzle attached to the syringes w.r.t to the surface agar plates which were retrieved from the 5° storage shortly before printing and taped to the print-bed of the Ultimaker. Calibration was carried out using the stock z-offset calibration tool of the Ultimaker 2+, whereas the nozzle was lowered until it came into contact with the agar plate after which is was raised 0.4mm. Once the calibration was complete, printing was carried out by execution desired g-code file, an example of which is shown in Figure 5.3, where the layer by layer buildup of a sample plate is depicted.

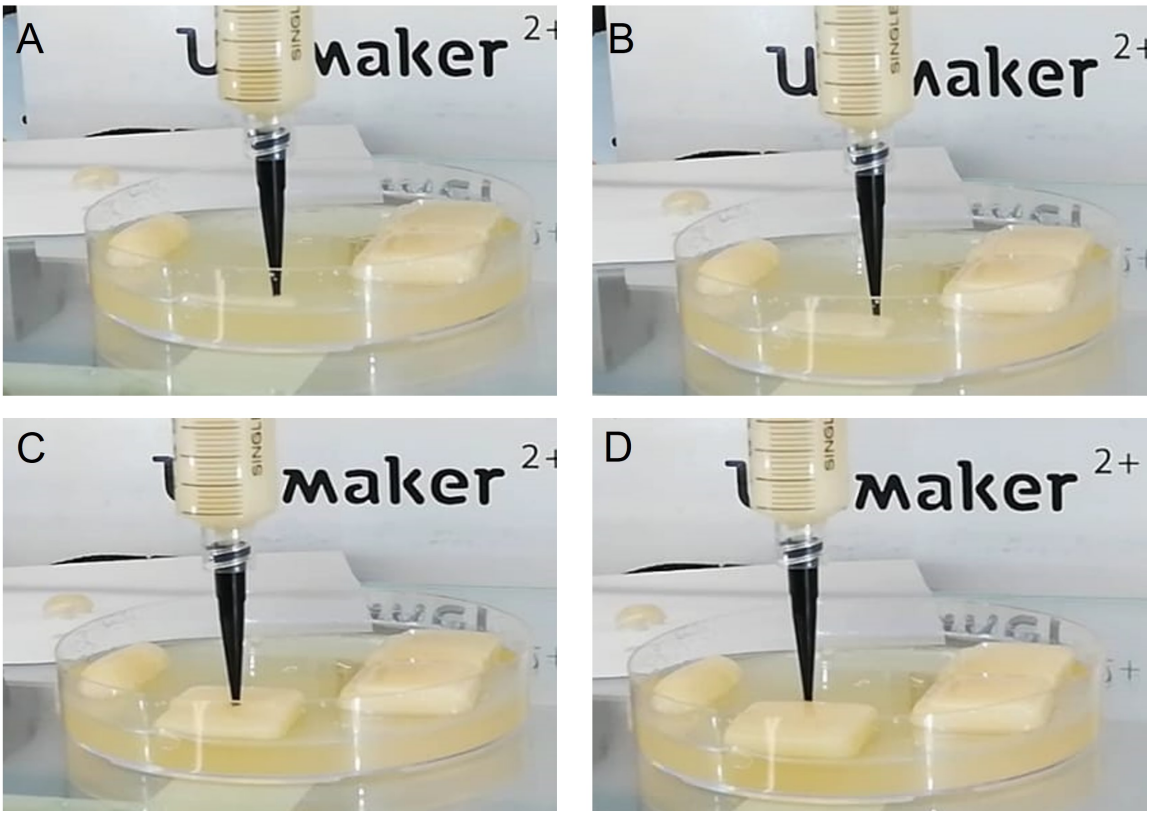

Figure 5.3: Images (A-D) show the progressive buildup of a three layer sample plate utilising the DIW setup

5.4. Growth & Drying

Once extruded onto the agar, the so created living structures were incubated in a temperature controlled growth chamber. Here the samples remained during their growth phase in a sterile environment at a constant temperature of 30°C and high humidity to allow the *G.hansenii* bacteria on the surface of the samples to utilise the nutrients within the ink to synthesise bacterial cellulose. An example of this overgrowth is shown in Figure 5.4, which depicts individual filament lines as printed compared to after incubation for 5 days. Clearly visible is the formation of white bacterial cellulose film on the surface of the filament lines after the growth period in image (B).

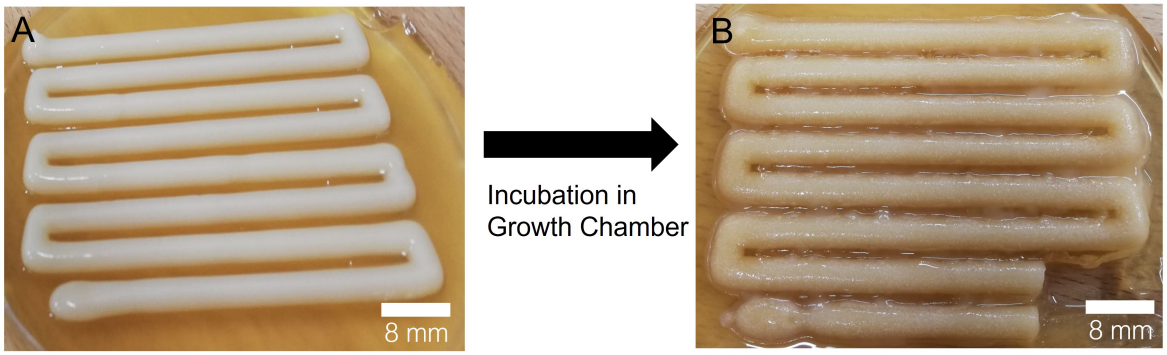

Figure 5.4: Ink scaffold before (A), and after overgrowth (B)

Samples were kept in this environment between 2 and 10 days depending on the growth regiment required after which the overgrown structures were peeled of the agar and placed on a petri-dish. Depending on the geometry created the samples were either directly dried within an oven at 50°C for 96hrs or in the case of flat geometries covered by a layer of peel-ply which was taped to the sides of

the petri-dish in order to clamp the structure down during drying which was found to prevent upwards warping as a consequence of differential shrinking during drying, further discussed in section 10.1. The impact of this final step is shown in Figure 5.5, where overgrown structures are shown before and after drying.

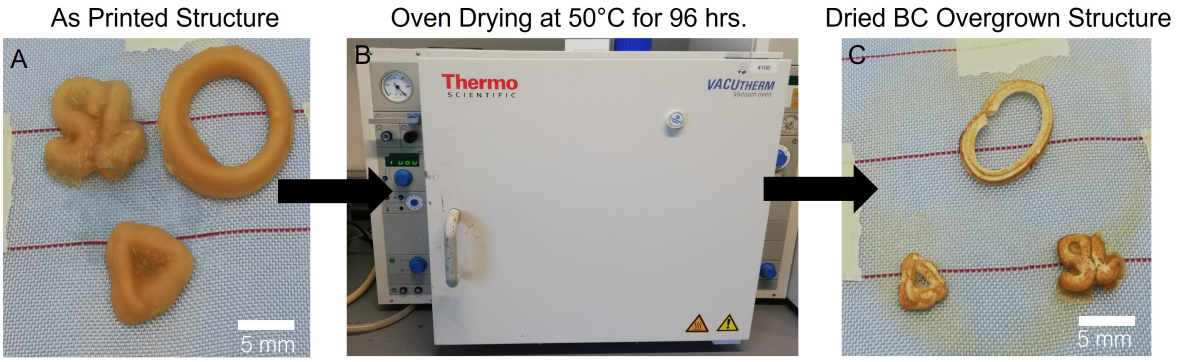

Figure 5.5: Overgrown hydrogel scaffold before (A) and after drying (C)

6

Printability

The developed manufacturing process described in chapter 5 was subsequently used to construct a range of geometries to determine both the improvements achieved by the here proposed ink while simultaneously gaining an understanding of the limitations of the process. As such this chapter first considers the improvements made in section 6.1, followed by an assessment of the limitations introduced as a consequence of the high shrinkage rate of BC in section 10.1.

6.1. Advances in Geometric Complexity

The objective of this section is to highlight the increases in shaping freedom achieved by the here developed ink formulation in order to verify the first aspect of the main research hypothesis, namely that the combination of reinforcing filler in the form of silicon dioxide platelets and fumed silica leads to an ink with higher shaping freedom, which can nonetheless be overgrown with BC.

Said improvements in printability are most clearly note-able when directly contrasting the structures created using the here developed ink formulation & process to those possible using the previous iteration ink formulation as developed by Balasubramanian et al.[4]. While the ink formulation without fumed silica and silicon dioxide platelets could be successfully used to create patterns on agar plates which were stabilised by the gellation of sodium alginate component of the ink, this gellation did require the diffusion of calcium chloride from the agar substrate throughout the ink limiting the maximum thickness achievable to $400\mu m$-$600\mu m$.

This is exemplary of the inherent trade-off at the heart of creating additively manufacturing structures stabilised by in-situ bacterial cellulose growth, similarly encounter by the works of Schaffner et al.[18], whereas the low conversion ratio from HS-medium input to bacterial cellulose yield requires the use of low viscosity inks, which results in inks of marginal printability, while nonetheless giving rise to a microstructure that provides little structural integrity as it is composed mostly of a liquid core held in place by a thin bacterial cellulose film as demonstrated by Shin et al.[20]

In contrast to the solution developed by the work of Balasubramanian et al.[4] to overcome this problem, the ink formulation developed in this work does not require the diffusion of calcium chloride from the agar throughout the printed part as the higher viscosity and yield point of the ink provides adequate stabilisation previous to the formation of the cellulose[18]. While this leads to a reduction in bacterial cellulose yield, as found in Figure 4.14, the incorporating of silicon dioxide platelets which form a scaffold around which the bacterial cellulose grows means that the stability of the structure is not entirely dependent on maximising the bacterial cellulose growth as even a thin layer is sufficient to compact and lock the silicon dioxide platelets into place during drying. Consequentially the ink presented here exhibits a higher printability which can be used to create mm-scale structures which show visible overgrowth by bacterial cellulose. One example to emphasize the substantially higher shaping freedom of the here developed ink is shown below, whereas a 12 mm tall, 6 mm diameter cylinder was printed, as shown in Figure 6.1 (A-B) and overgrown by bacterial cellulose, Figure 6.1 (C) , demonstrating both

the printability and bacteria survivability.

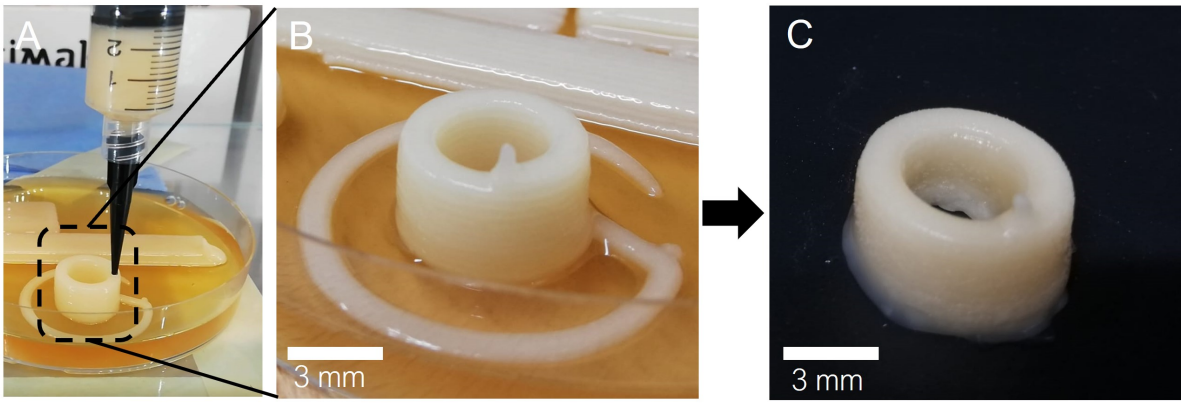

Figure 6.1: Increased shaping freedom of the scaffold ink formulation used to print a 3D cone shape (A-B), and overgrowth of the printed structure with BC (C).

Note that in addition to the observed BC growth on the macro-scale, the formation of BC around the structure was furthermore verified under SEM. The observed BC layer for the the aforedescribed 12mm x 6mm cone is shown in Figure 6.2, whereas (A) shows the cone after drying in the oven at 50°C for 96hrs. Note that the microstructure displayed in image (B) is included solely to verify the growth of a BC, with further analyses of its morphology outlined in the chapter 7.

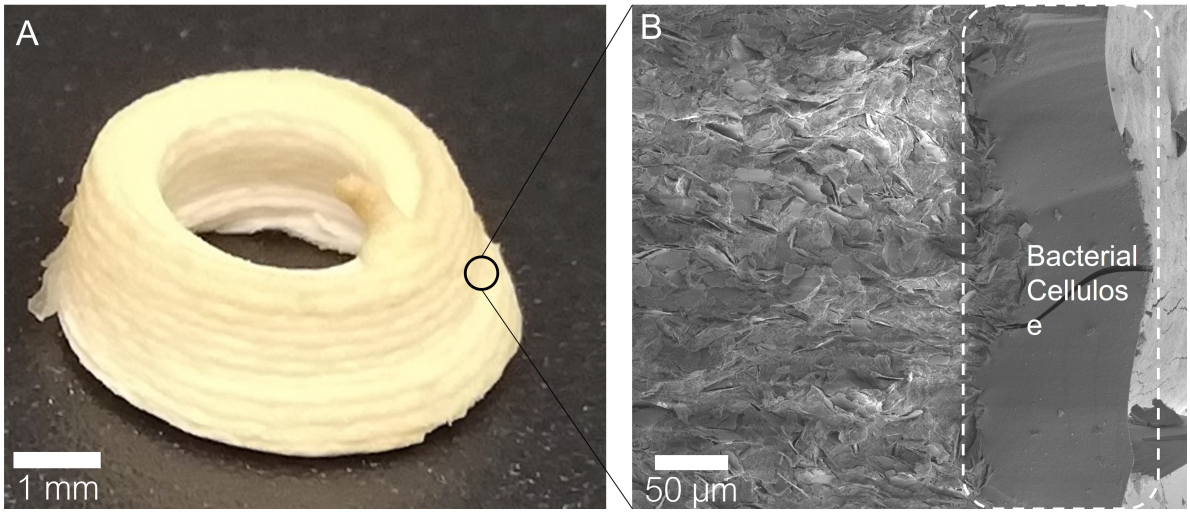

Figure 6.2: Overgrown and dried BC composite material (A), with its microstructure (B) highlighting the formation of a BC layer at the air-scaffold interface.

6.2. Limitations of the process

While the ink formulation and manufacturing processes were found to substantially increase the printability, consequentially verifying the shaping freedom aspect of the main research hypothesis, the complexity of parts which could be produced was found to be somewhat limited due to the material shrinkage of the BC layer during the drying step. Note that this applied to a higher extent to flat, high aspect ratio geometries. As outlined in the hypothesis and further highlighted in the previous section and in the analysis of the micro-mechanical properties in chapter 8, this shrinkage is required in order to compact the silicon dioxide platelets and consolidate the part into one integral component, however its extent did result in undesired warpage and fragmentation. Given the impact of this practical limitation, significant effort was invested to determine the origin of each in order to minimise its extent. The so-found

procedural steps are highlighted below.

Fragmention
The observed fragmentation behaviour is shown in Figure 6.3. The cause for this was investigated by varying the substrate on which the overgrown samples were dried, revealing that for substrates which could shrink with the part, fragmentation was prevented. As such the origin of the observed fragmentation was determined to be introduced by residual stresses caused by the substrate preventing the part from shrinking freely. In order to mitigate this, the bottom side of samples in contact with the substrate was covered with peel ply, a thin fabric used during composite production, which allowed for shrinkage of the drying part.

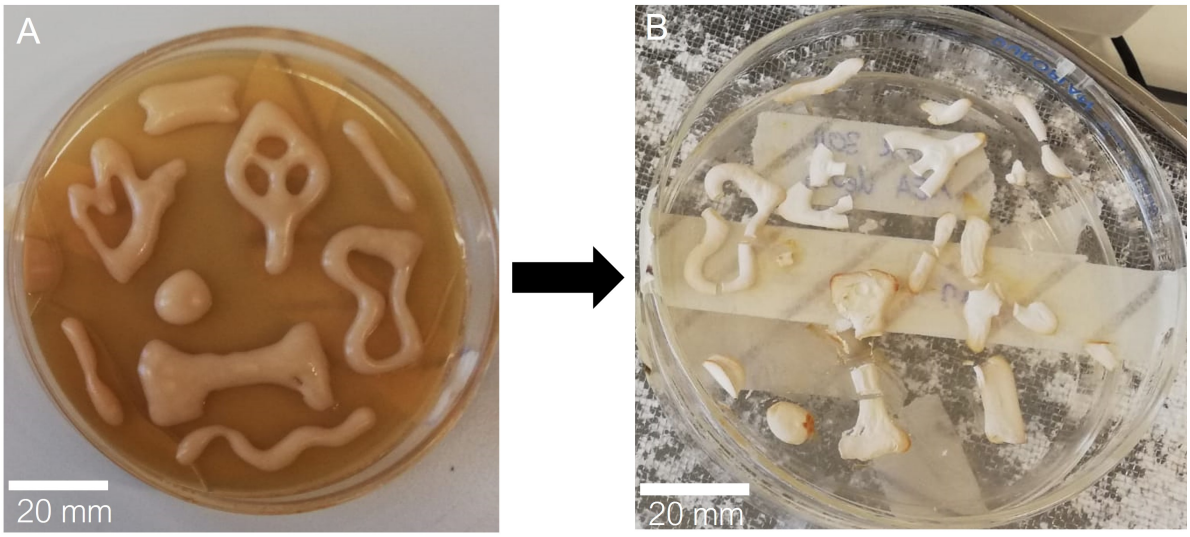

Figure 6.3: Fragmentation of overgrown sample prints (A) after drying (B).

which if left unopposed was found to introduce an out-of-plane upwards warpage for thin, high aspect ratio parts, schematically shown in Figure 6.4(a,b)

Warpage
In contrast to the observed fragmentation, the warpage, exhibited by printed samples during drying, imposed a stronger limitation on the geometries which could be manufactured. The reason for this is due to the inherent inhomogeneous nature of the bacterial cellulose growth in combination with its high water expulsion [29] and shrinkage during drying [29] which if left unopposed was found to introduce an out-of-plane upwards warpage for thin, high aspect ratio geometries, schematically shown in Figure 6.4 (A,B). Next to the more visible problematic of this warpage, namely the distortion of the printed sample, an example of which is shown in Figure 6.4 (C), the warpage furthermore causes no compression of the core as the stresses in the BC layer due to shrinkage are relaxed through the out of plane deformation rather than causing core compaction up to the point where the compressive stresses imposed on the core balance the tensile stresses in the BC layer.

Given the above insight into the origins of this deformation, the attempt was made to minimise it by using a layer of peel-ply to clamp the samples down during drying. While positive results were achieved using this method, such that instead of curling upwards the shrinkage was directed into a more uniform reduction of the printed geometry, as schematically shown in Figure 6.4 (A,D), with an example of a plate dried with this technique applied shown in Figure 6.4 (E), it was not possible to fully negate it, which for thin high aspect ratio samples caused undesired geometric distortions to occur.

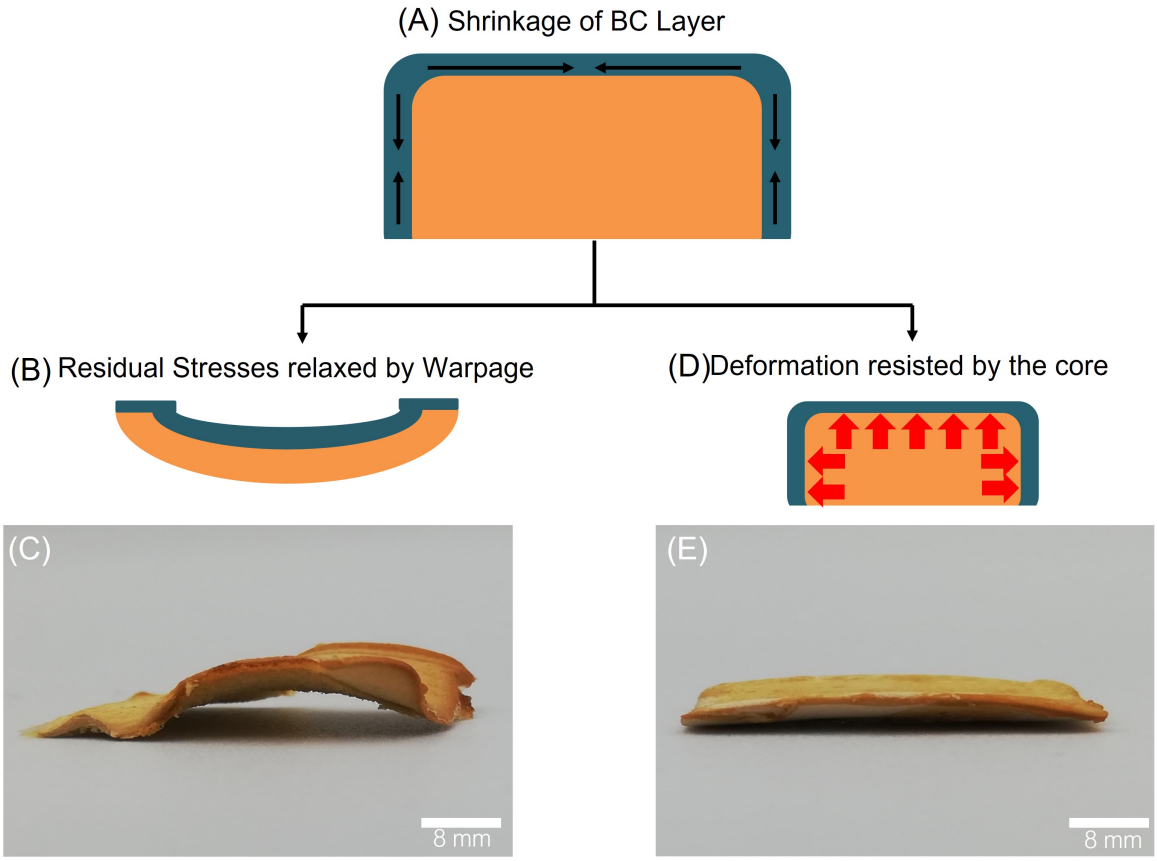

Figure 6.4: Shrinkage effect of the bacterial cellulose layer on the cross-section, showing the undesired warpage (A-C) and desired compaction effect (A,D-E).

7

Microstructure Characterisation

Having established ink formulation, printing procedure and the ability to print parts and overgrow them with bacterial cellulose it is subsequently imperative to on the one hand characterise the morphology of the microstructure created, while on the other hand investigating the origin of the observed growth in order to lay the foundation for further optimisation of the here developed process. To this end, this chapter first outlines the key characteristics observed for overgrown structures using Scanning Electron Microscopy (SEM) images of their respective cross-sections in section 7.1, followed by an explanation of the three competing diffusion models in section 7.2, which are derived from the known growth dynamics in static cultures. The applicability of the growth models to the process at hand is subsequently studied by quantifying the bacterial cellulose yield on the printed scaffolds after stagnation by varying the growth time, for which the methodology is described in section 7.3, followed by a presentation of the results and implications in section 7.4 and section 7.5 respectively.

7.1. Morphology of the Microstructure

The objective of this initial section is to establish the micro-structure of the created material based on Scanning Electron Microscopy images taken of the cross-section of printed sample plates. This includes both samples printed with and without *G.hansenii* glycerol stock added to the ink, in order to provide the reader with the necessary background knowledge for the diffusion models presented in section 7.2, while also highlighting the effect of the bacterial cellulose on the microstructure. Given the complexity of the observed microstructure, a distinction is made between the explanation of the general core-shell model which describes the observed microstructure on a high level, and a more focused analysis of both the core in subsection 7.1.2 and the shell in subsection 7.1.1.

On a high level the microstructure observed for all samples, which were printed using an ink which had been inoculated with *G.hansenii* glycerol stock, can be described by a core-shell model whereas the outside shell layer consists of the grown bacterial cellulose and the compacted core region consists of the SiO_2 platelets and a mixture of fumed silica, sodium alginate and HS-growth medium residue. The origin for this microstructure, and more specifically the exclusive growth of the bacterial cellulose at the air-scaffold interface can be explained by the high availability and concentration of oxygen which can support the *G.hansenii* bacteria population both in replication and cellulose synthesis. An example of this observed microstructure can be found in Figure 7.1, which shows the cross-section views of a one layer sample plate at x55 and x80 magnification, clearly showing the distinction between the platelet rich core and the smooth outside film.

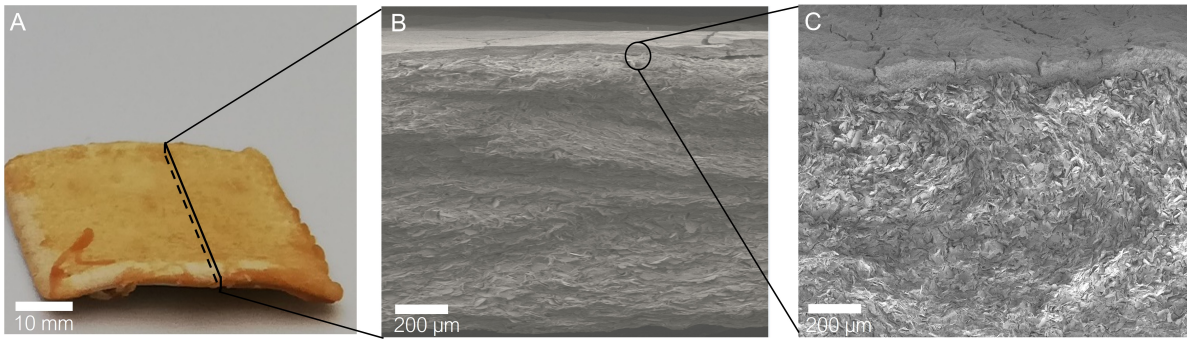

Figure 7.1: Overgrown sample plate (A), with the formed BC-shell and silicon dioxide core of the microstructure shown in (B,C).

The compaction effect of the bacterial cellulose shrinkage on the micro-structure can furthermore be emphasised by contrasting the lack of micron size voids with those observed for samples printed without *G.hansenii* glycerol stock added, which shows not only a lack of the characteristic core-shell distinction observed for all samples which include *G.hansenii* glycerol stock, but also leads to large scale ($> 100\mu m$) voids as highlighted in Figure 7.2. As a result the conclusion is drawn that the addition of cellulose forming bacteria to the ink yields in the formation of an outside film layer which causes compaction of the core, consequentially leading to the collapse of large scale voids which have formed during the manufacturing process.

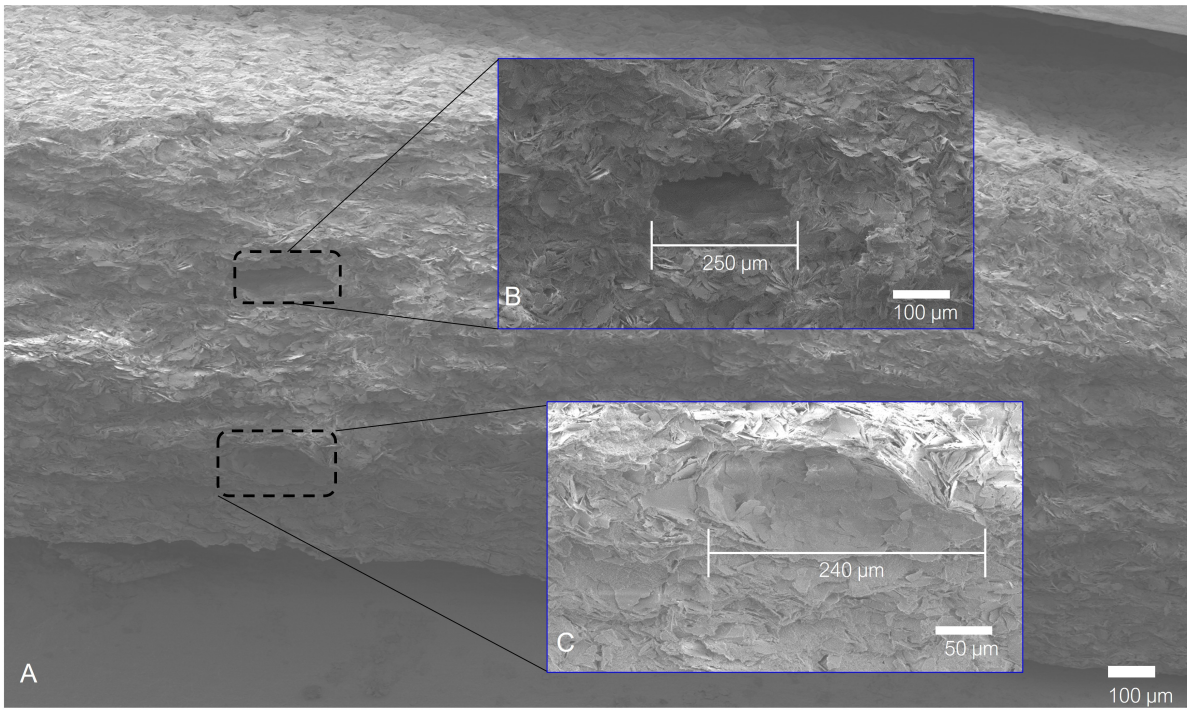

Figure 7.2: Cross-section of a sample plate (A) without BC shell layer, showing large scale($> 100\mu m$) voids (B,C) as a consequence of a lack of compression.

As stated the core-shell distinction is the prominent feature of the microstructure, which can be further highlighted when examining the distribution of carbon and silicon atoms. To this end, energy-dispersive X-ray Spectroscopy was used to decompose the SEM image shown inFigure 7.3 (C) into regions of high silicon concentration, highlighted in blue, and regions of high carbon concentration highlighted in pink, the results of which are shown in Figure 7.3.

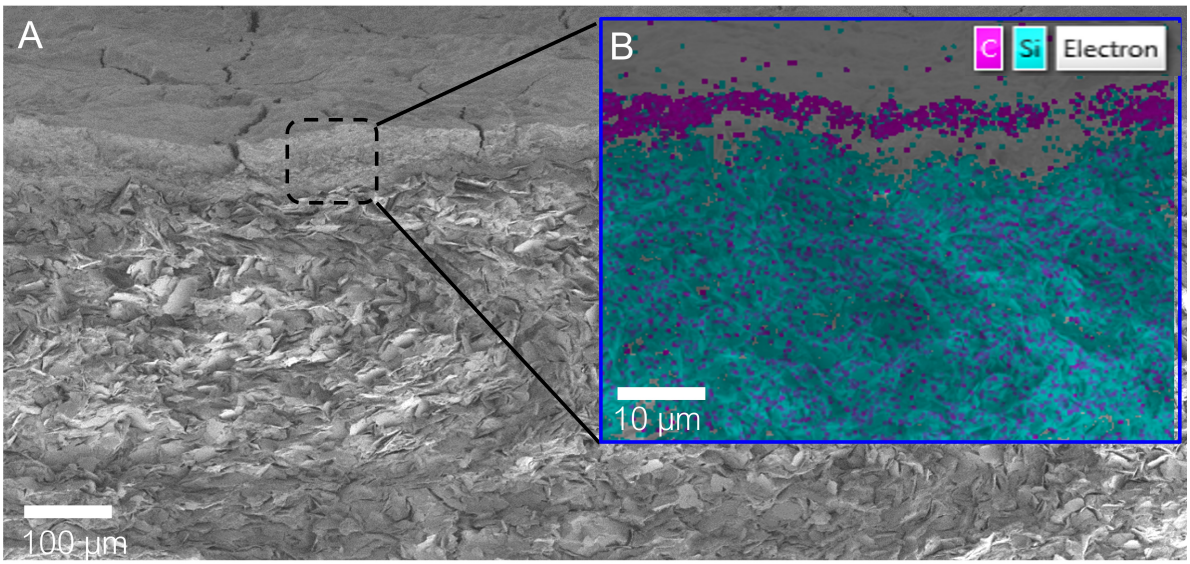

Figure 7.3: EDS image of cross-section close to the surface, showing the carbon rich shell vs silicone rich core (B).

Note that this observed distribution of carbon and silicon is distinctly different from the initially assumed homogeneous distribution within the ink and implies that a redistribution of the carbon has occurred as a consequence of the BC-shell growth. Note that an explanation for this observed redistribution can be extrapolated from the growth mechanics of BC and its chemical structure, whereas the *G.hansenii* bacteria in the shell use glucose from the substrate below to form ,an in thickness increasing, layer of BC, which locks the carbon contained in the glucose into the shell, consequentially causing the the observed carbon depleted core and carbon rich shell.

Having established the general core-shell microstructure it is now possible to analyse each of the individual components of the core and shell in more detailed which is done in subsection 7.1.2 and subsection 7.1.1 respectively.

7.1.1. Bacterial Cellulose Shell

The bacterial cellulose shell forms a consistent thin film on all surfaces which are in contact with the surrounding air. As a result the core is enclosed from all sides except the bottom which due to its contact with agar does not show any bacterial cellulose growth. In addition there is a distinction between the bacterial cellulose coverage which overgrows the top surface and that which grows on the sides, whereas the shell formed on the top surface exhibits a lower thickness than that on the sides in contact with the agar. The hypothesised reasoning for this is thought to be due to the increased nutrient availability close to the surface of the agar. This hypothesis is further elaborated on in section 7.5.

The film itself can be further discerned into the bodies of the *G.hansenii* bacteria, which appear as circular rods with a major axis of a approximately 3 microns, and the cellulose which they produced. Note that there is a stark distinction in the appearance of cellulose component of the shell layer depending on the drying regime applied. For samples which were not dried rigorously, the bacterial cellulose appeared much more fibrous as compared to samples which were dried for the full duration, where the bacterial cellulose film appears to be mostly made up of the bodies of the bacteria, with the cellulose having being compacted to the point where it is reduced to a thin layer inbetween the bodies of the bacteria. This is shown in Figure 7.4 and Figure 7.5 which show the fibrous and compacted morphology respectively.

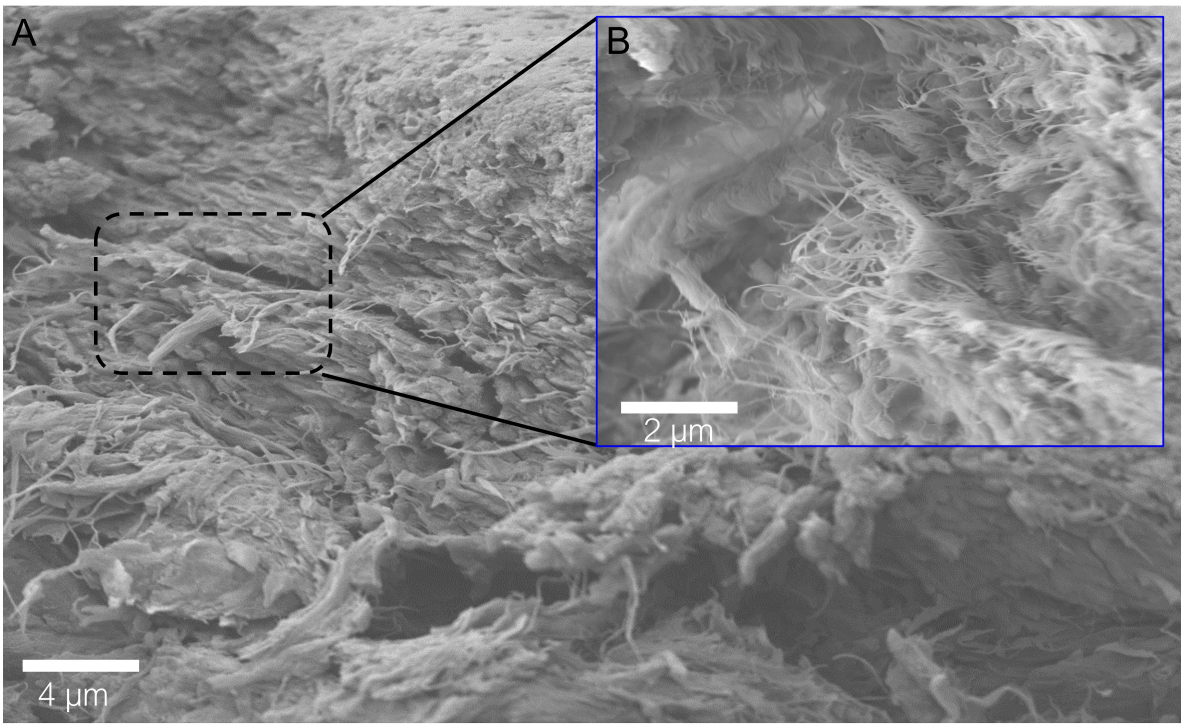

Figure 7.4: Morphology of the bacterial cellulose shell (A,B) showing its fibrous nature.

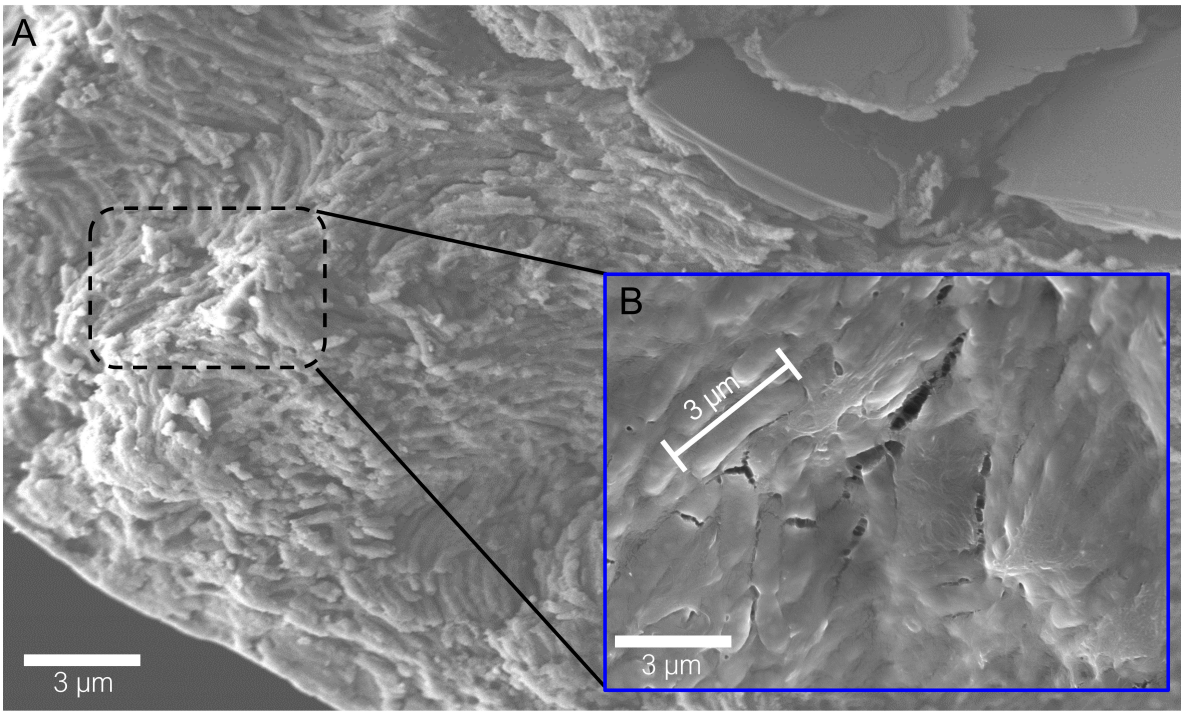

Figure 7.5: Compacted morphology of the bacterial cellulose shell (A,B).

7.1.2. Silicon Dioxide Platelet Core

Compared to the shell, the core makes up the majority of the total thickness for the printed sample plates with its thickness being in the range of multiple 100 microns as compared to the shell layers which as investigated in section 7.5 have thicknesses on the order of multiple 10s of microns. When

viewed under higher magnification two main entities can be discerned to comprise it, namely the SiO_2 platelets and a matrix material of fumed silica and sodium alginate, as can be seen from Figure 7.6.

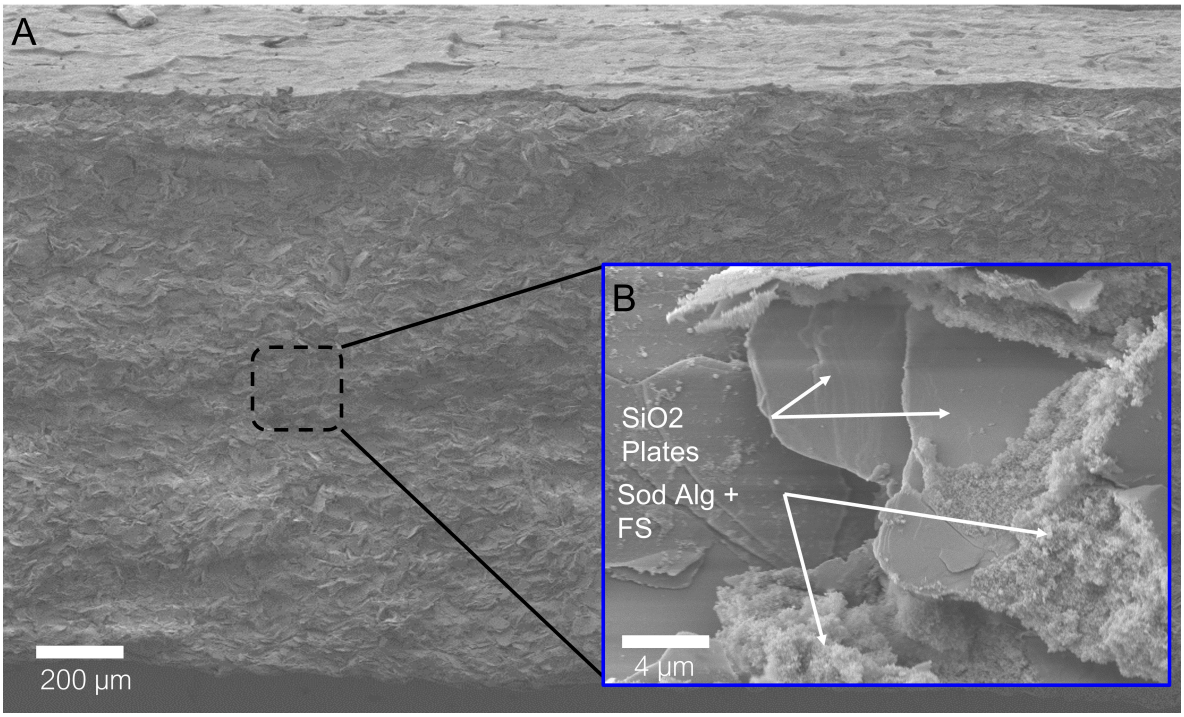

Figure 7.6: Core morphology (B) showing its two main constituents, the silicon dioxide platelets, and residue matrix consisting of sodium alginate, HS and fumed silica.

Note that while the focus of this chapter is on the growth of the BC on top of this core scaffold, further characterisation of its composition will be imperative in gaining a better understanding on how the platelets interact with each other and with the matrix material in which they are embedded under loading conditions.

7.2. Growth Model

Having established the observable core-shell morphology of the microstructure and redistribution of carbon atoms from the core towards the shell it is subsequently possible to establish three options which each describe a different scenario for the nutrient diffusion pathways to the active bacteria in the shell layer. Note that the underlying model of each scenario is equivalent and extrapolated from the known growth dynamics of bacterial cellulose under static conditions whereas, the bacteria combine oxygen at the surface with nutrients diffused from the growth-medium to replicate and produce bacterial cellulose.This is schematically depicted in Figure 7.7 which shows a idealised model of the cellulose formation in a static culture at the air-liquid interface.

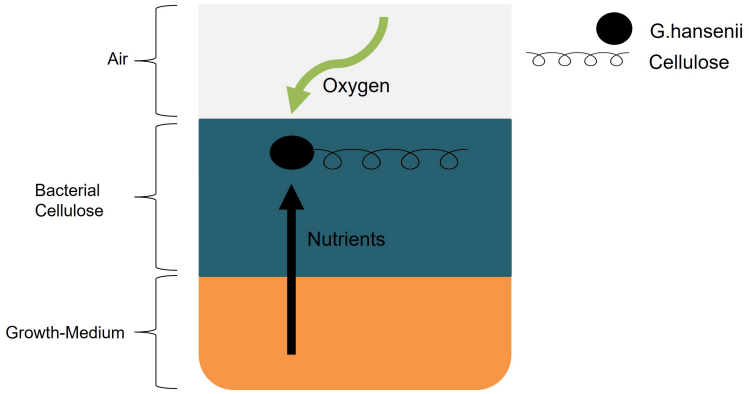

Figure 7.7: Fundamental growth mechanism of bacterial cellulose in static fermentation.

Applying this to the overgrowth of the printed structures thus means that the bacterial cellulose growth is similarly driven by a diffusion of nutrients from below the surface. As such the first of the three possible diffusion models describes the case where nutrients can diffuse from both the agar substrate on which the scaffold is printed as-well as from within the printed structure towards the air-scaffold interface were they can be utilised by the *G.hansenii* bacteria to metabolise cellulose. In essence this is the ideal scenario where-as the rheology of the ink does not limit the diffusion rate of the nutrients such that all input nutrients, including those supplemented by the agar, are used up by the bacteria. This state is schematically shown in Figure 7.8, whereas nutrients from both the agar substrate and the printed scaffold diffuse towards the *G.hansenii* bacteria at the air-scaffold interface.

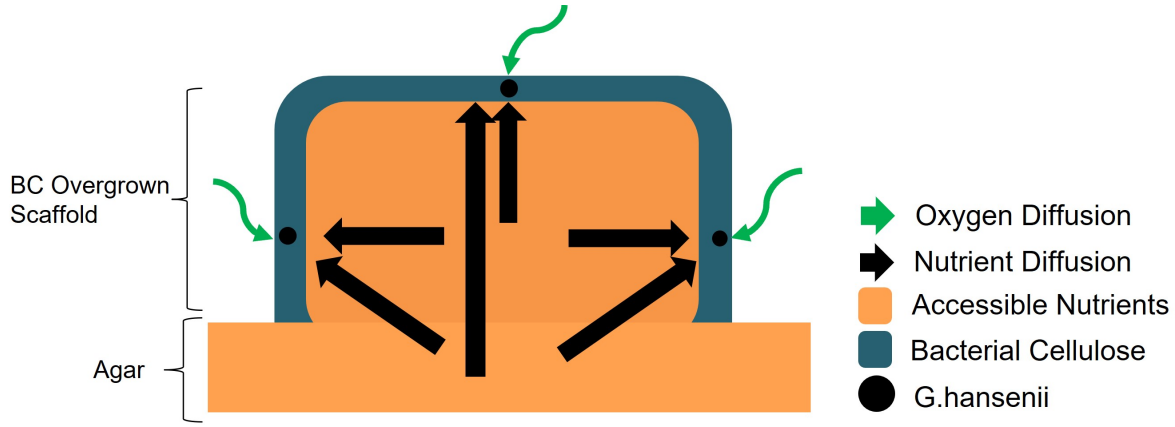

Figure 7.8: Maximum diffusion model where bacteria have access to nutrients within both the printed scaffold and the agar substrate.

The second model describes the case in which, in contrast to the ideal case described by the first model, nutrients cannot diffuse from the agar across the agar-scaffold interface and to the active *G.hanensii* bacteria within the BC-shell. As a result, the nutrients availlable to the *G.hansenii* bacteria are reduced to those present within the printed scaffold. Crucially this scenario assumes full conversion of the nutrients embedded within the printed scaffold such that the amount of bacterial cellulose produced as a consequence can be predicted using the conversion factor established in subsection 4.4.3. This is schematically shown in Figure 7.9, whereas the agar is highlighted in grey to denote that the nutrients within it are not able to diffuse to the bacterial cellulose layer.

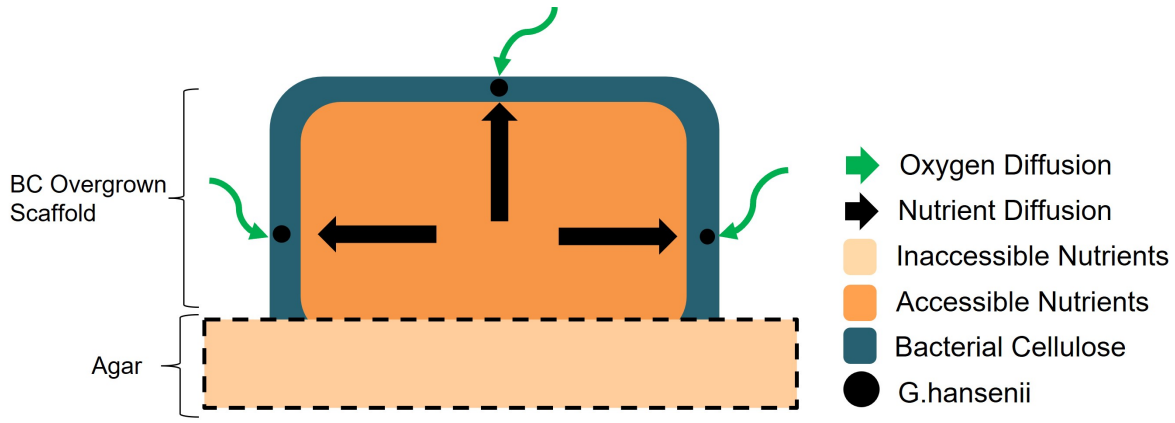

Figure 7.9: Threshold diffusion model where all nutrients from the printed scaffold are accessible for cellulose metabolism by the active bacteria in the shell layer.

Lastly the third model incorporates the consideration that the viscosity of the scaffold which the bacteria overgrow is higher, as compared to the liquid growth-media used for static fermentation, such that it may prevent total utilisation of nutrients from within the core region. This in essence limits the nutrient availlable to the *G.hansenii* bacteria for replication and cellulose formation to those within a certain distance of the surface, yielding in a reduced BC-shell thickness as a consequence of the reduction in nutrients availlable. This is similarly to the previous models, visually depicted in Figure 7.10, which shows the regions of nutrients which are inaccessible for bacterial cellulose growth highlighted in grey which applies not only to the agar but also to the core region of the printed scaffold as a result of the higher ink viscosity inhibiting effective diffusion.

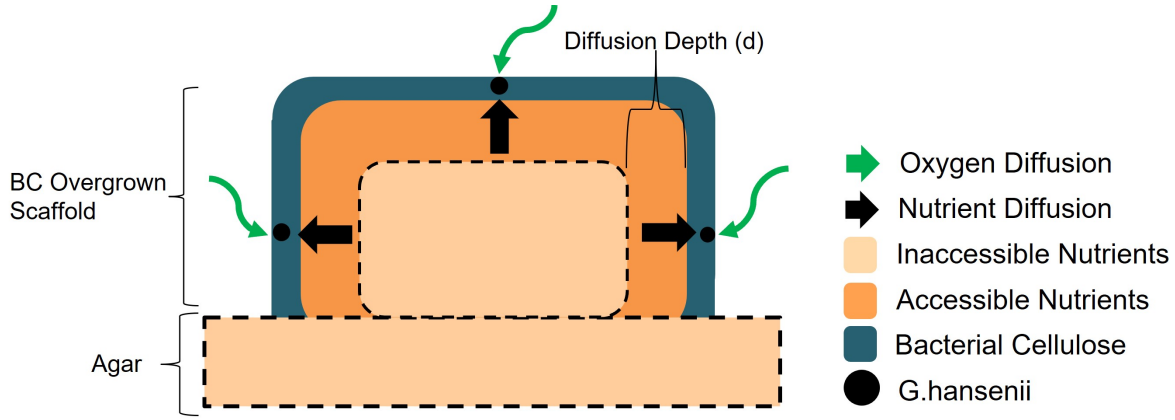

Figure 7.10: Limited diffusion model allowing nutrient diffusion to the surface depth lower than the characteristic diffusion depth (d), as a result limiting full nutrient utilisation from the printed scaffold.

Given these three possible diffusion pathways for nutrients to the bacterial cellulose shell, it is thus imperative to determine which occurs during the overgrowth of bacterial cellulose on the printed scaffolds. To this end an experiment was designed, which was aimed at quantifying the carrying capacity of one layer thick scaffolds in order to determine if the observed growth would exceed that predicted based on the input nutrients and nutrient conversion factor found in subsection 4.4.3, indicating that additional diffusion of nutrients from the agar substrate occurs, or if it would fall short, indicating that the rheology of the ink prevents full utilisation of the nutrients within the ink. The above is summarised in Figure 7.11, which discerns the two regions and the implication for the diffusion model selection depending on the measured bacterial cellulose yield after growth stagnation.

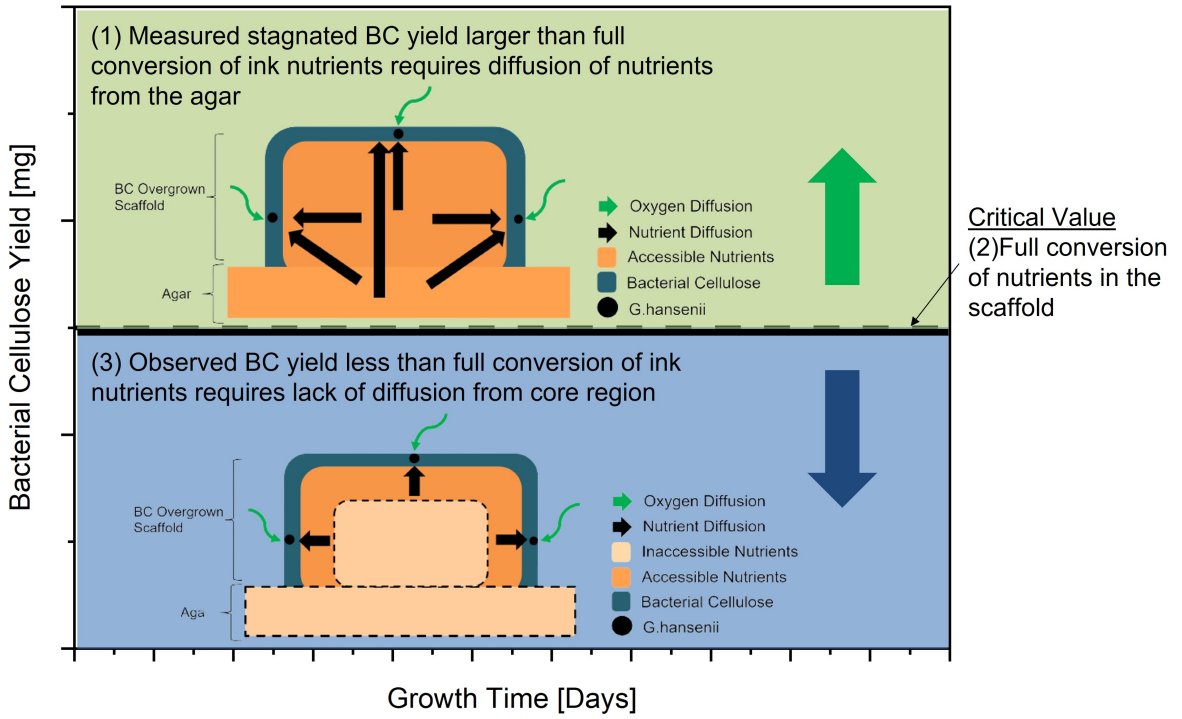

Figure 7.11: Applicability of the proposed growth models, depending on whether the observed bacteria cellulose yield is in excess (1) of the amount predicted based on full conversion of nutrients from the scaffold (2) or lower than predicted (3).

7.3. Bacterial Cellulose Yield at Growth Stagnation

In order to select the model appropriate to describe the diffusion of nutrients during the overgrowth of the BC-layer it was thus necessary to determine amount of BC at growth stagnation which indicates nutrient depletion. To achieve this an experiment was setup whereas the growth of the bacterial cellulose shell layer on-top of the sample plates was tracked until its growth stagnated. To ensure that this stagnation would occur within the scope of the experiment, which was limited to 10 days, the dimensions of the plates were limited to 30mm in length, 40mm in width and 1.2mm in thickness, as this limited the initial nutrient input to 1.44mL , which was deemed sufficiently small to be used to observe stagnation in the case of nutrient availability being limited to the printed scaffold.

All samples were prepared using the methodology established in chapter 5 with samples grown for 0,2,4,6,8,10 days after which they were removed and prepared for measuring the BC which had grown on top of each. To this end, SEM analysis of the cross-section was used to determine the average thickness of the bacterial cellulose shell layer from which the total quantity of BC formed could be calculated by assuming a uniform shell thickness and the known dimensions of the printed scaffold in combination with the density, which was found by measuring the dry mass of pure BC samples. In order to increase the accuracy of this assumption and encapsulate the variability of the shell thickness, the thickness was measured at eight locations across the top surface of each sample plate such that for each growth time a total of 8 datapoints was availlable for the subsequent calculation of the average bacterial cellulose shell thickness and standard deviation. This process is schematically shown in Figure 7.12. Note that the image magnifications was varied slightly in order to obtain a more clear distinction between shell and core, with the measurements being carried out using the inbuilt thickness measurement tool of the SEM.

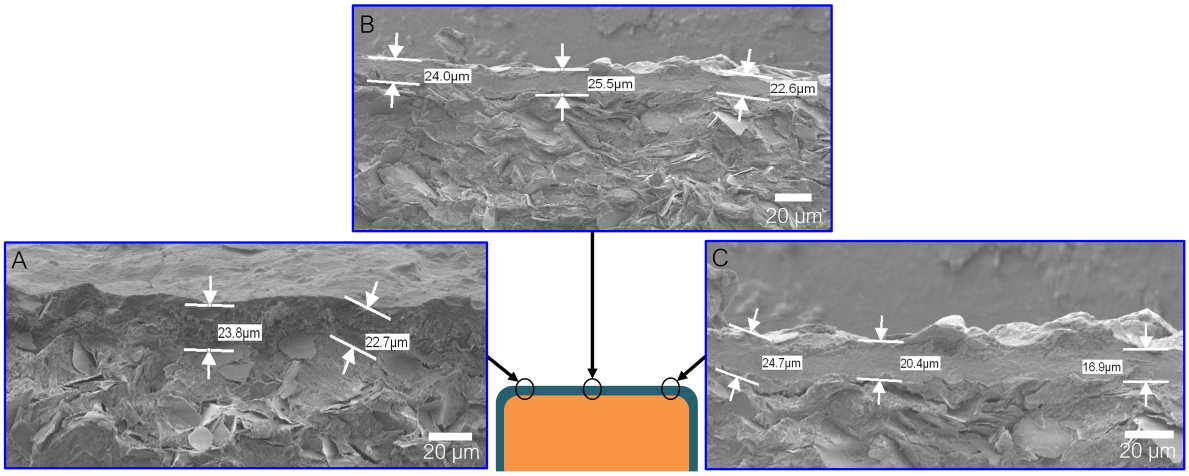

Figure 7.12: Procedure applied in order to obtain the average bacterial cellulose thickness, for which 8 measurements of the shell were done at 3 locations along the top surface.

As stated the average bacterial cellulose yield was subsequently found by assuming a constant bacterial cellulose thickness on all sides of the plate, excluding the agar-scaffold surface. For this, the total volume was first determined by decomposing the printed plate geometry into its core and shell components, after which the total BC shell volume was calculated by summing the individual volumes of BC covering the top surface, the front & back surfaces, and the left & right hand side surfaces according to Equation 7.1 and visually depicted in Figure 7.13. Note that all calculation assume thin-wall such that the contribution of the shell thickness to the overall dimensions of the sample was neglected.

$$V_{avg}^{obs} = V_{avg}^{\text{top}} + 2 \cdot \left(V_{avg}^{LHS,RHS} + V_{avg}^{\text{Front,Back}}\right) \tag{7.1}$$

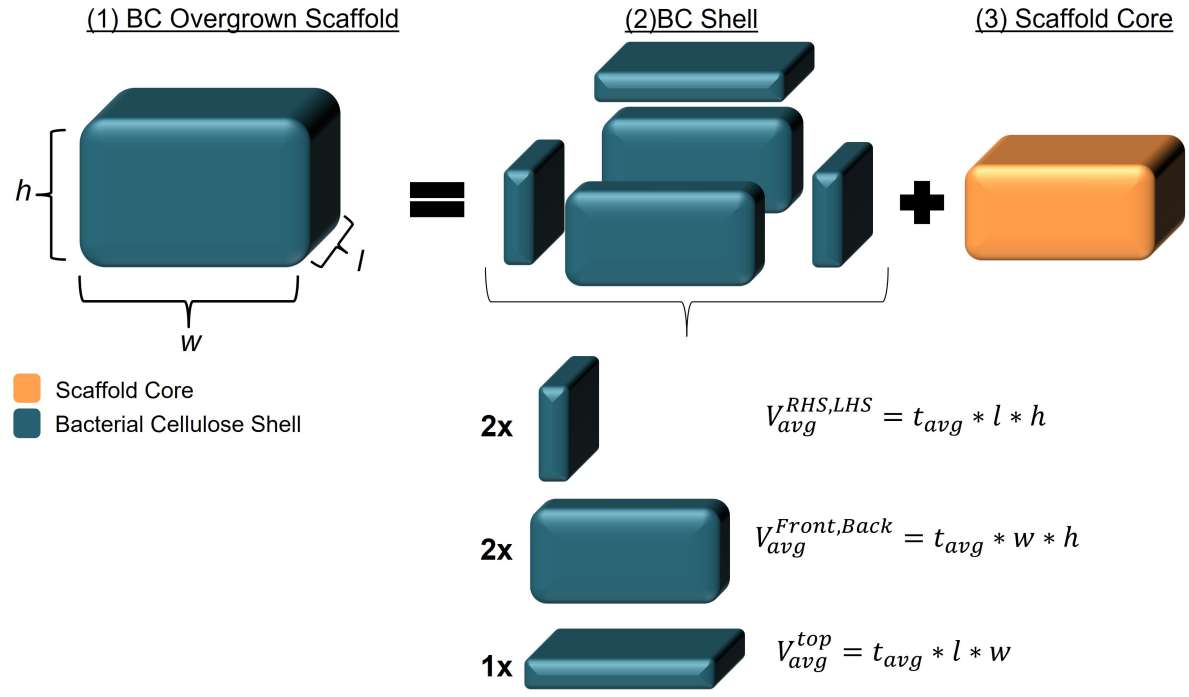

Figure 7.13: Decomposition of the BC overgrown sample geometries (1) into the BC shell layer (2) and the printed scaffold (3) to calculate the volume of the BC coverage.

The bacterial cellulose yield in mg was subsequently determined by multiplying the found total BC shell volume in mm^3 by the density of dried BC, experimentally determined to be $1.1mg/mm^3$, as summarised by Equation 7.2.

$$m_{avg}^{obs} = V_{avg}^{obs} \cdot \rho_{BC} \tag{7.2}$$

The calculation above was thus applied to each of the sample plates grown for 0,2,4,6,8, and 10 days after which the results were plotted in origin with the selection of a logistical fit following the reasoning in subsection 4.2.2.

7.4. Results

7.4.1. Sample Plate Dimensions

The dimensions of the sample plates before and after drying are shown below. Note that the dimensions as printed were taken from the executed G-code while the after drying dimensions were measured using a caliper.

	As Printed			After Drying		
Growth Time[days]	*Height[mm]*	*Width[mm]*	*Length[mm]*	*Height[mm]*	*Width[mm]*	*Length[mm]*
0	1.2	42	30	-	-	-
2	1.2	42	30	-	-	-
4	1.2	42	30	0.489	19.3	15.7
6	1.2	42	30	0.609	18.8	15.3
8	1.2	42	30	0.571	19.4	14.9
10	1.2	42	30	0.536	19.1	15.4

7.4.2. Sample Plate Average BC Yield

The average BC-shell thickness [μm] and the so-calculated average BC yield [mg] together with their respective standard deviations are summarised in the table below. Note that no measurement are shown for 0 and 2 days as no bacterial cellulose shell could be observed.

Growth Time[days]	*Avg BC-Shell Thickness[μm]*	*Std*	*Avg BC-Shell Yield[mg]*	*Std*
0	0	0	0	0
2	-	-	-	-
4	5.4	2.4	2.2	1.0
6	10.7	3.6	4.2	1.4
8	19.7	2.6	7.8	1.0
10	19.3	4.5	7.3	1.7

Table 7.1

The results of plotting the measured average bacterial cellulose yield on top of the 1 layer thick printed scaffolds as a function of growth time, as summarised by the table above, is shown in Figure 7.14.

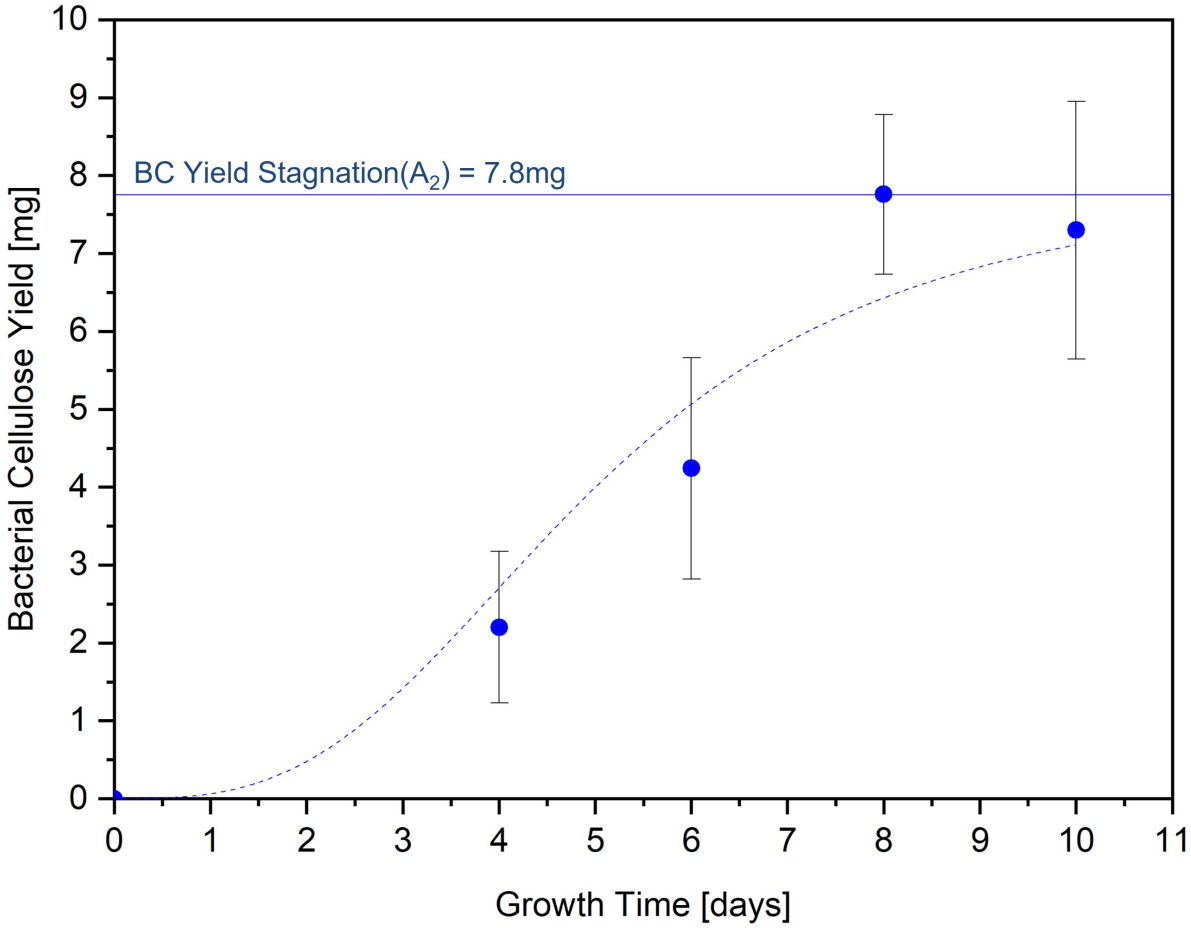

Figure 7.14: Bacterial cellulose yield as a function of growth time determined from the average bacterial cellulose shell thickness.

7.5. Discussion

The results of tracking the bacterial cellulose yield, which are depicted in Figure 7.14, show a measurable bacterial cellulose growth after 4 days of 2.2mg which increases to 4.2mg after 6 days and peaks after 8 days at 7.8mg. Crucially, no further increase in the bacterial cellulose yield is observed between 8 and 10 days indicating the the growth has stagnated in responds to a depletion of one or more resources. As result of the observed stagnation, the maximum carrying capacity of the 1 layer sample plate tested can be defined to be 7.8mg.

Having established the maximum carrying capacity of the given samples, it is subsequently possible to assess which of the three established models best describes the observed growth by calculating the threshold value, which describes the scenario whereas the *G.hansenii* bacteria have utilised all nutrients within the printed scaffold. This value is obtained using Equation 7.3, whereas the conversion factor of 9mg of BC per 1 ml of HS established in subsection 4.4.3 is used to calculate the BC yield assuming full nutrient utilisation. Note that the input HS-growth medium is obtained from the total ink extrusion mass(1.5g), reduced by a factor of 0.92 due to the addition of 4%wt fumed silica and 4%wtSiO_2 such that the total HS input per sample plate is given as 1.39(g), which given density of the HS-medium is close to that of water(0.997g/cc) gives rise to a HS-growth medium input per printed plate of 1.4mL.

$$m_{BC} = F_{BC}^{Nt} \cdot V_{HS}^{In} = 9[mg/mL] \cdot 1.4mL = 12.5mg \tag{7.3}$$

The so-obtained threshold value of 12.5mg, which describes full resource utilisation, can subsequently be compared to the the measured bacterial cellulose yield at growth stagnation, as visually depicted in

Figure 7.15.

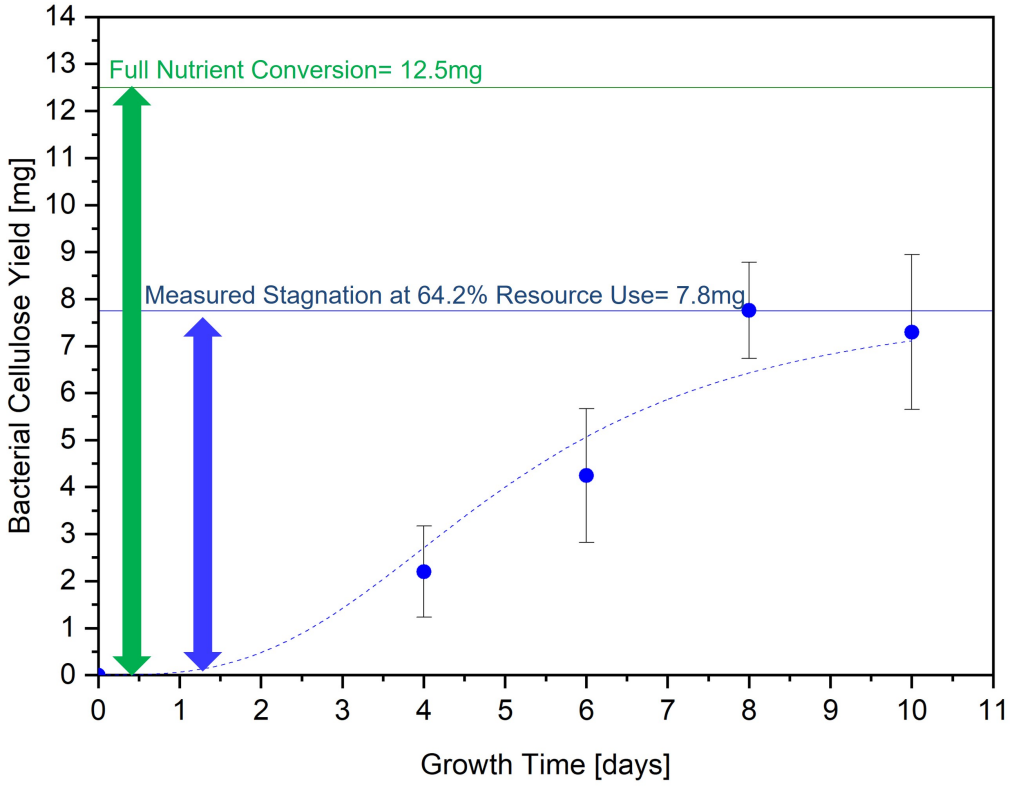

Figure 7.15: Comparison of the found stagnated bacterial cellulose yield around the printed scaffolds to the predicted for assuming full nutrient conversion from the scaffold.

This indicates that the BC growth on top of the printed scaffold utilised only 64.2% of the total nutrients within the printed scaffold such that the conclusion is drawn that nutrient diffusion cannot occur from the agar nor from all regions within the core but rather is limited to a certain depth close to the surface, as depicted in Figure 7.16.

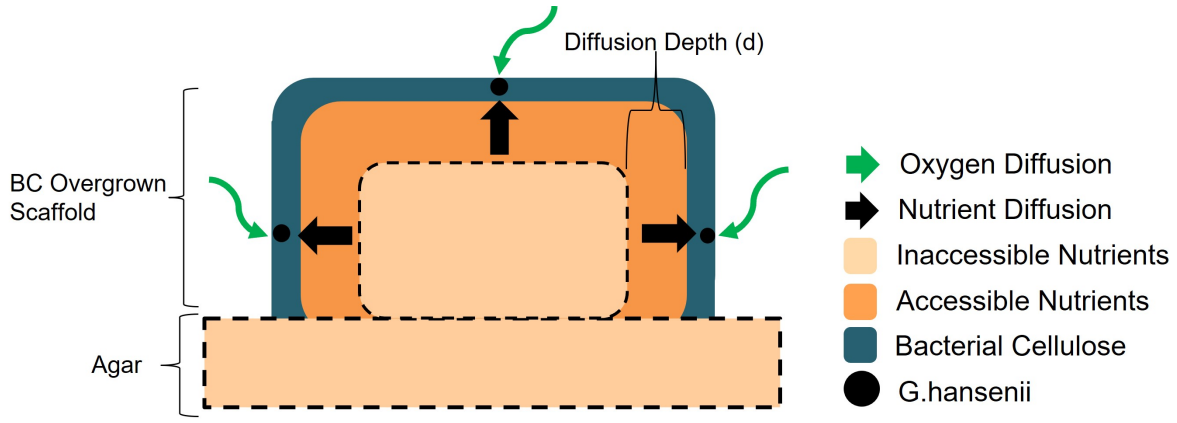

Figure 7.16: Applicable diffusion model, showing the limited utilisation of nutrients from the core.

At this point three implications based on the diffusion model established can be stated. First and foremost,the obtained results place an upper limit on the BC shell thickness of 19.7microns, see Table 7.1 at stagnation after 8 days of growth, regardless of the geometry of the printed scaffold implying that larger structures will simply have a larger core with an equivalent BC-Shell thickness. As such it will be imperative to determine if a %-wise thinner BC layer will nonetheless provide the compaction and stabilisation effect observed for the small scale structures printed as part of this thesis. Second, it puts

into question the use of the agar substrate, as the nutrients within it cannot be utilised effectively such that this aspect of its use should be excluded for future iterations of the process. Third and last, given the novelty of the diffusion model presented here, being the first of its kind reported for DIW of living inks, it is imperative to both further put it to the test and iterate on its complexity in order to describe phenomena such as the observed pockets of increased BC growth at the bottom corners of the sample, as noted in subsection 7.1.1 and shown in Figure 7.17, which are hypothesised to occur as a result of localised diffusion of nutrients from the agar.

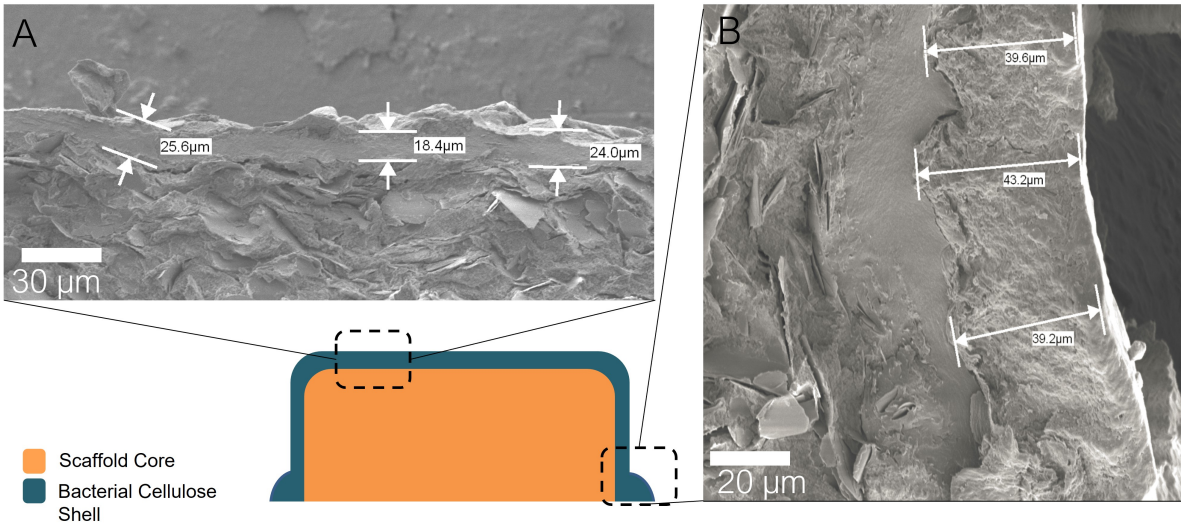

Figure 7.17: Observed increased cellulose growth at the intersection of the printed scaffold and agar substrate.

8

Micro-Mechanical Properties

The last component in order to fully characterise the $BC-silicondioxide$ composite material created by extrusion and subsequent overgrowth of the ink formulation developed here, after having established both the morphology of its microstructure and its diffusion characteristics during growth, is to define whether the synergy of silicon dioxide and BC overgrowth results in a measurable increase of the mechanical properties. To this end, this chapter investigates how the reduced Young's-modulus is effected by the overgrowth of the silicon dioxide scaffold by comparing samples with and without active *G.hansenii*, to pure BC. This is done by first detailing the rationale behind the selection of the reduced Youngs-Modulus as a parameter to compare the materials in section 8.1, followed by an outline of why nano-indentation was utilised to obtain measurements on the reduced Young's Modulus rather than more traditional testing techniques in section 8.2. Subsequent to this, the methodology applied for testing is detailed in section 8.3 and followed by the presentation of the results in section 8.4, with a discussion of their implications in section 8.5.

8.1. Quantifying Structural Integrity

As stated in the hypothesis of this thesis, the bacterial cellulose which encompasses the platelet rich core is argued to increase the structural integrity of the printed material. The rationale behind this is derived from the high shrinkage exhibited by the bacterial cellulose during drying [29], which is conjectured to induce compaction of the core given the lack of shrinkage of the silicon dioxide platelets, as such locking the platelets into place giving rise to a higher resistance against any further deformation. Crucially the resulting negation of micron sized voids as highlighted in the microstructural analysis in section 7.1 serves as an indication of this compaction behaviour while the macroscale observation of the formation of integral parts when prints are overgrown with bacterial cellulose as compared to the fragile and powdery parts obtained without it further demonstrates its effect. In order to verify this hypothesis it is however imperative to relate this observed increased structural integrity through compaction to a quantifiable mechanical property. As such the argument is made that the hypothesised increased structural integrity when samples are overgrown with BC is reflected in the elastic modulus of the material due to the following.

1. The inverse relationship between void content and Youngs modulus [12], such that the negation of large scale voids (>100microns) as a consequence of the compaction is echoed in an increase of the Youngs Modulus
2. A better load transfer between the stiffer silicon dioxide platelets as a result of the compressive pressure applied[13], which originates from the differential shrinkage of the BC shell layer and silicon dioxide dominated core.

In order to verify the above argument it is subsequently crucial to quantify the Youngs modulus of samples with and without BC overgrowth while quantification of the modulus of pure BC is required as a reference.

8.2. Characterising Biological Materials

The selection of an appropriate test type in order to characterise the Young's modulus was mainly driven by limitations imposed on the geometries which could be created as a result of the biological nature of the materials creation, previously highlighted in section 10.1, which caused warpage for high aspect ratio, large parts. As a consequence of this the constant cross-section,larger dimension samples required for the more commonly employed tensile and 3P-Bending tests could not be produced.

In comparison to the more commonly employed mechanical characterisation techniques(Tensile Testing & 3P-Bending), which for the reason considered above were not deemed applicable to characterise the mechanical properties of the overgrown BC-silicon dioxide, nano-indentation requires both smaller sample dimensions, and lower force clamping while nonetheless permitting for the measurement of both Hardness[MPa] and reduced Elastic Modulus [GPa]. As a result of this, in combination with its applicability to softer materials due to the lower forces required, nano-indentation was selected as the testing technique to characterise the impact of BC-overgrowth on the Youngs Modulus.

8.3. Methodology

The methodology applied in order to characterise the micro-mechanical properties of samples with and without bacterial cellulose overgrowth, as-well as those of pure bacterial cellulose prepared using static fermentation, is presented in this section, divided into the three preparatory steps, namely the sample preparation, subsection 8.3.1, the machine troubleshooting & calibration, subsection 8.3.2, and the selected loading configuration, subsection 8.3.3, and the two execution steps, namely the protocols used for testing and post-processing in subsection 8.3.4 & subsection 8.3.5 respectively.

8.3.1. Sample Production

Testing required the manufacture of three distinct sample types, namely samples which consisted of both the silicon dioxide core and BC-Shell layer, from here on referred to as BC-silicon dioxide, samples only consisting of the core-material without BC growth, referred to as silicon dioxide, and the bacterial cellulose reference samples, referred to as BC. Given the distinct production process for each, this section first outlines the manufacture of the BC-silicon dioxide samples and silicon dioxide samples followed by a description of the BC reference sample manufacture.

BC-Silicon Dioxide & Silicon Dioxide Sample Production

Both the samples with BC overgrowth and without BC overgrowth were prepared following the overarching printing methodology established in chapter 5 with the main difference being the addition of *G.hansenii* bacteria stock to the ink from which the BC-silicon dioxide samples were printed in order to induce the in-situ formation of the BC shell layer. Given the fact that nano-indentation requires relatively small plates, the same G-code as used for the printing of SEM samples could be applied such that the samples printed for the nano-indentation had as printed dimensions of 30mm in length, 40mm in width and 1.2mm in thickness. After extrusion, the samples were separated into those with & without *G.hansenii*, BC-silicon dioxide & silicon dioxide samples respectively, with the ones with *G.hansenii* stock (BC-silicon dioxide) being placed in the growth chamber for 10 days to allow for the in-situ growth of the BC shell. Subsequent to the growth, all sample plates, including the silicon dioxide samples, were removed from the agar substrate and placed on a petri-dish with either side of the plate being covered by a layer of peel ply. The peel-ply was then taped to the petri-dish in order to restrain the out of plane warpage of the samples during drying. The samples then dried at 50°C for 96hrs, after which they were glued to magnetic sliders, which allowed easy placement on the testing rig of the nano-indentor.

Bacterial Cellulose Samples

The reference sample in the form of statically grown bacterial cellulose(BC) was manufactured by preparing a liquid solution combining HS-growth medium and *G.hansenii* bacteria stock at a concentration of $30\mu l/100mL$, which subsequently incubated in the growth chamber for 10 days after which the pellicle was harvested, washed, dried and cut into rectangular pieces of similar dimension as those exhibited by the dried BC-silicon dioxide and silicon dioxide sample plates.

8.3.2. Machine Troubleshooting & Calibration

Nano-indentation testing was carried out using a Hysterion TI Premier Nanoindenter with a Berkovich diamond tip. Given the long idle time of the machine, with the last use being longer than one year ago, its use first required a re-calibration using a supplied quartz sample whereas the known Hardness and Young's-modulus of a quartz sample are leveraged to calibrate the area function of the berkovich probe, which is required in order to accurately relate the indentation depth to the projected indentation area based on which the elastic modulus is calculated from the measured force vs indentation depth.

Crucially this calibration required significant amounts of troubleshooting as the preset value for the threshold force which is used by the system to automatically detect the surface of the sample during testing, was found to be too low. As a result of this too low value, the system erroneously detected the sample surface before coming in contact with it caused by a force feedback when the stage moved, which triggered the indentation test to happen in mid air rather than in contact with the sample. In order to remedy the problem, the threshold force was increased from $5\mu N$ to $8\mu N$, which was just above the force feedback the system picked up due to its own movement which fixed this specific issue, after which the calibration could be completed.

8.3.3. Loading Configuration

Next to the calibration, the use of the nano-indentor required the definition of the appropriate testing parameter, as such requiring the selection of all variables to fully describe a single indent, while also necessitating the selection of the number of indents per sample and at the spacing between each.

Testing Parameters

For the force feedback controlled indentation test discussed here, the loading condition is characterised by three main components, namely the loading (1), holding (2) and unloading phase (3), as shown in Figure 8.1 (A).

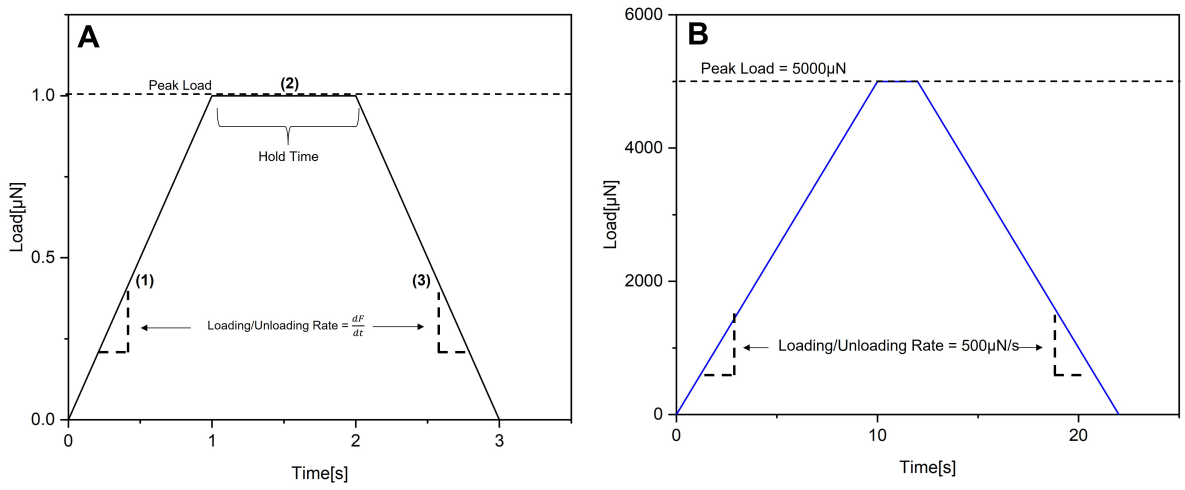

Figure 8.1: Main components of the loading curve (A) and the implemented loading curve (B).

The full characterisation of one indentation thus requires the selection of the peak load, holding time and both loading and unloading rates. While for the holding time and both the loading & unloading rate, this process was simplified by using the values recommended by the manufacturer, the peak load required a series of pre-test as it both had to be large enough to give rise to a sufficiently deep indent while being small enough such that the maximum indentation depth would not be reached at a force lower than the selected peak load. Based on the pre-test conducted, a peak force of $5000\mu N$ was found to provide for mid-range indentation depth, around 500-1000nm, with no issues of exceeding the maximum indentation depth of 5000nm for any of the samples tested. These above consideration subsequently yielded in the loading curve depicted in Figure 8.1 (B), which was used for all indents.

Indentation Geometry
Next to fully defining one indent, the nano-indentation system used further required the selection of the total of number of indents to execute per test and at what spacing. While the indentation process itself was fully automated, it nonetheless required up to 30 minutes per indent such that a maximum of 3 indents per sample were conducted. The spacing on the other hand was selected to be 20 microns, which represent a value slightly higher than suggested but was deemed appropriate in order to negate an potential interference between the individual indents.

8.3.4. Testing Execution
In order to execute the testing, the prepared magnetic sliders were placed on the testing bed of the nano-indentor after which the location and geometry of the tested samples was defined using the camera of the nano-indentor which allowed for the automation of the test. Subsequent to this the indentor probe was lowered close to the surface, as shown in Figure 8.2 (B) in order to decrease the approach time after which the the prepared 3-indents at a peak load of 5000μN were executed. Note that for each sample type, three samples were prepared such that a total of 9 indents per material (BC-silicon dioxide,BC,silicon dioxide) were made.

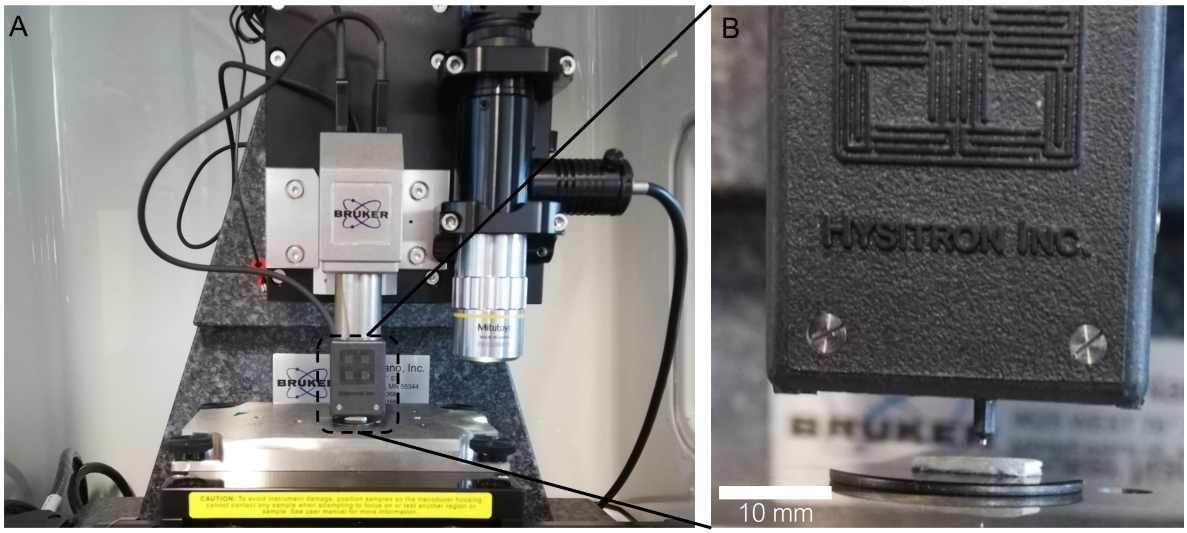

Figure 8.2: Nano-indentation setup (A) showing the Berkovisck probe during its approach to the sample surface (B).

8.3.5. Post-Processing
Once executed the data obtained from all nano-indentation test required very little post-processing as the software supplied with the testing machine automatically computes the hardness and reduced Youngs modulus based on the force vs indentation depth curve of each indent. As such only the average value and standard deviation for each material kind had to be computed, which was done using origin 2021 pro after which the results were plotted using a scatter plot to highlight the spread.

8.4. Results
The reduced Youngs moduli calculated for each indent and grouped by material type (BC-silicon dioxide,silicon dioxide,BC) are shown in Figure 8.3.

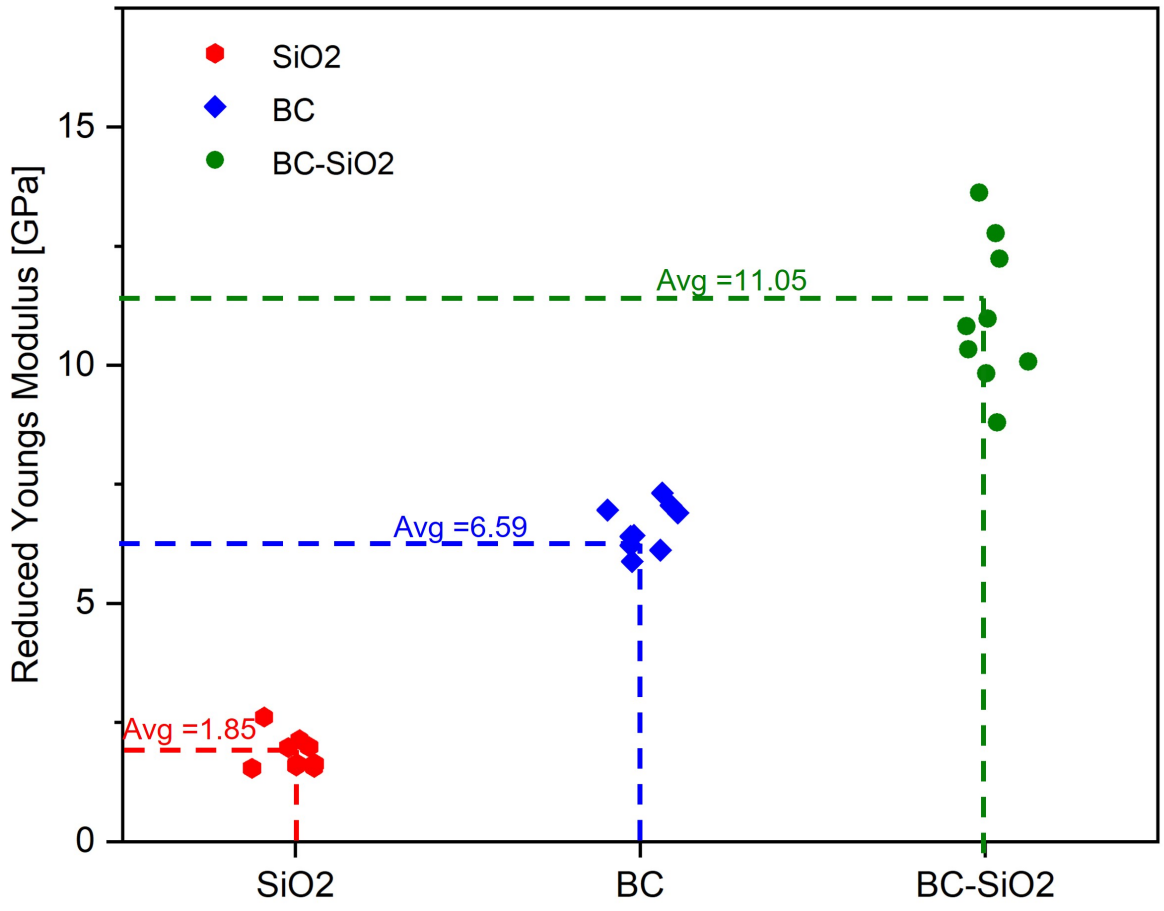

Figure 8.3: Reduced Youngs modulus per indent as a function of material type.

In addition the calculated average Youngs modulus per material type together with the respective standard deviation is summarised in Table 8.1.

	Average reduced Youngs Modulus[GPa]	Std[GPa]
SiO2	1.85	0.34
BC	6.59	0.46
BC-SiO2	11.05	1.46

Table 8.1: Average reduced Youngs modulus of the three material types tested together with their respective standard deviations

8.5. Discussion

The purpose of this section is to determine if the synergy of BC-shell and silicon dioxide core causes an increase in the reduced Youngs modulus in order to verify the hypothesis made in section 8.1. The key findings of the indentation testing carried which quantify the Youngs Modulus of the three distinct materials are listed below.

1. The measured Youngs Modulus of the samples combining a silicon dioxide core with a BC-shell layer exceed that of those without in-situ bacterial cellulose growth by a factor of 6.
2. The BC-silicon dioxide composite material created here shows a higher stiffness than that of the BC reference sample by more than 70%.

The conclusions which are drawn from the key findings listed above are two fold. First and foremost the results verify the hypothesis made in section 8.1 given that the higher stiffness of the overgrown BC-

silicon dioxide material as compared to pure BC indicates the at least partial loading of the added and much stiffer silicon dioxide platelets occurs, while the comparison of the BC overgrown material(BC-silicon dioxide) with the samples made without the in-situ bacterial cellulose growth(silicon dioxide), shows that without the growth of a BC-shell layer, the platelets cannot be loaded effectively such that the resulting material is to a lesser extent influenced by the properties of the silicon dioxide platelets but rather by the lack of load transfer between them.

Secondly the observed increase in Young's Modulus of the BC-$silicondioxide$ samples in comparison to the BC samples shows that the here used core-shell approach, whereas the shrinkage of the BC network around the core is leveraged to utilise the stiffness of the added fillers, can be effectively employed to tailor the mechanical properties of the resulting material. As such it presents an potential alternative route to the more frequently applied approach of integrating the reinforcing filler into the BC network on a micro-scale, which in comparison is more prone to issues of filler sedimentation or requires the need to disintegrate the BC network, while furthermore often being limited to 2D geometries [29]

9 Outlook

9.1. Significance of the Current Work

The need to curtail the effect of climate change is without a doubt one of the most monumental challenges which humanity has faced in its 300,000 years of existence. Crucially it is however also one of the few which, at least for the moment, lies fully within mankind's control to remedy. This necessity to act, is similarly reflected in the aerospace industry where long held believes about the environment friendliness of high performance materials such as carbon fibre composites have had to be re-evaluated given the substantial energy consumption required for their production.[22]

While there are many potential candidates to replace it, one of the most promising alternatives if fully utilised, is offered by bacterial cellulose, which due to its high purity and crystallinity offers outstanding mechanical properties while simultaneously requiring little energy input when leveraging its metabolism by bacteria from a glucose. Crucially its near term application to structural components is hindered by the restrictions that are imposed on the geometry of components which can be manufactured by currently used production techniques. One solution to overcome this lack of shaping freedom, is offered by the combination of in-situ bacterial cellulose growth and 3D printing. While a multitude of different approaches have been investigated, the one postulated in the work at hand, improves on previously explored techniques by utilising the in-situ cellulose overgrowth of a printed, nutrient rich, silicon dioxide platelet scaffold by embedded *G.hansenii* bacteria to allow for the manufacture of 3D components of previously unachievable shaping freedom with increased structural performance. As such this approach offers the unique ability to create living structures of high complexity making it ideally suited as the foundation for the manufacture of lightweight structural components within and beyond the field of aerospace engineering.

9.2. Conclusions

The main objective of this research was to iterate on the previous attempts made to combine in-situ bacterial cellulose growth and additive manufacturing by utilising the synergy of a printed scaffold core overgrown by bacterial cellulose in order to increase both shaping freedom and mechanical properties while simultaneously investigating and establishing the underlying growth dynamics.

As are result of the novelty of this approach, the thesis work commenced with a parametric study on the effect of a set of four processing parameters on the bacterial cellulose synthesis. This lead not only to the completion of the ink formulation, which was optimised for both initial bacteria count and fumed silica content, while simultaneously for the first time providing a quantification of the reduction in bacterial cellulose yield observed as a function of fumed silica, but also allowed for determination of the liquid nutrient conversion factor. Similar to the fumed silica reduction factor, the liquid nutrient conversion factor has not been previously investigated or reported given its lack of importance to traditional bacterial cellulose production. In contrast to this, its importance for DIW of living inks, cannot be overstated as it defines the amount of bacterial cellulose that can be expected to be metabolised by the bacteria from the nutrients embedded within the printed scaffold, such that it was used throughout

the thesis to understand the growth dynamics.

Using the established ink formulation, it was subsequently possible to investigate the improved shaping freedom facilitated by it, which showed that, in contrast to living inks without a scaffold core, the here developed ink formulation did not suffer any limitation w.r.t the thickness of the parts which could be produced. The implications of this were highlighted through the layer by layer manufacture of a 6mm tall cone shaped scaffold, which was fully overgrown by bacterial cellulose and whichs geometry was preserved after drying, giving rise to an BC based composite material. The observed increase in shaping freedom was subsequently used as evidence to conclude that the created ink formulation provides for an improved printability, as a result verifying one of the two core aspects of the main research hypothesis, namely that the synergy of a filler based scaffold core and in-situ bacterial overgrowth leads for an ink formulation which allows improved shaping freedom.

The second aspect of this thesis, next to the practicality of creating a living ink with improved printability, was to characterise the created material. This was first done using SEM imaging to analyse the microstructure of overgrown samples, from which it was concluded that on a high level the morphology of the microstructure follows a core-shell distinction whereas the bacterial cellulose forms an enclosing shell around the platelet rich scaffold core. In addition, the comparison with samples without a bacterial cellulose shell verified the proposed compaction effect its shrinkage during drying has on the core which was found to negate the formation of large scale voids (>100microns). The same cross-sectional analysis was subsequently used to fulfil the second objective this research posed, namely the need to establish a fundamental growth model for the printed scaffolds. For this the BC yield was tracked as a function of time to find the maximum carrying capacity of a set of sample plates which was compared to the bacterial cellulose yield based on the full conversion of nutrients contained within the printed scaffold using the liquid nutrient conversion factor established in the parametric study. As a result of the found lower than predicted bacterial cellulose yield, the conclusion was drawn that the bacterial cellulose formed around the core did not require the diffusion of nutrients from the agar substrate on which it was printed. Additionally the results indicated that the ink formulation did not lead to the complete utilisation of nutrients within the scaffold, as a result limiting the maximum bacterial cellulose shell thickness for the given ink formulation to $19.7\mu m$.

In addition to the analysis of the microstructure and the insights gained into the growth dynamics, the BC composite material created based on the living ink formulation developed was investigated using nano-indentation to compare the elastic modulus of samples with and without a bacterial cellulose shell. The testing campaign found that the overgrowth of the silicon dioxide core by bacterial cellulose increased the reduced Young's modulus by a factor of six, while showing a reduced Youngs modulus 1.7x higher than that of the statically grown bacterial cellulose reference sample. Based on these results, the conclusion was drawn, that the bacterial cellulose growth and subsequent shrinkage during drying compacts the core and gives rise to loading response whereas the material acts more integral, resulting in a more effective loading of the stiff silicon dioxide platelets contained in its core. As such the observed increase in reduced Youngs modulus was used as evidence to conclude that the synergy of a filler based scaffold core and in-situ bacterial overgrowth leads to an increase in the structural integrity of the created material, thus verifying the second aspect of the main research hypothesis.

The increased printability and mechanical integrity observed for the living ink formulation developed, as outlined above, allows for a positive verdict on the main research hypothesis, namely that

"The addition of silicon dioxide platelets and fumed silica to a living ink can be utilised to act as a scaffold for in-situ bacterial cellulose growth which allows for the additive manufacture of 3-dimensional shapes giving rise to an increase in the achievable shaping freedom and micro-mechanical properties."

In addition, the detailed characterisation of the materials microstructure in combination with a first of its kind diffusion model to describe the nutrient flow during bacterial cellulose growth around the printed scaffold, provides the fundamental understanding required for further developing living inks for in-situ bacterial cellulose growth.

10

Perspective for Future Research

10.1. Limitations

There are two main limitations which require an iteration on the ink formulation and process developed as part of this research. The first is that despite the increase in shaping freedom achieved, the process nonetheless restricts the geometric complexity of parts which can be constructed, as a result of the ink rheology and drying characteristic as further discussed in section 10.1. Next to the limitations imposed on the geometry, the nutrient diffusion model established in this work reveals a further restriction of the process which places an upper limit on the obtainable bacterial cellulose growth independent of the nutrients contained within the printed scaffold, similarly detailed in section 10.1.

Geometric Limitations

The origin for the geometric limitations of the process are introduced in both the printing and drying step of the manufacturing procedure.

The ink rheology as such imposes restriction due to its lack of bridging capability which inflicts substantial limitations on the overhangs which can be printed. While this issue is commonly encountered in direct ink writing with low-viscosity inks and can be traced back to to a too low yield stress, the appropriate mitigation strategy often applied of increasing the yield stress by increasing the filler content is not applicable to the work at hand. This is due to the fact that any further increase of the ink yield stress by increasing the %wt fumed silica was found to have a detrimental effect on the bacterial cellulose yield, as quantified by the fumed silica reduction factor, see Figure 4.14, such that for samples with a fumed silica content in excess of 4%wt no BC overgrowth could be observed. As a result, this requires the proposed process alteration to necessitate no further ink viscosity or yield stress increases, while nonetheless preventing the ink from sagging under its own weight.

Next to the geometric restrictions imposed by the ink rheology, the drying characteristics of the created material furthermore limit the geometric complexity which can be achieved. Note that this concept has been discussed in detail in section 10.1, with the origin of the observed geometric distortions being the differential shrinkage introduced by the lack of uniform growth around the scaffold. As a result the proposed solution is required to allow for homogeneous bacterial cellulose growth around the printed scaffold, which in turn necessitates an equal and sufficient oxygen availability on all sides.

Nutrient Supply Limitations

As outlined in section 7.5, the maximum bacterial cellulose coverage around the printed silicon dioxide scaffolds is solely dependent on the nutrients within close proximity of the surface leading to an underutilisation of the nutrients within the core of the printed scaffold. This lack of diffusion from the core can in part be explained by the, relatively high viscosity, which as similarly noted by the work of Schaffner et al.[18], hinders the diffusion of nutrients. Note that in addition to the qualitative observations provided as a basis for this argument in the work of Schaffner et al.[18], it can furthermore be extrapolated from a theoretical standpoint, whereas viscosity (η) and diffusion are inversely related through the diffusion coefficient(D) as denoted by Equation 10.1.[2]

$$D = \frac{k_B T}{6\pi\eta r_H} \tag{10.1}$$

As a result, the desire to more effectively utilise nutrients throughout the printed scaffold requires a ink formulation which gives rise to a lower viscosity.

10.2. Proposed Process Improvement

The following requirements on the proposed process alteration can be derived from the above discussion on the current limitations.

1. Prevent ink sagging under its own weight without increasing the ink viscosity
2. Allow for a homogeneous bacterial cellulose growth around the printed scaffold, by having an equal and sufficient oxygen availability on all surfaces
3. Reduce the ink viscosity to increase the availability of nutrients from within the printed scaffold

In order to overcome the above requirements it is proposed to investigate the extrapolation of the direct ink writing process used here to in-gel direct ink writing, whereas the ink is extruded into a gel bath which encapsulates and supports it, allowing for the manufacture of geometries untethered from gravitational limitations, Figure 10.1.

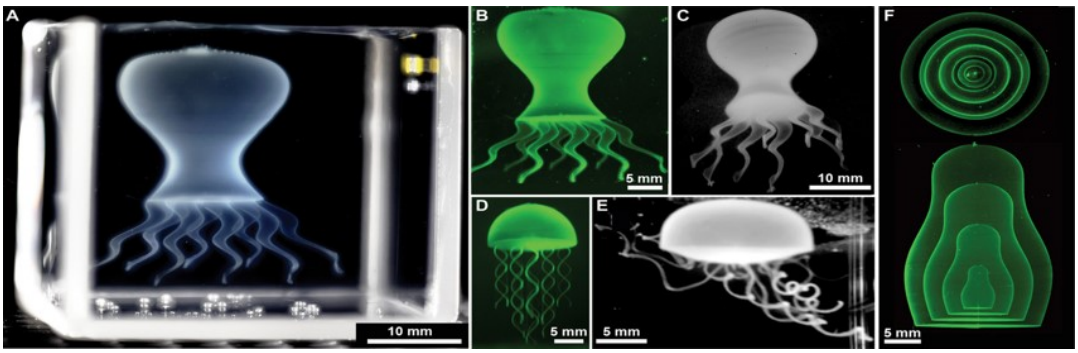

Figure 10.1: Examples of achievable shaping freedom when extruding low-viscosity inks into a gel support bath[5].

As a result this technique has found frequent and successful application to low viscosity inks without sacrificing geometric complexity, such that the argument is made that the extrapolation of in-gel printing to the process at hand would allow for the %wt FS to be reduced, leading to a more efficient diffusion of nutrients from the scaffold to the BC-shell layer without sagging issues as such fulfilling both the first and third requirement imposed on the alteration of the process.

In contrast to the fulfilment of requirements 1 & 3 by extrapolating the here developed process to in-gel direct ink writing, the need to supply sufficient oxygen to all surface of the printed structure opens up the opportunity for further research, as the aerobic cellulose producing bacteria strain (*G.hansenii*), as shown in subsection 4.4.4, requires a sufficient supply and concentration of oxygen in order to metabolise cellulose. As a result it is unclear if the gel support bath used in in-gel printing allows for a high enough diffusion rate of oxygen from the air-gel interface to the active bacteria on the surface of the printed scaffold.

While this remains a hurdle of unknown severity for the *G.hansenii* bacteria used, the fundamental issue, namely the need to supply oxygen to organisms within a liquid enviroment can be found many times over within the natural world, offering a rich source of inspiration for how to overcome it. While a in detail discussion of these options facilitates a thesis on its own, one possible mechanisms is proposed here for future research.

Microbial Symbiosis

In stark contrast to the approach taken here, whereas the organisms of interest was isolated and supported by the artificial supply of resources, the natural world often relies on an intricate balance between

a range of organisms, working in symbiosis to support each other. By extrapolating this approach to the work at hand the proposal is made that the integration of algae microbes into the gel medium could allow the formation of a symbiotic relationship, whereas the algae microbes use the carbon dioxide from the cellulose producing bacteria and light to increase the oxygen availability within the gel. Note that the viability of this approach has been demonstrated by the work of Das et al.[7], which showed that a symbiotic relationship between algae microbes and cellulose producing bacteria is fundamentally possible.

References

[1] Clemens M. Altaner et al. “How Cellulose Stretches: Synergism between Covalent and Hydrogen Bonding”. In: *Biomacromolecules* 15.3 (2014), pp. 791–798. DOI: 10.1021/bm401616n.

[2] I. Avramov. “Relationship between diffusion, self-diffusion and viscosity”. In: *Journal of Non-Crystalline Solids* 355.10-12 (2009), pp. 745–747. DOI: 10.1016/j.jnoncrysol.2009.02.009.

[3] *Bacterial cellulose - Alchetron, the Free Social Encyclopedia*. Sept. 2021. URL: https://alchetron.com/Bacterial-cellulose.

[4] Srikkanth Balasubramanian et al. “Emergent biological endurance depends on extracellular matrix composition of three-dimensionally printed escherichia coli biofilms”. In: *ACS Publication* (Oct. 2021). DOI: https://doi.org/10.1021/acssynbio.1c00290.

[5] Tapomoy Bhattacharjee et al. “Writing in the granular gel medium”. In: *Science Advances* 1.8 (2015). DOI: 10.1126/sciadv.1500655.

[6] Mikaela Börjesson and Gunnar Westman. “Crystalline Nanocellulose — Preparation, Modification, and Properties”. In: *Cellulose - Fundamental Aspects and Current Trends* (2015). DOI: 10.5772/61899.

[7] Anupam A. Das et al. “Fabrication of living soft matter by symbiotic growth of unicellular microorganisms”. In: *Journal of Materials Chemistry B* 4.21 (2016), pp. 3685–3694. DOI: 10.1039/c5tb02489g.

[8] *Dissolved oxygen*. Jan. 2019. URL: https://www.fondriest.com/environmental-measurements/parameters/water-quality/dissolved-oxygen/.

[9] Johnsy George and Sabapathi S N. “Cellulose nanocrystals: synthesis, functional properties, and applications”. In: *Nanotechnology, Science and Applications* (2015), p. 45. DOI: 10.2147/nsa.s64386.

[10] Gorgieva and Trček. “Bacterial Cellulose: Production, Modification and Perspectives in Biomedical Applications”. In: *Nanomaterials* 9.10 (2019), p. 1352. DOI: 10.3390/nano9101352.

[11] Gorgieva and Trček. “Bacterial cellulose: Production, modification and perspectives in biomedical applications”. In: *Nanomaterials* 9.10 (2019), p. 1352. DOI: 10.3390/nano9101352.

[12] P.-O. Hagstrand, F. Bonjour, and J.-A.E. Månson. “The influence of void content on the structural flexural performance of unidirectional glass fibre reinforced polypropylene composites”. In: *Composites Part A: Applied Science and Manufacturing* 36.5 (2005), pp. 705–714. DOI: 10.1016/j.compositesa.2004.03.007.

[13] M. L. Hentschel and N. W. Page. “Elastic properties of powders during compaction. part 1: Pseudo-isotropic Moduli”. In: *Journal of Materials Science* 42.4 (2006), pp. 1261–1268. DOI: 10.1007/s10853-006-1145-x.

[14] Ivy Tech Lumen Learning. *Biology I*. URL: https://courses.lumenlearning.com/ivytech-bio1-1/chapter/reading-types-of-carbohydrates/.

[15] Kunal Masania. *Additive Manufacturing: Direct Ink Writing*. University Lecture. 2020.

[16] Daisuke Miyashiro, Ryo Hamano, and Kazuo Umemura. “A review of applications using mixed materials of cellulose, nanocellulose and carbon nanotubes”. In: *Nanomaterials* 10.2 (2020), p. 186. DOI: 10.3390/nano10020186.

[17] Patrick A. Rühs et al. “3D bacterial cellulose biofilms formed by foam templating”. In: *npj Biofilms and Microbiomes* 4.1 (2018). DOI: 10.1038/s41522-018-0064-3.

[18] Manuel Schaffner et al. “3D printing of bacteria into functional complex materials”. In: *Science Advances* 3.12 (2017). DOI: 10.1126/sciadv.aao6804.

[19] Giuseppe Scionti. 2010. URL: https://hdl.handle.net/20.500.12380/129263.

[20] Sungchul Shin et al. “Solid matrix-assisted printing for three-dimensional structuring of a viscoelastic medium surface”. In: *Nature Communications* 10.1 (2019). DOI: 10.1038/s41467-019-12585-9.

[21] Adam M. Sokolnicki et al. “Permeability of bacterial cellulose membranes”. In: *Journal of Membrane Science* 272.1-2 (2006), pp. 15–27. DOI: 10.1016/j.memsci.2005.06.065.

[22] Young S. Song, Jae R. Youn, and Timothy G. Gutowski. “Life cycle energy analysis of fiber-reinforced composites”. In: *Composites Part A: Applied Science and Manufacturing* 40.8 (2009), pp. 1257–1265. DOI: 10.1016/j.compositesa.2009.05.020.

[23] *Strength Stiffness*. URL: https://netcomposites.com/guide/resin-systems/strength-stiffness/.

[24] Hao Sun et al. “Mechanically Strong, cost-efficiency, and sustainable fully wood-derived structural materials by Micro/Nanoscale Design”. In: *Journal of Materials Research and Technology* 14 (2021), pp. 3043–3050. DOI: 10.1016/j.jmrt.2021.08.153.

[25] *UCI Human Resources: Staff Service Awards - History*. URL: https://hr.uci.edu/partnership/staff-service/history.php.

[26] Leire Urbina et al. “Hybrid and biocompatible cellulose/polyurethane nanocomposites with water-activated shape memory properties”. In: *Carbohydrate Polymers* 216 (2019), pp. 86–96. DOI: 10.1016/j.carbpol.2019.04.010.

[27] *Washington State University*. URL: https://labs.wsu.edu/mpml/projects/.

[28] Shoichiro Yano et al. “Preparation and mechanical properties of bacterial cellulose nanocomposites loaded with silica nanoparticles”. In: *Cellulose* 15.1 (2007), pp. 111–120. DOI: 10.1007/s10570-007-9152-x.

[29] K. Yu. *Biological Production of Spatially Organized Functional Materials*. June 2021. URL: https://repository.tudelft.nl/islandora/object/uuid:57651a9a-5dab-4459-a320-302b6c680b8e.

Appendix A

A.1. Nitrogen Leak Test

To verify sufficient sealing of the oxygen limited test tubes the sealing method was tested using a nitrogen leak test. Here the flask were filled with nitrogen such that the initial oxygen concentration was close to zero after which the variation in oxygen level was tracked over 15 hrs, the results of which are shown in Figure A.1.

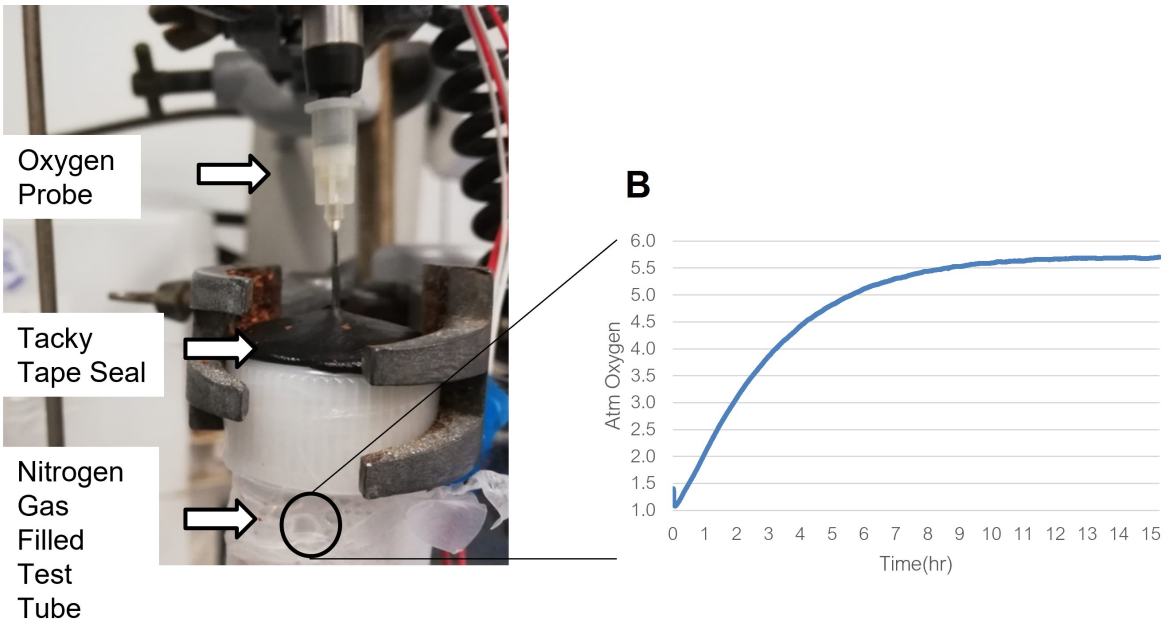

Figure A.1: Experimental setup for the nitrogen leak test (A) and the oxygen concentration as a function of time (B).

A.2. Initial Nutrient Supply Experiment

Results of the initial nutrient supply experiment used to determine the the maximum growth time and volumes levels investigated.

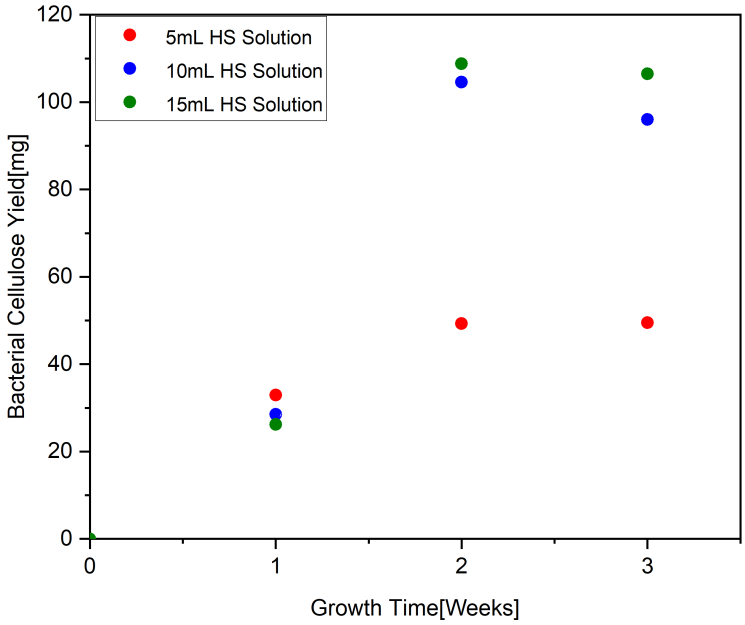

Figure A.2: BC yield of the initial nutrient supply parametric study as a function of time and HS-medium supplemented.

A.3. Oxygen N=1

Initial oxygen limitation experiment showing the effect of insufficient sealing, indicated by the rapid increase in bacterial cellulose growth after previous stagnation, see oxygen limited datapoints week 3 Figure A.3.

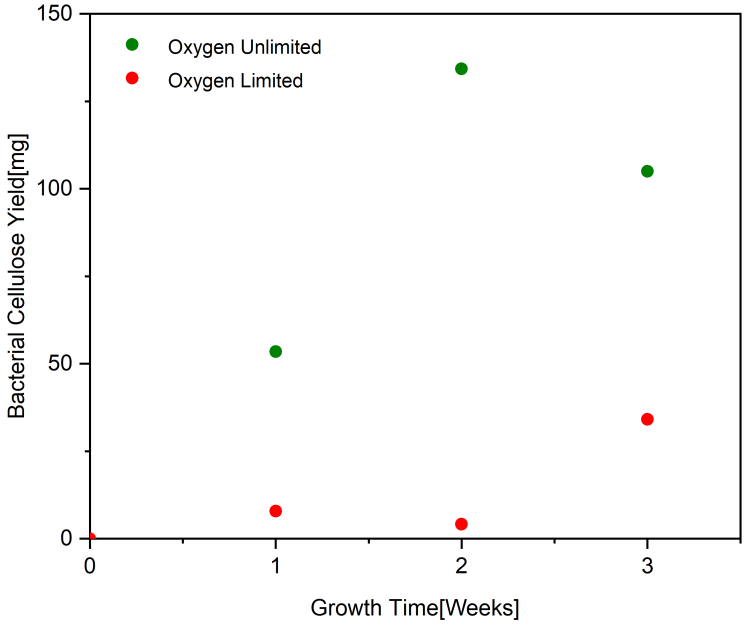

Figure A.3: BC yield of the initial oxygen limited parametric study as a function of time and oxygen availability.